

THE SPIRITS SAMPLE OF LUMINOUS INFRARED TRANSIENTS: UNCOVERING HIDDEN SUPERNOVAE AND DUSTY STELLAR OUTBURSTS IN NEARBY GALAXIES

JACOB E. JENCSON,^{1,*} MANSI M. KASLIWAL,¹ SCOTT M. ADAMS,¹ HOWARD E. BOND,^{2,3} KISHALAY DE,¹ JOEL JOHANSSON,⁴
VIRAJ KARAMBELKAR,⁵ RYAN M. LAU,^{1,6} SAMAPORN TINYANONT,¹ STUART D. RYDER,^{7,8} ANN MARIE CODY,⁹ FRANK J. MASCI,¹⁰
JOHN BALLY,¹¹ NADEJDA BLAGORODNOVA,¹² SERGIO CASTELLÓN,¹³ CHRISTOFFER FREMLING,¹ ROBERT D. GEHRZ,¹⁴
GEORGE HELOU,¹⁰ CHARLES D. KILPATRICK,¹⁵ PETER A. MILNE,¹⁶ NIDIA MORRELL,¹³ DANIEL A. PERLEY,¹⁷ MARK PHILLIPS,¹³
NATHAN SMITH,¹⁶ SCHUYLER D. VAN DYK,¹⁰ AND ROBERT E. WILLIAMS^{15,3}

¹*Cahill Center for Astronomy and Astrophysics, California Institute of Technology, Pasadena, CA 91125, USA*

²*Department of Astronomy & Astrophysics, Pennsylvania State University, University Park, PA 16802, USA*

³*Space Telescope Science Institute, 3700 San Martin Dr., Baltimore, MD 21218, USA*

⁴*Department of Physics and Astronomy, Division of Astronomy and Space Physics, Uppsala University, Box 516, SE 751 20 Uppsala, Sweden*

⁵*Department of Physics, Indian Institute of Technology Bombay, Mumbai 400076, India*

⁶*Institute of Space & Astronautical Science, Japan Aerospace Exploration Agency, 3-1-1 Yoshinodai, Chuo-ku, Sagami-hara, Kanagawa 252-5210, Japan*

⁷*Australian Astronomical Observatory, 105 Delhi Road, North Ryde, NSW 2113, Australia*

⁸*Department of Physics & Astronomy, Macquarie University, NSW 2109, Australia*

⁹*NASA Ames Research Center, Moffet Field, CA 94035*

¹⁰*Caltech/IPAC, Mailcode 100-22, Pasadena, CA 91125, USA*

¹¹*Astrophysical and Planetary Sciences Department University of Colorado, UCB 389 Boulder, Colorado 80309, USA*

¹²*Department of Astrophysics/IMAPP, Radboud University, Nijmegen, The Netherlands*

¹³*Las Campanas Observatory, Carnegie Observatories, Casilla 601, La Serena, Chile*

¹⁴*Minnesota Institute for Astrophysics, School of Physics and Astronomy, University of Minnesota, 116 Church Street, S. E., Minneapolis, MN 55455, USA*

¹⁵*Department of Astronomy and Astrophysics, University of California, Santa Cruz, CA 95064, USA*

¹⁶*University of Arizona, Steward Observatory, 933 N. Cherry Avenue, Tucson, AZ 85721, USA*

¹⁷*Astrophysics Research Institute, Liverpool John Moores University, IC2, Liverpool Science Park, 146 Brownlow Hill, Liverpool L3 5RF, UK*

ABSTRACT

We present a systematic study of the most luminous (M_{IR} [Vega magnitudes] brighter than -14) infrared (IR) transients discovered by the SPitzer InfraRed Intensive Transients Survey (SPIRITS) between 2014–2018 in nearby galaxies ($D < 35$ Mpc). The sample consists of 9 events that span peak IR luminosities of $M_{[4.5],\text{peak}}$ between -14 and -18.2 , show IR colors between $0.2 < ([3.6] - [4.5]) < 3.0$, and fade on timescales between $55 < t_{\text{fade}} < 480$ days. The two reddest events ($A_V > 12$) show multiple, luminous IR outbursts over several years and have directly detected, massive progenitors in archival imaging. With analyses of extensive, multi-wavelength follow-up, we infer the following likely classifications: 5 obscured core-collapse supernovae (CCSNe), 2 erupting massive stars, 1 massive stellar merger, and 1 possible electron capture SN. We define a control sample of all optically discovered transients recovered in SPIRITS galaxies and satisfying the same selection criteria. The control sample consists of 8 core-collapse supernovae (CCSNe) and 1 Type Iax SN. We find that 7 of the 13 CCSNe in the SPIRITS sample have lower bounds on extinction of $2 < A_V < 8$, suggesting that a large population of CCSNe is heavily obscured. We estimate a nominal fraction of CCSNe in nearby galaxies that are missed by optical surveys of $38.5^{+26.0}_{-21.9}\%$ (90% confidence). This may resolve long-standing discrepancies between measurements of the CCSN rate and the cosmic star-formation rate.

Keywords: infrared: general — stars: massive — dust, extinction — supernovae: general — supernovae: individual (SPIRITS 14buu, SPIRITS 15c, SPIRITS 15ud, SPIRITS 16ix, SPIRITS 16tn, SPIRITS 17lb, SN 2014bi, SN 2014df, ASASSN-14ha, SN 2014dt, SN 2016C, SN 2016bau, SN 2016bkv, SN 2016cok, SN 2017eaw)

Corresponding author: Jacob E. Jencson

jj@astro.caltech.edu

* National Science Foundation Graduate Research Fellow

1. INTRODUCTION

While there are now several known classes of stellar transient phenomena for which the observable emission is predominantly infrared (IR), exploration of the landscape of IR-dominated transients is just beginning. Often due to the effects of astrophysical dust, a host of eruptive and explosive stellar phenomena may be best observed in the IR. In particular, otherwise optically luminous transients such as supernovae (SNe), may be significantly obscured by dust in their host galaxies and/or local environments. Dust in the immediate circumstellar environment of a luminous transient, which may have condensed in a steady wind of the progenitor or formed during previous eruptive mass loss events, may also efficiently reprocess shorter wavelength emission into the IR. Some transients, particularly those associated with cool, low-velocity outflows, are themselves copious dust producers, leading to IR-dominated spectral energy distributions (SEDs).

Since 2014, we have been conducting the *Spitzer* InfraRed Intensive Transients Survey (SPIRITS; PIDs 11063, 13053, 14089; PI M. Kasliwal, [Kasliwal et al. 2017](#)) to discover transients in nearby $D \lesssim 35$ Mpc galaxies using the 3.6 and 4.5 μm imaging bands ([3.6] and [4.5]) of the Infrared Array Camera (IRAC; [Fazio et al. 2004](#)) on board the warm *Spitzer* Space Telescope (*Spitzer*; [Werner et al. 2004](#); [Gehrz et al. 2007](#)). In this paper, we focus on a thorough investigation of all luminous ($M_{[4.5]}$ [Vega magnitudes] brighter than -14) IR transients discovered by SPIRITS in the last five years (Section 2.3). We compare this sample to a well-defined control sample of all optically discovered and spectroscopically classified transients hosted by SPIRITS galaxies and satisfying the same selection criteria (Section 2.4). Our sample of luminous infrared transients may represent diverse origins, including obscured core-collapse supernovae (CCSNe) and other known classes of IR-dominated transients such as stellar mergers or massive star eruptions (MSEs).

Core-collapse SNe (CCSNe), the explosive deaths of stars of initial masses $\gtrsim 8 M_{\odot}$, are now found in numbers exceeding several hundreds of events per year by numerous, primarily optical, searches. Arising from recently formed, massive stars, CCSNe may be subject to significant extinction from the dusty regions of active star formation in their host galaxies. The fraction of CCSNe missed optically due to the obscuring effects of dust is therefore an important consideration for measurements of the CCSN rate (e.g., [Grossan et al. 1999](#); [Maiolino et al. 2002](#)). [Horiuchi et al. \(2011\)](#) claimed half of all SNe were missing from observed CCSN rate estimates in comparison to the rate of massive star formation both locally and across cosmic time from redshifts $0 < z < 1$; however, other studies have found better agreement (e.g., [Cappellaro et al. 2015](#)). Accounting for obscured or otherwise optically dim CCSNe may also resolve this dis-

crepancy (e.g., [Mannucci et al. 2007](#); [Mattila et al. 2012](#)). Direct searches for CCSNe at wavelengths less sensitive to extinction are thus required to accurately measure the CCSN rate. Significant work (e.g., [Kool et al. 2018](#); [Varenius et al. 2017](#), and references therein) has been dedicated to uncovering extinguished CCSNe in the densely obscured and highly star forming regions of starburst and (ultra-) luminous infrared galaxies (U/LIRGS). In contrast, our SPIRITS sample of galaxies focuses on local galaxies encompassing a wide variety of galaxy morphologies, masses and star-formation rates (Section 2.1).

Other categories of luminous IR transients include intermediate luminosity red transients (ILRTs), luminous red novae (LRNe), and giant eruptions of luminous blue variables (LBVs). The prototypical objects for ILRTs are the “imposter” SN 2008S and the 2008 transient in NGC 300 (NGC 300 2008OT-1; [Bond et al. 2009](#)), suggested to be explosions of extreme asymptotic giant branch (AGB) stars of intermediate mass ($\approx 10\text{--}15 M_{\odot}$) self-obscured by a dusty wind ([Prieto et al. 2008](#); [Bond et al. 2009](#); [Thompson et al. 2009](#)). Extragalactic LRNe are believed to be more massive analogs of stellar mergers observed in the Galaxy, including the striking example of the $\approx 1\text{--}3 M_{\odot}$ contact binary merger V1309 Sco ([Tylenda et al. 2011](#)) and the B-type stellar merger V838 Mon ([Bond et al. 2003](#); [Sparks et al. 2008](#)). While sharing many observational properties with ILRTs, a key difference is that LRNe have surviving remnants (e.g., NGC 4490 OT2011-1; [Smith et al. 2016](#)). Surviving dust in the circumstellar environments of LBVs may also result in an observed IR excess during some non-terminal giant eruptions (e.g., UGC 2773OT; [Smith et al. 2010](#)). It is particularly telling that known examples and even class prototypes of these IR-dominated events have almost exclusively been identified via their optical emission. SPIRITS overcomes the selection biases of optical discovery and is sensitive to redder events that may lack optical counterparts altogether.

We have undertaken extensive follow-up including optical/IR photometry, spectroscopy, and radio imaging to characterize the nature of each luminous IR transient presented in this work (Section 3). We describe our analysis of the full data set including host galaxy properties, progenitors constraints, photometric evolution, spectroscopic feature identification, and extinction estimates in Section 4. In Section 5, we combine all available observational constraints and compare to well-studied objects to classify each luminous SPIRITS transient. In Section 6, we discuss the A_V distribution of nearby, luminous IR transients and CCSNe in particular, and in Section 7, we derive statistically robust estimates of the rate of CCSNe missed in nearby galaxies relative to the control sample of optically discovered CCSNe in SPIRITS galaxies. Finally, in Section 8, we summarize the main results and conclusions of this work.

2. SURVEY DESIGN AND SAMPLE SELECTION

2.1. Galaxy sample and imaging cadence

A full description of the SPIRITS survey design is given in Kasliwal et al. (2017). It is a targeted search of nearby galaxies using the 5×5 arcmin field of view of the IRAC camera. SPIRITS monitored a sample of 190 nearby galaxies for 3 years from 2014–2016. The sample was selected based on the following criteria: 1) The 37 galaxies within 5 Mpc including both early and late-type galaxies, dwarf galaxies and giant galaxies, 2) the 116 most luminous galaxies between 5 and 15 Mpc, including 83% if the B -band starlight within 15 Mpc, and 3) the 37 most luminous and massive galaxies in the Virgo Cluster at 17 Mpc.

In 2014, each galaxy was observed 3 times at ~ 1 month and ~ 6 month intervals. In 2015–2016, baselines of one- and three-week timescales were added. In 2017–2018, the galaxy sample was reduced to focus on only the 105 galaxies most likely to host new transients and SNe, including the 58 galaxies that had previously hosted at least one IR transient, and the 47 remaining most luminous and star-forming galaxies ($L > 2 \times 10^{10} L_{\odot}$). Our cadence was also reduced to ~ 6 month intervals, typically with one observation per galaxy per visibility window. Each SPIRITS observation consists of 7 dithered 100 s exposures in both IRAC bands. The nominal 5σ point source limiting magnitude of these observations are 20.0 mag at [3.6] and 19.1 mag at [4.5].

2.2. Image subtraction and transient identification

For reference images, we make use of archival *Spitzer*, including Super Mosaics¹ or S4G (*Spitzer* Survey of Stellar Structure in Galaxies; PID 61065; PI K. Sheth; Sheth et al. 2010; Muñoz-Mateos et al. 2013; Querejeta et al. 2015), or stacks of archival “bcd” images (where Super Mosaics or S4G images were not available). Further details of our image subtraction and transient identification pipelines are provided in Kasliwal et al. (2017).

Photometry was performed at the location of saved transients in the reference-subtracted images using a 4 mosaicked-pixel (2.4 arcsec) aperture and background annulus from 4–12 pixels (2.4–7.2 arcsec). The extracted flux was multiplied by the aperture corrections of 1.215 for [3.6] and 1.233 for [4.5] as described in the IRAC instrument handbook². Fluxes then were converted to Vega system magnitudes using the handbook-defined zero magnitude fluxes for each IRAC channel.

2.3. Luminous IR transient sample selection

We selected events having M_{IR} brighter than -14 in either the [3.6] or [4.5] channels of *Spitzer*/IRAC, and we required at least two SPIRITS detections and that these events were not present in the first epoch of SPIRITS imaging. We list basic properties for these objects in Table 1. One source, SPIRITS 14buu (first presented in Jencson et al. 2017), was identified in the first epoch of SPIRITS imaging of the galaxy IC 2163. As such, we have no constraint on the age of this object from SPIRITS data, and thus exclude it from the primary sample. The sample then consists of 9 events discovered in SPIRITS between 2014–2017 that, to our knowledge, were not identified and spectroscopically classified as by any other survey³. The *Spitzer*/IRAC [4.5] discovery images for each object, including the new science frame, reference image, and science – reference subtractions, are shown in Figure 1.

2.4. Optically discovered control sample

To place our sample of luminous IR transients in context, we define a control sample of optically discovered and classified transients recovered during normal operation of the SPIRITS survey, employing the same selection criteria as for the IR selected sample. A total of 14 transients hosted by SPIRITS galaxies and discovered at optical wavelengths have been reported since the start of the survey in 2014. We summarize basic properties of these events in Table 2.

Three events, SN 2014C (Type Ib/IIn), SN 2014J (Type Ia), and SN 2014L (Type Ic), were present in the first epoch of SPIRITS observations such that we would not have a meaningful constraint on the explosion epoch from SPIRITS data alone. Two additional events were not recovered in SPIRITS by our automated image subtraction and transient identification pipeline due to saturation of the IRAC detector at the location of the transient. SN 2014bc (Type II) was located only 3.4 arcsec from the bright nucleus of NGC 4258, which is saturated in all epochs of SPIRITS imaging. SN 2016adj (Type Ib) is the nearest SN in the optically discovered sample at only 3.7 Mpc, and is saturated in all epochs where the SN is present in SPIRITS imaging.

Thus, we define our primary comparison sample as the 9 objects that were recovered by SPIRITS and have constraints on their explosion dates from SPIRITS data. By optical spectroscopic subtype this sample includes 6 SNe II, 2 SNe Ib, and 1 SN Iax.

¹ Super Mosaics are available as *Spitzer* Enhanced Imaging Products through the NASA/IPAC Infrared Science Archive: <https://irsa.ipac.caltech.edu/data/SPITZER/Enhanced/SEIP/overview.html>

² <http://irsa.ipac.caltech.edu/data/SPITZER/docs/irac/iracinstrumenthandbook/>

³ An optical transient at the location of SPIRITS 15ade was first discovered on 2015 September 11.5 and reported by M. Aoki as PSN J15220552+0503160 through the Central Bureau for Astronomical Telegrams (<http://www.cbat.eps.harvard.edu/unconf/followups/J15220552+0503160.html>). To our knowledge, no spectroscopy for classification or host confirmation was reported before this work.

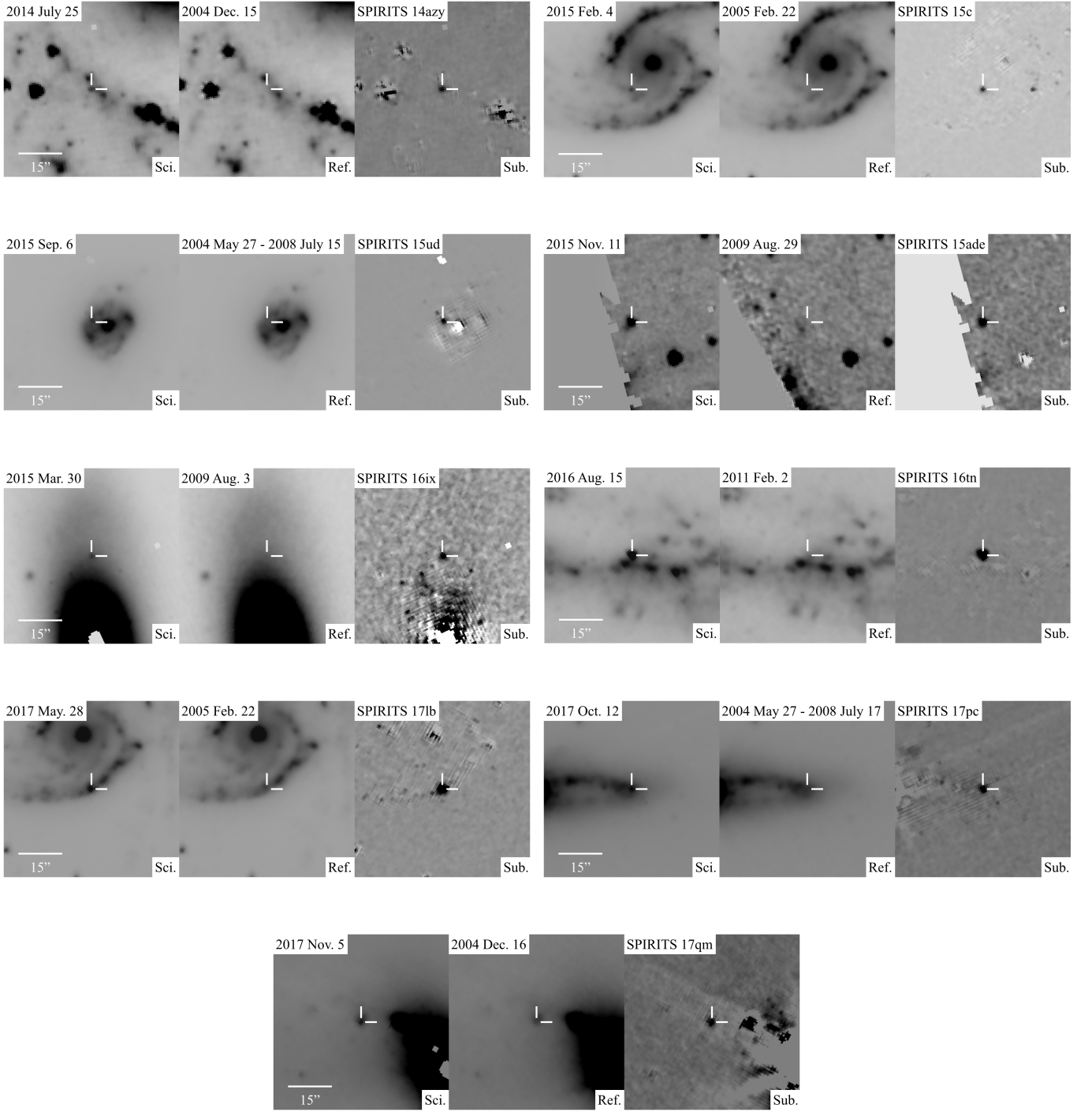


Figure 1. We show the *Spitzer*/IRAC [4.5] discovery images for each SPIRITS obscured SN candidate in our sample. In each panel, from left to right, we show the new science frame, reference frame, and science-minus-reference subtraction image. The dates of each image and labels for each object are shown along the top of each panel, and the locations of the transients are indicated by white crosshairs. Each image is $1' \times 1'$, oriented with N up and E left.

Table 1. Luminous, IR-discovered SPIRITS transients

| Name | RA (J2000) | Dec (J2000) | Host (Type) | μ^a mag | Distance (Mpc) | $E(B-V)_{\text{MW}}^b$ mag | UT discovery | Host offset (") (kpc) | |
|---------------|---------------|----------------|------------------------------|------------------|-------------------|-------------------------------|-----------------------------|--------------------------|------|
| SPIRITS 14buu | 06:16:27.2 | -21:22:29.2 | IC 2163 (SBc pec) | 32.75 ± 0.4 | 35.5 | 0.077 | 2014 Jan. 13.9 ^c | 11.5 | 2.0 |
| SPIRITS 14azy | 09:45:40.92 | -31:12:07.8 | NGC 2997 (SABc) | 30.43 ± 0.16 | 12.2 | 0.027 | 2014 Jul 26.0 | 48.4 | 2.9 |
| SPIRITS 15c | 06:16:28.49 | -21:22:42.2 | IC 2163 (SBc pec) | 32.75 ± 0.4 | 35.5 | 0.077 | 2015 Feb 04.4 | 11.6 | 2.0 |
| SPIRITS 15ud | 12:22:55.29 | +15:49:22.0 | M100 (SABbc) | 30.72 ± 0.06 | 13.9 | 0.023 | 2015 Sep 06.7 | 7.5 | 0.5 |
| SPIRITS 15ade | 15:22:05.55 | +05:03:15.9 | NGC 5921 (SBbc) | 31.9 ± 0.2 | 24.0 | 0.036 | 2015 Nov 11.9 | 146.3 | 17.0 |
| SPIRITS 16ix | 12:29:03.16 | +13:11:30.7 | NGC 4461 (SB0 ⁺) | 31.48 ± 0.25 | 19.8 | 0.02 | 2016 Mar 30.9 | 29.2 | 2.8 |
| SPIRITS 16tn | 11:11:20.40 | +55:40:17.3 | NGC 3556 (SBcd) | 29.7 ± 0.4 | 8.7 | 0.015 | 2016 Aug 15.0 | 89.9 | 3.8 |
| SPIRITS 17lb | 06:16:27.78 | -21:22:51.7 | IC 2163 (SBc pec) | 32.75 ± 0.4 | 35.5 | 0.077 | 2017 May 28.7 | 18.8 | 3.2 |
| SPIRITS 17pc | 12:25:44.43 | +12:39:44.5 | NGC 4388 (SAB) | 31.3 ± 0.4 | 18.2 | 0.029 | 2017 Oct 12.8 | 33.9 | 3.0 |
| SPIRITS 17qm | 03:33:38.85 | -36:08:09.4 | NGC 1365 (SBb) | 31.31 ± 0.06 | 18.3 | 0.018 | 2017 Nov 05.2 | 34.1 | 3.0 |

^aReferences for distance moduli: NGC 2997 (Hess et al. 2009), IC 2163 (Theureau et al. 2007), M100 and NGC 4461 (Tully et al. 2013), NGC 5921 (Rodríguez et al. 2014), NGC 3556 and NGC 4388 (Sorce et al. 2014), NGC 1365 (Riess et al. 2016).

^bGalactic extinction estimates taken from NED using the Schlafly & Finkbeiner (2011) recalibration of the Schlegel et al. (1998) IR-based dust map assuming a Fitzpatrick (1999) extinction law with $R_V = 3.1$.

^cTransient present in first 2014 SPIRITS epoch, and therefore excluded from the primary sample.

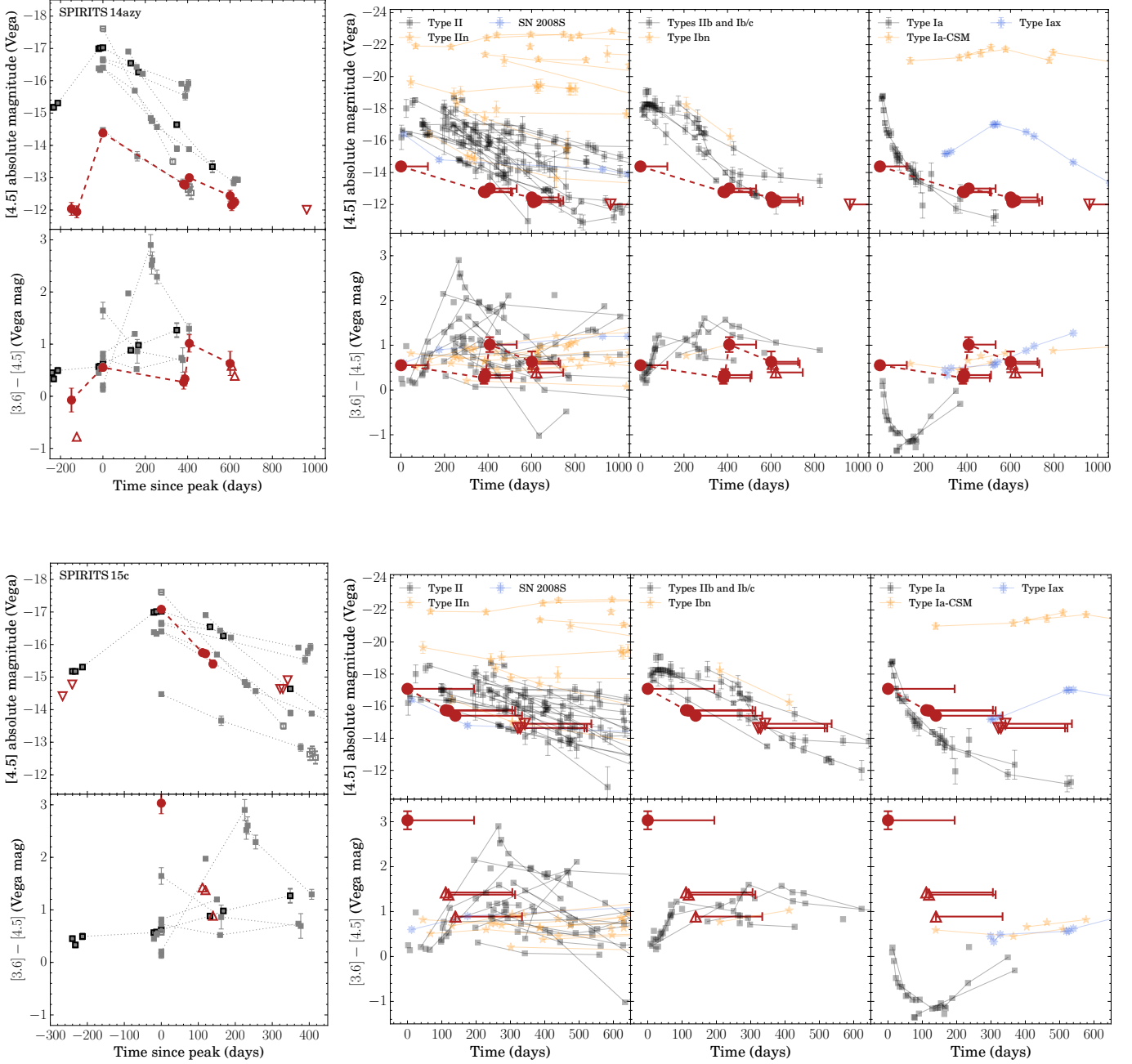


Figure 2. For each SPIRITS obscured SN candidate, we show the [4.5] light curve (top row) and [3.6] – [4.5] color curve (bottom row) as the large, red circles. In the left panel for each object, the phase is measured in days since the observed IR peak, and we compare to the control sample of optically discovered SNe recovered in SPIRITS as described in Section 2.4 including SNe II (light gray squares), stripped-envelope SNe Ib (unfilled squares), and the Type Iax SN 2014dt (black-outlined squares). In the right panel for each object, we compare to the full sample of SNe detected by *Spitzer* compiled by Szalai et al. (2018), including previous compilations by Szalai & Vinkó (2013), Tinyanont et al. (2016), and Johansson et al. (2017), and references therein. Additionally, we include the SNe observed by SPIRITS since 2014 and presented in this work. From left to right, we compare to SNe II (IIn), stripped-envelope SNe Ib and Ib/c (Ibn), and SNe Ia (Ia CSM) as light grey squares (orange stars). The blue, eight-pointed stars indicate the prototypical for its class SN 2008S, and the unusual, dusty Type Iax SN 2014dt. The phase for comparison SNe is measured as days since discovery, and for obscured SN candidates we represent our uncertainty in the phase of the primary outburst by the horizontal error bars. Upper- (lower-) limits from non-detections are indicated by unfilled, downward- (upward-) pointing triangles.

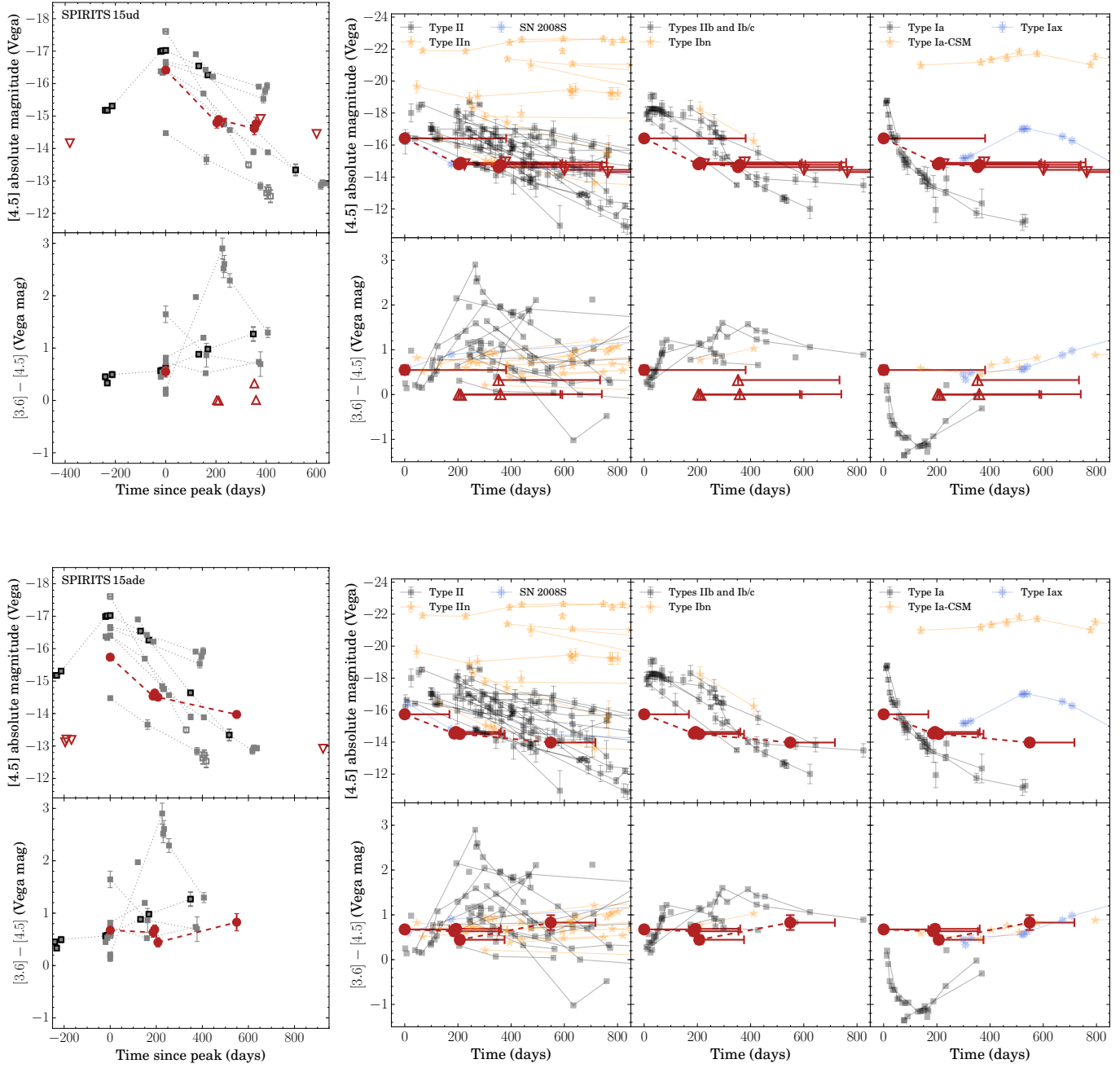


Figure 2, continued.

Table 2. Optically discovered and classified transients in SPIRITS

| Name | SPIRITS name ^a | RA (J2000) | Dec (J2000) | Host (Type) | μ^b (mag) | D (Mpc) | $E(B-V)_{\text{MW}}^c$ (mag) | A_V^d (mag) | UT discovery ^e | Host offset ($''$) | Type |
|-------------|---------------------------|---------------|----------------|---------------------|------------------|--------------|---------------------------------|------------------|----------------------------|-------------------------|------------|
| SN 2014C | SPIRITS 14aom | 22:37:05.60 | +34:24:31.9 | NGC 7331 (SAB) | 30.71 \pm 0.08 | 13.9 | 0.08 | 0.22 | 2014 Jan 05.1 ^g | 31.0 | 2.1 Ib/IIn |
| SN 2014J | SPIRITS 14pw | 09:55:42.14 | +69:40:26.0 | M82 (I0) | 27.74 \pm 0.08 | 3.5 | 0.14 | 0.98 | 2014 Jan 21.8 ^g | 58.6 | 1.0 Ia |
| SN 2014L | SPIRITS 14we | 12:18:48.68 | +14:24:43.5 | NGC 4254 (SAC) | 30.7 \pm 0.2 | 13.8 | 0.11 | ... | 2014 Jan 26 ^g | 20.8 | 1.4 Ic |
| SN 2014bc | ... | 12:18:57.71 | +47:18:11.3 | NGC 4258 (SABbc) | 29.32 \pm 0.05 | 7.3 | 0.01 | ... | 2014 May 19.3 | 3.7 | 0.1 II |
| SN 2014bi | SPIRITS 15bx | 12:06:02.99 | +47:29:33.5 | NGC 4096 (SABc) | 30.4 \pm 0.4 | 12.1 | 0.02 | 4.3 | 2014 May 31.3 | 54.4 | 3.2 IIP |
| SN 2014df | SPIRITS 14bse | 03:44:23.99 | -44:40:08.1 | NGC 1448 (SACd) | 31.31 \pm 0.05 | 18.3 | 0.01 | \sim 0 | 2014 Jun 03.2 | 121.1 | 10.7 Ib |
| ASASSN-14ha | SPIRITS 15yp | 04:20:01.41 | -54:56:17.0 | NGC 1566 (SAB pec?) | 31.1 \pm 0.4 | 16.8 | 0.01 | \sim 0 | 2014 Sep 10.3 | 8.6 | 0.7 II |
| SN 2014dt | SPIRITS 15sd | 12:21:57.57 | +04:28:18.5 | M61 (SABbc) | 31.43 \pm 0.07 | 19.3 | 0.02 | \sim 0 | 2014 Oct. 29.8 | 40.5 | 3.8 Iax |
| SN 2016C | SPIRITS 16ot | 13:38:05.30 | -17:51:15.3 | NGC 5247 (SABc) | 31.7 \pm 0.4 | 21.9 | 0.07 | \sim 0.2 | 2016 Jan 03.8 | 111.9 | 11.9 IIP |
| SN 2016adj | ... | 13:25:24.11 | -43:00:57.5 | Cen A (S0 pec) | 27.82 \pm 0.06 | 3.7 | 0.10 | 0.23 | 2016 Feb. 08.6 | 40.1 | 0.7 Ib |
| SN 2016bau | SPIRITS 16is | 11:20:59.02 | +53:10:25.6 | NGC 3631 (SAC) | 31.2 \pm 0.4 | 17.4 | 0.01 | \sim 3.3 | 2016 Mar. 14.0 | 37.8 | 3.2 Ib |
| SN 2016bkv | SPIRITS 17eb | 10:18:19.31 | +41:25:39.3 | NGC 3184 (SABcd) | 30.79 \pm 0.05 | 14.4 | 0.01 | 0.0 | 2016 March 21.7 | 30.3 | 2.1 IIP |
| SN 2016cok | SPIRITS 17ft | 11:20:19.10 | +12:58:56.0 | M66 (SABb) | 29.78 \pm 0.07 | 9.0 | 0.03 | 0.16 | 2016 May 28.5 | 69.1 | 3.0 IIP |
| SN 2017eaw | SPIRITS 18k | 20:34:44.24 | +60:11:35.9 | NGC 6946 (SABcd) | 28.73 \pm 0.05 | 5.6 | 0.30 | \lesssim 0.13 | 2017 May 14.2 | 154.1 | 4.2 IIP |

^a SN 2014bc was located near the saturated nucleus of NGC 4258 in the *Spitzer*/IRAC images and not detected in SPIRITS. SN 2016adj was saturated in the *Spitzer*/IRAC images of Centaurus A and not detected in SPIRITS.

^b References for distance moduli: NGC 7331, M82, NGC 4254, NGC 4258, Centaurus A, M66 (Tully et al. 2013), NGC 4096, (Sorce et al. 2014), NGC 1448 (Riess et al. 2016), NGC 1566 (Nasonova et al. 2011), M61 and NGC 6946 (Rodríguez et al. 2014), NGC 5247 (Tully 1988), NGC 3631 (Theureau et al. 2007), NGC 3184 (Ferrearese et al. 2000).

^c Galactic extinction estimates taken from NED using the Schlafly & Finkbeiner (2011) recalibration of the Schlegel et al. (1998) IR-based dust map assuming a Fitzpatrick (1999) extinction law with $R_V = 3.1$.

^d References for host extinction estimates: SN 2014C (Milisavljevic et al. 2015), SN 2014J (with $R_V = 1.4$, Amanullah et al. 2014), SN 2014bi (J. Johansson et al., in preparation), SN 2014dt (Foley et al. 2015), SN 2016adj (with $R_V = 2.57$, Banerjee et al. 2018), SN 2016bkv (Hosseinzadeh et al. 2018), SN 2016cok (Kochanek et al. 2017), SN 2017eaw (Kilpatrick & Foley 2018).

^e References for SN discovery: SN 2014C (Kim et al. 2014), SN 2014J (Fossey et al. 2014), SN 2014L (Zhang et al. 2014), SN 2014bc (Smartt et al. 2014), SN 2014bi (Kumar et al. 2014), SN 2014df (Monard et al. 2014), ASASSN-14ha (Kiyota et al. 2014), SN 2014dt (Nakano et al. 2014), SN 2016C (Aoki 2016), SN 2016adj (Marples et al. 2016), SN 2016bau (Arbour 2016), SN 2016bkv (Itagaki 2016), SN 2016cok (Bock et al. 2016), and SN 2017eaw (Wiggins 2017).

^f References for SN classification: SN 2014C (Kim et al. 2014; Milisavljevic et al. 2015), SN 2014J (Cao et al. 2014), SN 2014L (Li et al. 2014), SN 2014bc (Cortini et al. 2014), SN 2014bi (Kumar et al. 2014), SN 2014df (Monard et al. 2014), ASASSN-14ha (Arcavi et al. 2014), SN 2014dt (Ochner et al. 2014), SN 2016C (Sahu et al. 2016), SN 2016adj (Stritzinger et al. 2016), SN 2016bau (Granata et al. 2016), SN 2016bkv (Hosseinzadeh et al. 2016), SN 2016cok (Zhang et al. 2016), and SN 2017eaw (Cheng et al. 2017).

^g SN present in first 2014 SPIRITS epoch, and therefore excluded from the control sample.

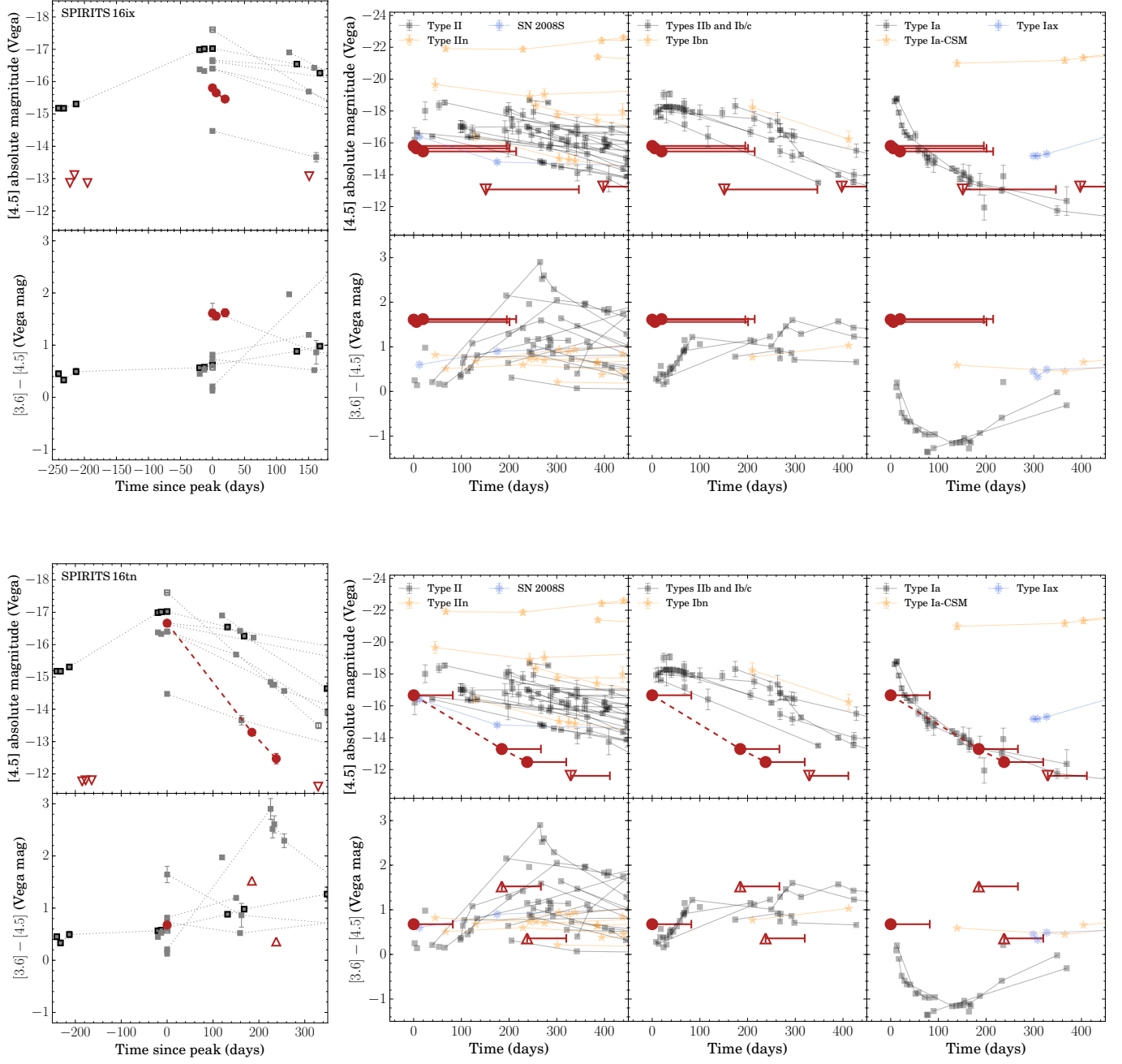


Figure 2, continued.

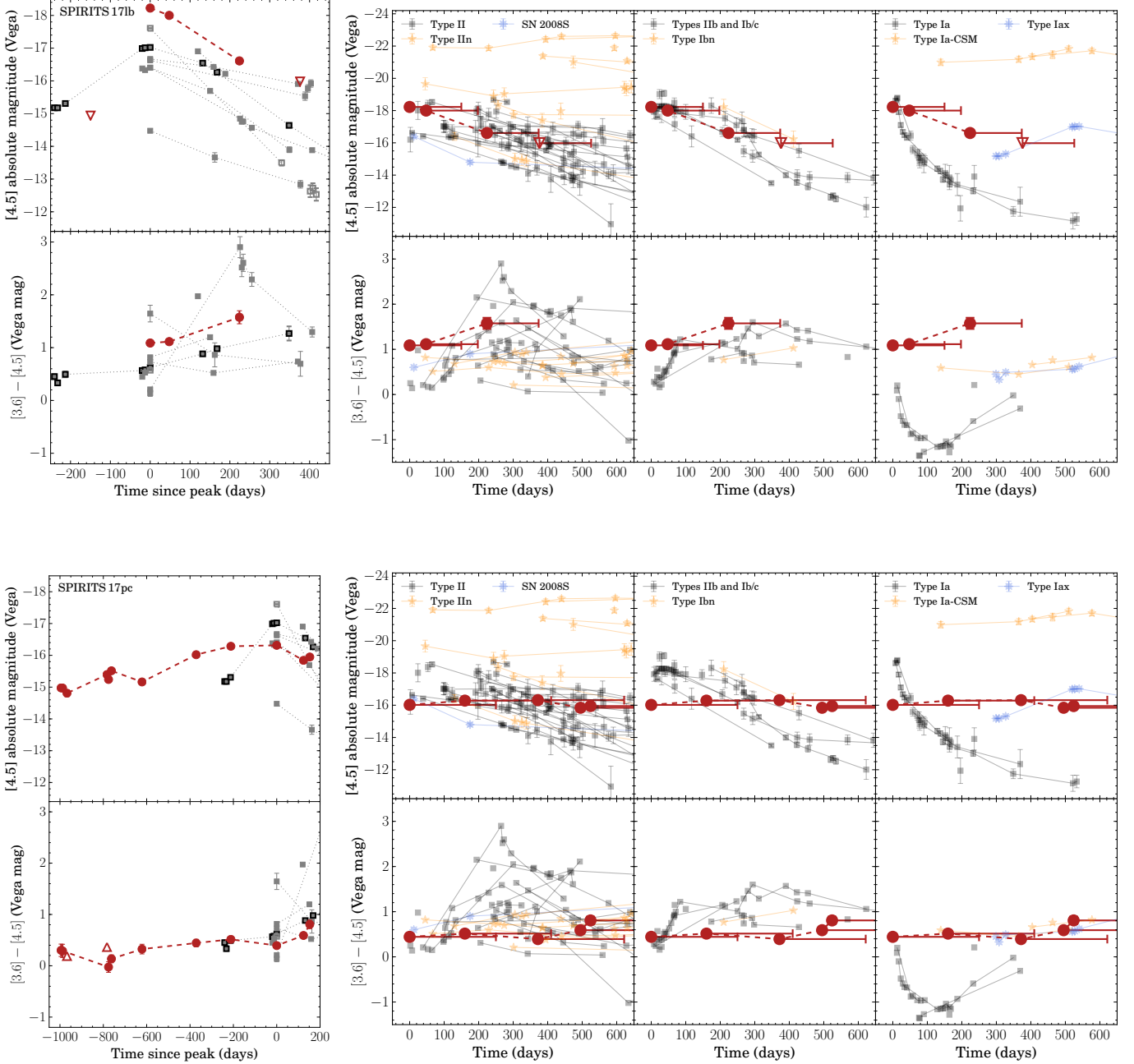


Figure 2, continued.

3. FOLLOW-UP AND SUPPLEMENTARY OBSERVATIONS

3.1. Space-based imaging

For transients that were inaccessible to ground-based observing at the time of discovery with *Spitzer*, we attempted to trigger Target of Opportunity (ToO) observations with the *Neil Gehrels Swift Observatory* UV/Optical Telescope (*Swift*/UVOT; Gehrels et al. 2004; Nousek 2004; Roming

et al. 2005) to detect an optical counterpart or obtain limits on the contemporaneous optical flux. For SPIRITS 16tn we triggered a 2000 s observation on 2016 August 29.1 split between the *U*, *B*, and *V* bands, with limits reported in (Adams et al. 2016a) and (Jencson et al. 2018c). For SPIRITS 17lb we obtained a 1200 s integration in the *V* band on 2017 June 9.4, and derive a 5σ limiting magnitude of $V > 17.7$ mag. For SPIRITS 17pc we obtained a 2000 s observation on 2017 November 9.1 split between *U*, *B*, and *V*. NGC 4388 was

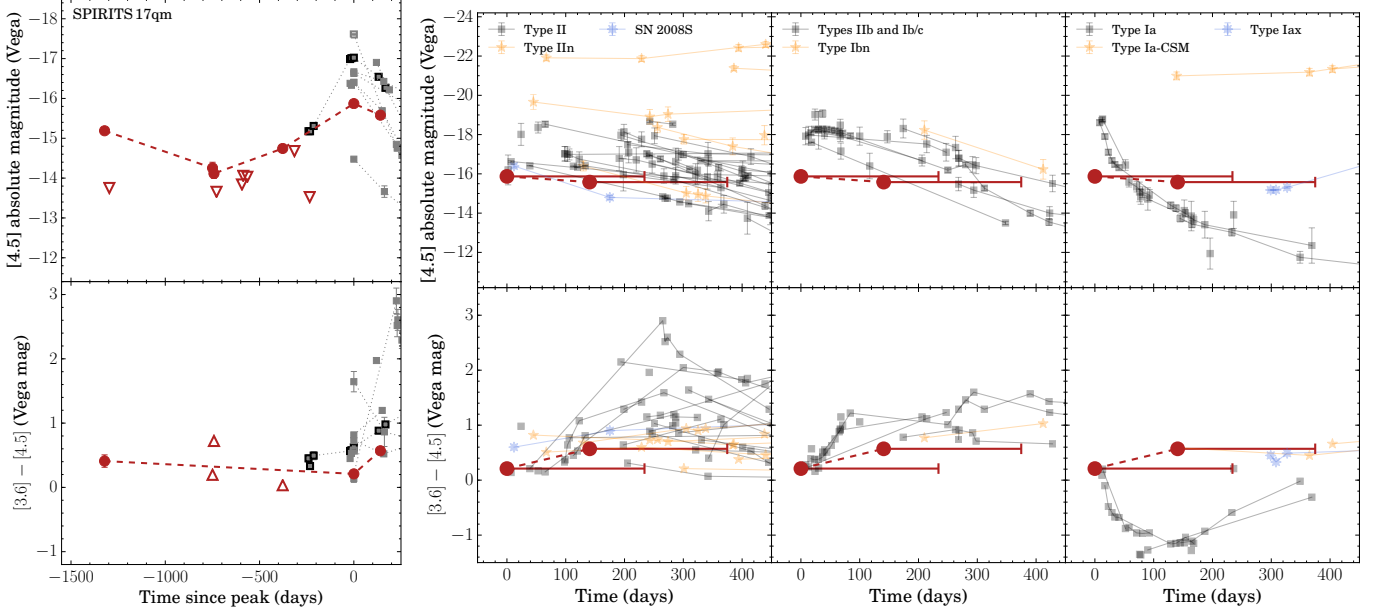


Figure 2, continued.

previously observed by *Swift*/UVOT one year prior on 2016 November 8.8, but with shorter integrations of only ≈ 60 s in each band. We find no evidence of significant variability at the location of SPIRITS 17pc between the two epochs. We derive limits for the earlier (later) epochs of $U > 18.0$ (18.8), $B > 18.2$ (18.8), and $V > 17.2$ (18.0) mag.

We also executed *Hubble Space Telescope* (*HST*) ToO observations of SPIRITS 16tn using the Wide Field Camera 3 (WFC3) in UVIS channel with the F814W filter and the IR channel with the F110W and F160W filters as part of our program to follow-up SPIRITS transients (GO-14258; PI: H. Bond) on 2016 September 25 as described in Jencson et al. (2018c).

3.2. Ground-based imaging

SPIRITS galaxies were regularly monitored from the ground in the optical and near-IR with several telescopes. For the SPIRITS transient host galaxies discussed here, sequences of optical $g'r'i'$ -band images of IC 2163, M100, NGC 4461, NGC 3556, and NGC 4388 were obtained with the CCD camera on the fully automated Palomar 60 inch telescope (P60; Cenko et al. 2006) throughout 2014–2018 and reduced by a fully automated pipeline. Where available, we used SDSS images as templates for image subtraction to remove host-galaxy background emission and obtain deeper limits on optical emission from the transients.

Similarly for SPIRITS galaxies located in the Southern Hemisphere, namely NGC 2997, IC 2163, and NGC 1365, sequences of optical gri -band images were obtained with the CCD camera on the 1-m Swope Telescope at Las Campanas

Observatory (LCO) throughout 2014–2015. Near-IR YJH -band images were also obtained throughout 2014–2015 with the RetroCam IR camera (Morgan et al. 2005) on the 2.5-m du Pont Telescope at LCO. Photometry was performed at the locations of the transients by fitting the point-spread-function (PSF) of the images, measured using stars in the field, simultaneously with the background emission, modeled using low-order polynomials.

Post-discovery, ground-based follow-up imaging in the optical and near-IR was also obtained for several SPIRITS transients. Near-IR JHK_s -band images were obtained with the Multi-object Spectrometer for Infra-red Exploration (MOS-FIRE; McLean et al. 2010, 2012) on the 10-m Keck I Telescope of the W. M. Keck Observatory on the summit of Mauna Kea, the Wide Field Infrared Camera (WIRC; Wilson et al. 2003) on the 200-inch telescope at Palomar observatory (P200), and the FourStar IR camera (Persson et al. 2013) on the Magellan Baade Telescope at LCO. Flat-fielding, background subtraction, astrometric alignment, and final stacking of images in each filter were performed using a custom pipeline.

Additional near-IR imaging was obtained with the Wide Field Camera (WFCAM; Casali et al. 2007) on the United Kingdom Infrared Telescope (UKIRT) at Mauna Kea Observatories. Simultaneous optical/near-IR $rizYJH$ were obtained with the Reionization and Transients InfraRed camera (RATIR; Butler et al. 2012) on the 1.5-m Johnson Telescope at the Mexican Observatorio Astronómico Nacional on the

Sierra San Pedro Martir in Baja California, Mexico (Watson et al. 2012).

3.3. Spectroscopy

We obtained near-IR spectroscopy of the SPIRITS obscured SN candidates at several epochs using the Folded-port InfraRed Echellette spectrograph (FIRE; Simcoe et al. 2008, 2013) on the Magellan Baade Telescope at LCO, MOSFIRE on the Keck I Telescope, the Near-Infrared Echellette Spectrometer⁴ (NIREs) on the Keck II Telescope, the Gemini Near-InfraRed Spectrograph (GNIRS; Elias et al. 2006) on the 8.1 m Gemini N Telescope (PIs GN-2016B-FT-25, GN-2017B-Q-14; PI J. Jencson), the FLAMINGOS-2 spectrograph (Eikenberry et al. 2006) on the 8.1 m Gemini S Telescope (PID GS-2017B-Q-15; PI J. Jencson). Optical spectroscopy was obtained for SPIRITS 16tn, SPIRITS 17pc, and SPIRITS 17qm with the Low Resolution Imaging Spectrometer (LRIS; Goodrich & Cohen 2003) on the Keck I telescope. Our spectroscopic observations, including the integration times used, are summarized in Table 3.

The FIRE and MOSFIRE spectra of SPIRITS 15c, and the GNIRS and LRIS spectra of SPIRITS 16tn and details of the data reduction procedures were previously published in (Jencson et al. 2017) and (Jencson et al. 2018c).

For the LRIS observations of SPIRITS 17pc and SPIRITS 17qm, we used the D560 dichroic to split the light between the red and blue sides, and we used a 1'' longslit with the 400/8500 grating on the red side and the 400/3400 grism on the blue side providing the resolution and wavelength coverage given in Table 3. Spectroscopic reductions for LRIS were performed using the analysis pipeline LPIPE⁵ developed by D. Perley. For SPIRITS 17pc, a weak trace is visible at the position of the transient on the red-side camera. For SPIRITS 17qm, there is no obvious continuum trace, however we detect several emission lines associated with the transient on the red side. No emission was detected on the blue side for either object. The 1D spectra were extracted at these positions along the slit and flux calibrated using observations of the standard stars G191-B2B and BD+75 325. Our optical spectra of SPIRITS 16tn, SPIRITS 17pc, and SPIRITS 17qm are shown in Figure 3.

For observations with the near-IR spectrographs the target was nodded along the slit between exposures to allow for accurate subtraction of the sky background. Observations of an A0V telluric standard star near the target location were also taken immediately before or after each science target observation for flux calibration and correction of the strong near-IR telluric absorption features. For MOSFIRE, we used

a 0.''7 slit with the standard grating/filter setups for each of the *YJHK* spectral regions, providing the wavelength coverage and resolution listed for each observation in Table 3. For GNIRS, we used the cross-dispersed (XD), multi-order mode providing coverage of the full near-IR spectral region at once, with a 0.''45 slit, the 32 line mm⁻¹ grating, and the short blue camera with its XD prism, providing an average spectral resolution of $R = 1200$. For, FLAMINGOS-2 we use the longslit mode and the low-resolution HK grism with a 3-pixel, 0.''54 slit providing wavelength coverage from 13500–24000 Å and an average spectral resolution of $R = 600$. NIREs employs a 0.''55 slit and provides wavelength coverage from 9500–24600 Å across 5 spectral orders at a mean resolution of $R = 2700$.

Reductions for MOSFIRE, including flat-fielding, the wavelength solution, background subtraction, and frame stacking for each object on a given night were performed with the MOSFIRE Data Reduction Pipeline. 1D extractions, where the continuum trace of the target and/or emission lines were visible in the reduced 2D spectra, were performed using standard tasks in IRAF⁶. For GNIRS and FLAMINGOS-2 reductions, including detector pattern noise cleaning and radiation event removal (GNIRS only), flat-fielding, background subtraction, spatial distortion corrections (GNIRS only), wavelength calibration, and 1D extractions, we used standard tasks in the Gemini IRAF package following procedures outlined on the Gemini webpage⁷. NIREs data were reduced, including flat-fielding, wavelength calibration, background subtraction, and 1D spectral extractions steps, using a version of the IDL-based data reduction package Spextool developed by (Botticella et al. 2009a), updated by M. Cushing specifically for NIREs. Corrections for the strong near-IR telluric absorption features and flux calibrations for spectra from all instruments were performed with the A0V standard star observations using the method developed by (Vacca et al. 2003) implemented with the IDL tools XTELLCOR or XTELLCOR_GENERAL developed by (Botticella et al. 2009a) as part of Spextool.

We did not detect any emission from the transient in the MOSFIRE spectrum of SPIRITS 15ud, the MOSFIRE 2016 April 16.6 *Y*-band and 2016 May 30.5 *H*-band spectra of SPIRITS 15ade, the MOSFIRE spectrum of SPIR-

⁶ IRAF is distributed by the National Optical Astronomy Observatory, which is operated by the Association of Universities for Research in Astronomy (AURA) under a cooperative agreement with the National Science Foundation.

⁷ Procedures for reducing GNIRS XD spectra are found at <http://www.gemini.edu/sciops/instruments/gnirs/data-format-and-reduction/reducing-xd-spectra>. Procedures for FLAMINGOS-2 are found at https://gemini-iraf-flamingos-2-cookbook.readthedocs.io/en/latest/Tutorial_Longslit.html

⁴ <https://www2.keck.hawaii.edu/inst/nires/>

⁵ Software available at <http://www.astro.caltech.edu/~dperley/programs/lpipe.html>.

Table 3. Spectroscopic observations

| Name | UT Date | MJD | Phase (days) | Tel./Instr. | Range (Å) | Resolution ($\lambda/\delta\lambda$) | Integration |
|---------------|---------------|---------|-----------------|----------------------|--------------|---|-------------------|
| SPIRITS 15c | 2015 Mar 14.1 | 57095.1 | 204.7 | Baade/FIRE | 8000–24000 | 300–500 | 4×120 s |
| | 2015 Mar 31.2 | 57112.2 | 221.8 | Keck I/MOSFIRE | 9700–11100 | 3400 | 8×180 s |
| | 2015 Mar 31.3 | 57112.3 | 221.9 | Keck I/MOSFIRE | 11400–13100 | 3300 | 6×120 s |
| | 2015 Mar 31.3 | 57112.3 | 221.9 | Keck I/MOSFIRE | 14500–17500 | 3700 | 10×120 s |
| | 2015 Mar 31.3 | 57112.3 | 221.9 | Keck I/MOSFIRE | 19500–23500 | 3600 | 6×180 s |
| | 2015 Sep 19.3 | 57284.6 | 394.2 | Keck I/MOSFIRE | 9700–11100 | 3400 | 10×180 s |
| SPIRITS 15ud | 2016 Jan 23.6 | 57410.6 | 138.9 | Keck I/MOSFIRE | 19500–23500 | 3600 | 12×180 s |
| SPIRITS 15ade | 2016 Jan 23.6 | 57410.6 | 134.1 | Keck I/MOSFIRE | 19500–23500 | 3600 | 30×180 s |
| | 2016 Apr 16.6 | 57494.6 | 218.1 | Keck I/MOSFIRE | 9700–11100 | 3400 | 2×180 s |
| | 2016 Apr 16.6 | 57494.6 | 218.1 | Keck I/MOSFIRE | 11400–13100 | 3300 | 10×120 s |
| | 2016 May 30.5 | 57538.5 | 262.0 | Keck I/MOSFIRE | 14500–17500 | 3700 | 6×120 s |
| SPIRITS 16ix | 2016 Apr 16.5 | 57494.5 | 16.6 | Keck I/MOSFIRE | 19500–23500 | 3600 | 10×180 s |
| SPIRITS 16tn | 2016 Nov 2.6 | 57694.6 | 79.5 | Keck I/LRIS | 3500–6000 | 600 | 1800 s |
| | 2016 Nov 2.6 | 57694.6 | 79.5 | Keck I/LRIS | 5500–10300 | 1000 | 2×860 s |
| | 2016 Dec 29.5 | 57751.5 | 136.4 | Gemini N/GNIRS | 8500–25000 | 1200 | 14×300 s |
| | 2017 Jan 9.6 | 57762.6 | 147.5 | Gemini N/GNIRS | 8500–25000 | 1200 | 10×300 s |
| SPIRITS 17lb | 2017 Sep 28.6 | 58024.6 | 122.9 | Keck I/MOSFIRE | 19500–23500 | 3600 | 24×180 s |
| | 2017 Nov 1.3 | 58058.3 | 156.6 | Gemini S/FLAMINGOS-2 | 13500–24000 | 600 | 24×150 s |
| | 2017 Nov 20.6 | 58077.6 | 175.9 | Keck I/MOSFIRE | 11400–13100 | 3300 | 6×120 s |
| | 2017 Nov 20.6 | 58077.6 | 175.9 | Keck I/MOSFIRE | 19500–23500 | 3600 | 8×180 s |
| SPIRITS 17pc | 2017 Nov 11.6 | 58071.6 | 192.8 | Keck I/LRIS | 3500–6000 | 600 | 1200 s |
| | 2017 Nov 11.6 | 58071.6 | 192.8 | Keck I/LRIS | 5500–10300 | 1000 | 2×560 s |
| | 2017 Nov 20.6 | 58077.6 | 198.8 | Keck I/MOSFIRE | 9700–11100 | 3400 | 6×180 s |
| | 2017 Nov 20.7 | 58077.7 | 198.9 | Keck I/MOSFIRE | 19500–23500 | 3600 | 4×180 s |
| | 2017 Dec 7.6 | 58094.6 | 215.8 | Gemini N/GNIRS | 8500–25000 | 1200 | 4×180 s |
| | 2017 Dec 8.6 | 58095.6 | 216.8 | Gemini N/GNIRS | 8500–25000 | 1200 | 8×180 s |
| | 2017 Dec 11.6 | 58098.6 | 219.8 | Gemini N/GNIRS | 8500–25000 | 1200 | 12×180 s |
| | 2018 Jan 8.5 | 58126.5 | 247.7 | Keck I/MOSFIRE | 9700–11100 | 3400 | 6×180 s |
| | 2018 Jan 8.6 | 58126.6 | 247.8 | Keck I/MOSFIRE | 11400–13100 | 3300 | 6×120 s |
| | 2018 Jan 8.6 | 58126.6 | 247.8 | Keck I/MOSFIRE | 14500–17500 | 3700 | 6×120 s |
| | 2018 Jan 8.6 | 58126.6 | 247.8 | Keck I/MOSFIRE | 19500–23500 | 3600 | 6×180 s |
| | 2018 May 4.4 | 58242.4 | 363.6 | Keck II/NIRES | 9500–24600 | 2700 | 6×300 s |
| SPIRITS 17qm | 2017 Nov 11.5 | 58071.5 | 9.3 | Keck I/LRIS | 3500–6000 | 600 | 2×1200 s |
| | 2017 Nov 11.5 | 58071.5 | 9.3 | Keck I/LRIS | 5500–10300 | 1000 | 4×560 s |
| | 2017 Nov 20.5 | 58077.5 | 15.3 | Keck I/MOSFIRE | 9700–11100 | 3400 | 14×180 s |
| | 2018 Jan 8.2 | 58126.2 | 64.0 | Keck I/MOSFIRE | 9700–11100 | 3400 | 8×180 s |
| | 2018 Jan 8.3 | 58126.3 | 64.1 | Keck I/MOSFIRE | 11400–13100 | 3300 | 12×120 s |
| | 2018 Jan 8.3 | 58126.3 | 64.1 | Keck I/MOSFIRE | 14500–17500 | 3700 | 12×120 s |
| | 2018 Jan 8.3 | 58126.3 | 64.1 | Keck I/MOSFIRE | 19500–23500 | 3600 | 10×180 s |

ITS 16ix, or the 2017 November 20.6 MOSFIRE spectra of SPIRIST 17lb. The full sequence of near-IR spectra for which we detected emission from the transient, either a continuum trace or specific emission lines, are shown in Figure 4.

3.4. Radio Observations

We obtained radio continuum imaging observations of each of our luminous IR transients, primarily using the Karl G. Jansky Very Large Array (VLA) between 2017 June and 2018 April in the C, B, and A configurations with 3.4, 11.1, and 36.4 km maximum baselines, respectively (PIDs 16B-388, 17A-365, 17B-331, 18A-418; PI J. Jencson). The bulk of our observations were carried out in 1-hour blocks in C band (6 GHz central frequency) using the full, wide-band capabilities of the upgraded VLA with 3-bit samplers offering 4 GHz bandwidth. For some objects and epochs, we split the block between multiple bands including the *S* (3 GHz central frequency, 2 GHz bandwidth with 8-bit samplers), *X* (10 GHz central frequency, 4 GHz bandwidth), and *Ku* bands (15.5 GHz central frequency, 4 GHz bandwidth). Each observing block included observations of the VLA standard calibrators 3C286 or 3C138 for calibration of the flux density scale and instrument bandpass. For complex gain calibrations, we took observations of a nearby calibrator source, cycling between the calibrator and science target at sufficient intervals for the given array configuration and observing frequency based on recommendations in the VLA observing guide⁸.

We also analyzed the 2016 February 19 observations of IC 2163 targeting the unrelated event SN 2010jp, but fortuitously covering the sites of SPIRITS 14buu, SPIRITS 15c, SPIRITS 17lb (PID 16A-101; PI C. Kilpatrick). These observations used the 8-bit sampler setup providing 2×1 GHz bandwidth tuned to the ranges 4.5–5.5 GHz and 6.9–7.9 GHz in C band, and 8.0–9.0 GHz and 10.5–11.5 GHz in X band.

The data for each observation were run through the VLA CASA calibration pipeline⁹, suitable for automated flagging and calibration of Stokes I continuum data sets. The calibrated data were carefully inspected, and additional flagging and recalibration were performed as necessary. We imaged our data using the standard CLEAN task in CASA. First-pass images of SPIRITS 17pc in NGC 4388 were limited in sensitivity due to artifacts from residual phase errors of the bright nucleus of the host, a known Seyfert 2 active galactic nucleus. We performed self-calibration of the visibility phases on the nucleus, which significantly improved the final im-

ages, reaching near the theoretical thermal noise sensitivity for our observations.

We inspected the location of the transients in each image for the presence of a coincident point source and report our flux measurements with 1σ errors, estimated as the rms noise in a relatively clean region of the image, in Table 4. In several cases, the location of the transients suffered significant contamination from extended emission from the host galaxy or nearby star-forming regions, particular in the lower-resolution C-configuration observations. For non-detections or when possible emission from the transient cannot be distinguished from background contamination, we report upper limits on the transient flux as either 5σ ($5 \times$ image rms), or the level of the contaminating flux at the location plus $2 \times$ image rms, whichever is larger.

Specifically for the 2016 February 19.1 C-band measurement of SPIRITS 15c, a source is clearly detected at the position and has faded significantly in the subsequent image on 2017 June 10.8 (taken in the same configuration with similar resolution) confirming its association with the transient. We note however, that possible residual emission from the transient in the later epoch is blended with a nearby, somewhat extended contaminating source. We adopt the flux at the transient location as an estimate of the maximum contamination for our previous measurement, and adopt this as a lower bound on the flux in Table 4. In the subsequent epochs in the larger B and A configurations, the contaminating emission appears resolved out, and the radio counterpart to SPIRITS 15c is clearly detected as a relatively isolated, fading point source.

Radio observations of SPIRITS 16tn were also obtained with the Arcminute Microkelvin Image Large Array (AMILA), which were previously reported in (Jencson et al. 2018c). Additional observations of IC 2163 containing SPIRITS 14buu, SPIRITS 15c, and SPIRITS 14buu were obtained with the Australia Telescope Compact Array (ATCA) on 2017 September 4 at 9.0 and 5.5 GHz, and we report limiting fluxes in Table 4.

3.5. Limits from wide-field optical surveys

We obtained limits on the optical emission from SPIRITS transients that were fortuitously covered by the intermediate Palomar Transient Factory (iPTF; Cao et al. 2016; Masci et al. 2017) survey during their outbursts in the *g*, *R*, and/or *i* filters. To obtain deeper constraints, we stacked limits from individual observations within 10 day windows. Constraints on the optical emission from our sample transients from iPTF are included in Figure 12.

4. ANALYSIS

4.1. Host environments and archival imaging

⁸ VLA calibration information available here: <https://science.nrao.edu/facilities/vla/docs/manuals/obsguide/calibration>

⁹ <https://science.nrao.edu/facilities/vla/data-processing/pipeline/scripted-pipeline>

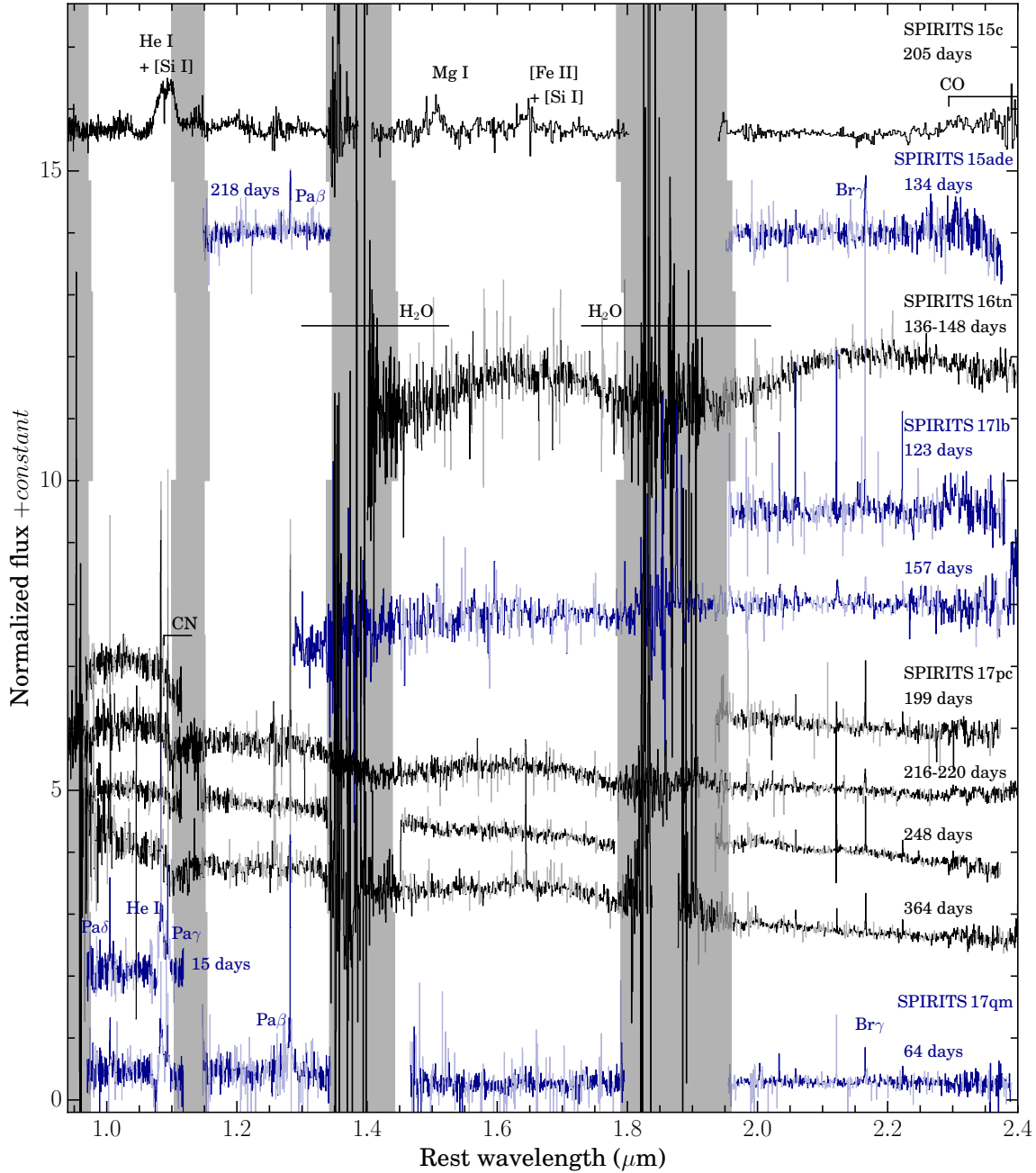


Figure 4. The full sequence of near-IR spectra obtained for the SPIRITS luminous IR transient sample. Spectra correspond to the objects and phases (measured from t_0 as in Table 4.2) listed along the right side of the figure, shown in alternating colors so spectra for separate objects may be easily distinguished. The spectra for each object are shifted to the rest frame of their respective host galaxies, and regions of low S/N due to coincidence with OH airglow emission lines are shown in lighter colors. The spectra have been scaled in flux and shifted by arbitrary constants for clarity. The major features identified in each spectrum and discussed in the text are labeled, including the SN I/Ib emission features in the spectrum of SPIRITS 15c, the $\sim 200 \text{ km s}^{-1}$ width emission lines of H I in the spectra of SPIRITS 15ade, the possible broad H_2O absorption features in the spectrum of SPIRITS 16tn, the broader $\sim 2000 \text{ km s}^{-1}$ features of H I and He I in the spectrum of SPIRITS 17qm, and the $\text{CO } \delta\nu = 2$ vibrational transition band heads detected in the spectra of SPIRITS 15c, SPIRITS 17lb, and SPIRITS 17pc.

Table 4. Radio observations of SPIRITS obscured SN candidates

| Name | UT Date | MJD | Phase (days) | Inst. | Max. Baseline (km) | Frequency (GHz) | Flux (mJy) | Luminosity (erg s ⁻¹ Hz ⁻¹) |
|---------------|---------------|---------|-----------------|--------|-----------------------|--------------------|--|---|
| SPIRITS 14buu | 2016 Feb 19.1 | 57437.1 | 786.8 | VLA | 3.4 | 10.0 | < 0.04 | < 6.0 × 10 ²⁵ |
| | 2016 Feb 19.1 | 57437.1 | 786.8 | VLA | 3.4 | 6.0 | < 0.13 | < 2.0 × 10 ²⁶ |
| | 2017 Jun 10.8 | 57914.8 | 1264.5 | VLA | 3.4 | 6.0 | < 0.12 | < 1.8 × 10 ²⁶ |
| | 2018 Jan 6.2 | 58124.2 | 1473.9 | VLA | 11.1 | 6.0 | < 0.039 | < 5.9 × 10 ²⁵ |
| | 2018 May 9.0 | 58247.0 | 1596.7 | VLA | 36.4 | 6.0 | < 0.035 | < 5.3 × 10 ²⁵ |
| | 2018 May 9.0 | 58247.0 | 1596.7 | VLA | 36.4 | 6.0 | < 0.055 | < 8.3 × 10 ²⁵ |
| SPIRITS 14azy | 2017 Jun 12.9 | 57916.9 | 1144.9 | VLA | 3.4 | 6.0 | < 0.075 | < 1.3 × 10 ²⁵ |
| SPIRITS 15c | 2016 Feb 19.1 | 57437.1 | 546.7 | VLA | 3.4 | 10.0 | 0.12 ± 0.01 | 1.8 × 10 ²⁶ |
| | 2016 Feb 19.1 | 57437.1 | 546.7 | VLA | 3.4 | 6.0 | 0.23 ^{+0.01} _{-0.09} | 3.5 × 10 ²⁶ |
| | 2017 Jun 10.8 | 57914.8 | 1024.4 | VLA | 3.4 | 6.0 | < 0.11 | < 1.7 × 10 ²⁶ |
| | 2017 Sept. 4 | 58000 | 1110 | ATCA | 3.0 | 9.0 | < 1.7 | 2.6 × 10 ²⁷ |
| | 2017 Sept. 4 | 58000 | 1110 | ATCA | 3.0 | 5.5 | < 7.6 | 1.1 × 10 ²⁸ |
| | 2018 Jan 6.2 | 58124.2 | 1233.8 | VLA | 11.1 | 6.0 | 0.055 ± 0.007 | 8.3 × 10 ²⁵ |
| | 2018 May 9.0 | 58247.0 | 1356.6 | VLA | 36.4 | 6.0 | 0.051 ± 0.008 | 7.7 × 10 ²⁵ |
| | 2018 May 9.0 | 58247.0 | 1356.6 | VLA | 36.4 | 3.0 | 0.082 ± 0.014 | 1.2 × 10 ²⁶ |
| SPIRITS 15ud | 2017 Jun 14.1 | 57918.1 | 646.4 | VLA | 3.4 | 6.0 | < 1.1 | < 2.5 × 10 ²⁶ |
| SPIRITS 15ade | 2017 Jun 16.0 | 57920.0 | 643.5 | VLA | 3.4 | 6.0 | < 0.045 | < 3.1 × 10 ²⁵ |
| SPIRITS 16ix | 2017 Jun 16.0 | 57920.0 | 442.1 | VLA | 3.4 | 6.0 | < 0.025 | < 1.2 × 10 ²⁵ |
| SPIRITS 16tn | 2016 Sep 3 | 57634 | 19 | AMI-LA | 0.11 | 15.0 | < 0.3 | < 2.8 × 10 ²⁵ |
| | 2016 Sep 4.0 | 57635.0 | 20.0 | VLA | 11.1 | 10.0 | < 0.047 | < 4.4 × 10 ²⁴ |
| | 2016 Sep 4.0 | 57635.0 | 20.0 | VLA | 11.1 | 6.0 | < 0.075 | < 7.0 × 10 ²⁴ |
| | 2016 Sep 4.0 | 57635.0 | 20.0 | VLA | 11.1 | 3.0 | < 0.10 | < 9.3 × 10 ²⁴ |
| | 2017 Jan 12.4 | 57765.4 | 150.4 | VLA | 36.4 | 15.5 | < 0.029 | < 2.7 × 10 ²⁴ |
| | 2017 Jan 12.4 | 57765.4 | 150.4 | VLA | 36.4 | 6.0 | < 0.029 | < 2.7 × 10 ²⁴ |
| | 2018 Jan 23.6 | 58141.6 | 526.6 | VLA | 11.1 | 15.5 | < 0.030 | < 2.8 × 10 ²⁴ |
| | 2018 Jan 23.6 | 58141.6 | 526.6 | VLA | 11.1 | 6.0 | < 0.030 | < 2.8 × 10 ²⁴ |
| SPIRITS 17lb | 2017 Jun 10.8 | 57914.8 | 13.1 | VLA | 3.4 | 6.0 | < 0.25 | < 3.8 × 10 ²⁶ |
| | 2017 Sep 4 | 58000 | 99 | ATCA | 3.0 | 9.0 | < 1.7 | < 2.6 × 10 ²⁷ |
| | 2017 Sep 4 | 58000 | 99 | ATCA | 3.0 | 5.5 | < 6.5 | < 9.8 × 10 ²⁷ |
| | 2018 Jan 6.2 | 58124.2 | 222.5 | VLA | 11.1 | 6.0 | 0.059 ± 0.006 | 8.9 × 10 ²⁵ |
| | 2018 May 9.0 | 58247.0 | 345.3 | VLA | 36.4 | 6.0 | 0.039 ± 0.009 | 5.9 × 10 ²⁵ |
| | 2018 May 9.0 | 58247.0 | 345.3 | VLA | 36.4 | 3.0 | 0.067 ± 0.013 | 1.0 × 10 ²⁶ |
| SPIRITS 17pc | 2017 Oct 30.5 | 58056.5 | 177.7 | VLA | 11.1 | 6.0 | < 0.090 | > 3.6 × 10 ²⁵ |
| | 2018 Jan 21.7 | 58139.7 | 260.9 | VLA | 11.1 | 6.0 | < 0.13 | > 5.2 × 10 ²⁵ |
| | 2018 Apr 14.2 | 58222.1 | 343.3 | VLA | 36.4 | 6.0 | < 0.025 | > 9.9 × 10 ²⁴ |
| SPIRITS 17qm | 2017 Nov 23.3 | 58080.3 | 18.1 | VLA | 11.1 | 6.0 | < 0.05 | > 2.0 × 10 ²⁵ |
| | 2018 Apr 16.8 | 58224.8 | 162.6 | VLA | 36.4 | 6.0 | < 0.025 | > 1.0 × 10 ²⁵ |

The host galaxy morphological types (obtained from NED) of our sample of IR-selected transients are given in Table 1. With the exception of SPIRITS 16ix in the lenticular SB0⁺ galaxy NGC 4461, these events were found in late-type, star-forming galaxies. Similarly, the entire control sample of optically discovered SNe was also found in star-forming galaxies (Table 2). In Figure 5, we indicate the locations of the IR-selected transients in the Digitized Sky Survey (DSS) *R*-band images of their host galaxies, showing a clear trend of positional associations with the active star-forming regions of the hosts' spiral arms. This indicates a likely physical association of the bulk of the sample to ongoing star formation and young, massive stars. Of particular note, SPIRITS 15ade was discovered in the outskirts of NGC 5921 at a projected distance from the galaxy center of 146.''3 (17.0 kpc), while SPIRITS 15ud was found very near the nucleus of M100 at a projected distance of only 7.''5 (0.5 kpc).

We examined the location of each source in the IR-selected sample in the archival *Spitzer*/IRAC [3.6] and [4.5] reference images for the presence of possible IR progenitor stars. The regions near the objects in our sample were typically crowded by several sources or dominated by the bright, spatially variable background emission from the host galaxy. To identify possible progenitors, we constructed source catalogs and performed PSF photometry for each *Spitzer*/IRAC reference image using the DAOPHOT/ALLSTAR package (Stetson 1987), where a model of the PSF was constructed using isolated stars in the image. The PSF-fitting and photometry procedure, including corrections for the finite radius of the PSF (using the method of Khan 2017), will be described in Karambelkar et al. (in preparation).

With the exception of SPIRITS 17qm, there are no sources in our catalogs consistent with the transient positions in *Spitzer*/IRAC reference images. We estimate upper limits on the progenitor flux as 5 times the standard deviation in a 25×25 pixel box at the transient position. The limits at [3.6] and [4.5] on the progenitor flux of each object in our sample are given in Table 5.

For SPIRITS 17qm, we identified a source in the [3.6] and [4.5] reference image PSF catalogs of NGC 1365, separated from the location of the transient by only 0.''12 and 0.''24, respectively, less than one IRAC mosaicked pixel. However, we note that this source is heavily blended with several other sources in our catalogs, and its centroid is slightly offset from the optical progenitor star identified in archival *HST* imaging below. While the coincident IR PSF-catalog sources likely contain flux from the progenitor, we consider the PSF-magnitudes given in Table 5 as upper-limits given the possibility of significant contamination from nearby sources.

We also examined the available archival *Hubble Space Telescope* (*HST*) imaging for each source in our sample. To determine the precise locations of our transients in the

archival *HST* frames, we registered the archival images with a detection image of the transient, usually a *Spitzer*/IRAC image where the transient is strongly detected. We used higher resolution images of the active transients where they were available and where registration with *Spitzer* frames was insufficient to determine a precise location of the transient. To preform the registrations, we used centroid measurements of several (at least 10), relatively isolated, bright stars detected in both frames. We then determined the geometric transformations from the archival *HST* frame to the frame containing the transient using the Space Telescope Science Data Analysis System (STSDAS)¹⁰ GEOMAP task. By applying the GEOTRAN task to the archival frames and blinking this transformed images against the transient detection images, we verified the quality of the registrations. We then examined the precise location of each transient in the available archival frames to search for the presence of a possible progenitor star.

For SPIRITS 15c and SPIRITS 16tn, we discussed the limits we obtained on their progenitors from this procedure in Jencson et al. (2017) and Jencson et al. (2018c). We obtained precise registrations of the *HST*/WFPC2 F555W and F814W images taken 1998 November 11.7 with program GO-6483 (PI: D. Elmegreen) using a Baade/IMACS WB6226-7171 image of the SPIRITS 15c from 2015 January 20.0. We derived 5σ limiting magnitudes on the progenitor of $V > 25.1$ and $I > 24.0$ mag, corresponding to limits on the absolute magnitude of the progenitor of $M_V > 7.9$ and $M_I > 8.9$ mag, correcting for Galactic extinction to IC 2163 only. We constrained the flux from the progenitor of SPIRITS 16tn to $V \gtrsim 24.5$ mag in an archival WFPC2/WFC F606W frame from 1994 July 4.8 (PID SNAP-5446; PI: G. Illingworth), corresponding to limits on the absolute magnitude of $M_V > -5.2$ mag (correcting for Galactic extinction only; $L < 2.9 \times 10^4$ for a red supergiant [RSG] progenitor of spectral type M0), however the limit is not constraining for an SN II progenitor if one assumes heavy extinction of $A_V \sim 8$ mag as was inferred for SPIRITS 16tn in Jencson et al. (2018c) based on the optical/near-IR SED of the transient.

The location of SPIRITS 14azy was imaged with WFC3/UVIS in the F336W filter on 2010 October 28.8 with program SNAP-12229 (PI L. Smith), nearly four years before the discovery of the transient, which we registered with the *Spitzer*/IRAC [4.5] discovery image of the transient. The rms uncertainty in the registration is 0.9 WFC3 pixels (0.''036) in both the *x* and *y* directions. As shown in Figure 6, the location is within an apparent dust lane, completely devoid of stars consistent with the transient position. The limiting

¹⁰ STSDAS is a product of STScI, which is operated by AURA for NASA.

Table 5. Archival imaging progenitor constraints

| Name | UT Date | Tel./Inst. | Program/PI | Band | Vega Mag. (mag) | Abs. Mag. ^a (mag) |
|---------------|-------------------------------|-----------------------|--------------------------|-------|--------------------|---------------------------------|
| SPIRITS 14azy | 2004 Dec 16.7 | <i>Spitzer</i> /IRAC | PID 3333/M. Barlow | [3.6] | > 16.7 | > -13.8 |
| | 2004 Dec 16.7 | <i>Spitzer</i> /IRAC | PID 3333/M. Barlow | [4.5] | > 16.5 | > -14.0 |
| | 2010 Oct 28.8 | <i>HST</i> /WFC3 UVIS | SNAP-12229/L. Smith | F336W | > 25.5 | > -5.4 |
| SPIRITS 15c | 2005 Feb 22.7 | <i>Spitzer</i> /IRAC | Super Mosaic | [3.6] | > 15.5 | > -17.3 |
| | 2005 Feb 22.7 | <i>Spitzer</i> /IRAC | Super Mosaic | [4.5] | > 15.5 | > -17.3 |
| | 1998 Nov 11.7 | <i>HST</i> /WFPC2 WFC | GO-6483/D. Elmegreen | F555W | > 25.1 | > -7.9 |
| | 1998 Nov 11.7 | <i>HST</i> /WFPC2 WFC | GO-6483/D. Elmegreen | F814W | > 24.0 | > -8.9 |
| SPIRITS 15ud | 2004 May 27.5 – 2008 Jul 15.7 | <i>Spitzer</i> /IRAC | Super Mosaic | [3.6] | > 12.8 | > -17.9 |
| | 2004 May 27.5 – 2008 Jul 15.7 | <i>Spitzer</i> /IRAC | Super Mosaic | [4.5] | > 12.7 | > -18.0 |
| | 2001 Nov 12.1 | <i>HST</i> /WFC3 UVIS | GO-11646/A. Crotts | F775W | > 24.5 | > -6.3 |
| | 2005 May 31.0 | <i>HST</i> /ACS HRC | GO-9776/D. Richstone | F814W | > 24.4 | > -6.4 |
| SPIRITS 15ade | 2009 Aug 29.4 | <i>Spitzer</i> /IRAC | S4G/K. Sheth | [3.6] | > 19.7 | > -12.2 |
| | 2009 Aug 29.4 | <i>Spitzer</i> /IRAC | S4G/K. Sheth | [4.5] | > 19.1 | > -12.8 |
| SPIRITS 16ix | 2010 Aug 3.5 | <i>Spitzer</i> /IRAC | S4G/K. Sheth | [3.6] | > 16.3 | > -15.2 |
| | 2010 Aug 3.5 | <i>Spitzer</i> /IRAC | S4G/K. Sheth | [4.5] | > 16.3 | > -15.2 |
| SPIRITS 16tn | 2011 Feb 7.6 | <i>Spitzer</i> /IRAC | S4G/K. Sheth | [3.6] | > 15.0 | > -14.7 |
| | 2011 Feb 7.6 | <i>Spitzer</i> /IRAC | S4G/K. Sheth | [4.5] | > 14.8 | > -14.9 |
| | 1994 Jul 4.8 | <i>HST</i> /WFPC2 WFC | SNAP-5446/G. Illingworth | F606W | > 24.5 | > -5.2 |
| SPIRITS 17lb | 2005 Feb 22.7 | <i>Spitzer</i> /IRAC | Super Mosaic | [3.6] | > 14.9 | > -17.9 |
| | 2005 Feb 22.7 | <i>Spitzer</i> /IRAC | Super Mosaic | [4.5] | > 14.8 | > -18.0 |
| | 2012 Dec 4.5 | <i>HST</i> /WFC3 UVIS | SNAP-13029/A. Filippenko | F625W | > 26.8 | > -9.4 |
| | 2012 Dec 4.5 | <i>HST</i> /WFC3 UVIS | SNAP-13029/A. Filippenko | F814W | > 26.2 | > -8.9 |
| SPIRITS 17pc | 2004 May 27.6 - 2008 Jul 17.7 | <i>Spitzer</i> /IRAC | Super Mosaic | [3.6] | > 14.6 | > -16.7 |
| | 2004 May 27.6 - 2008 Jul 17.7 | <i>Spitzer</i> /IRAC | Super Mosaic | [4.5] | > 14.4 | > -16.9 |
| | 2011 Jun 8.3 | <i>HST</i> /WFC3 UVIS | GO-12185/J. Greene | F336W | > 26.06 | > -5.4 |
| | 2011 Jun 8.4 | <i>HST</i> /WFC3 UVIS | GO-12185/J. Greene | F438W | > 26.2 | > -5.2 |
| | 2011 Jun 8.4 | <i>HST</i> /WFC3 UVIS | GO-12185/J. Greene | F814W | 24.21 ± 0.05 | -7.1 |
| | 2011 Jun 8.2 | <i>HST</i> /WFC3 IR | GO-12185/J. Greene | F110W | 21.76 ± 0.04 | -9.6 |
| | 2011 Jun 8.2 | <i>HST</i> /WFC3 IR | GO-12185/J. Greene | F160W | 20.60 ± 0.02 | -10.7 |
| SPIRITS 17qm | 2004 Dec 16.4 | <i>Spitzer</i> /IRAC | Super Mosaic | [3.6] | > 15.3 | > -16.0 |
| | 2004 Dec 16.4 | <i>Spitzer</i> /IRAC | Super Mosaic | [4.5] | > 14.9 | > -16.5 |
| | 2001 Mar 8.3 | <i>HST</i> /WFPC2 PC | SNAP-8597/M. Regan | F606W | 22.45 | -9.3 |
| | 2001 Jun 9.1 | <i>HST</i> /WFPC2 WFC | SNAP-8597/M. Regan | F606W | 20.77 | -11.0 |

^aCorrected for Galactic extinction only.

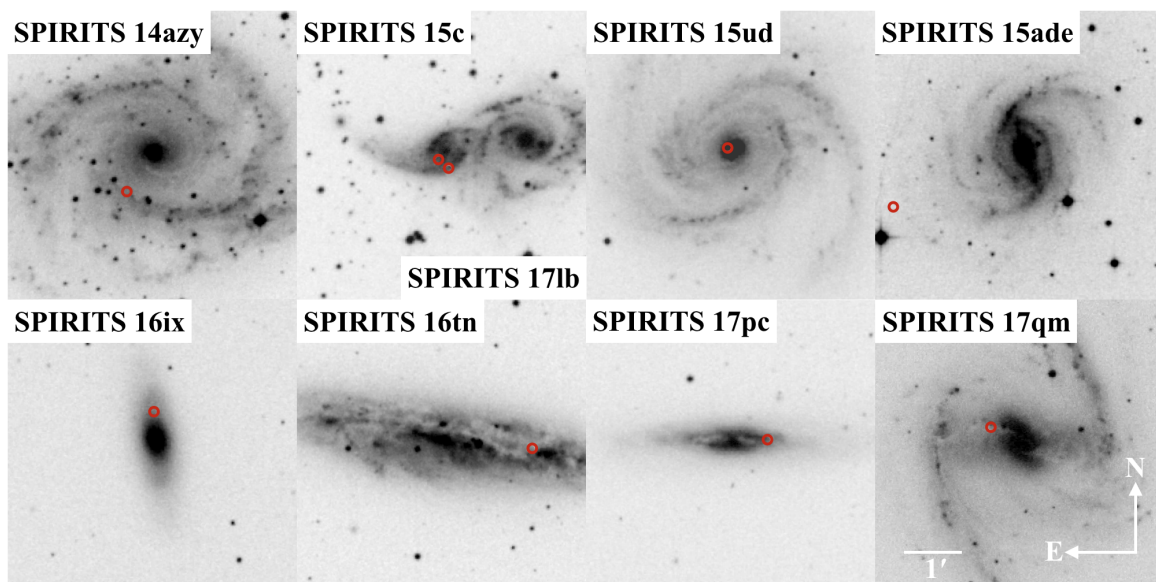


Figure 5. We show the DSS *R*-band images of the host galaxies of the IR-selected sample of SPIRITS transients. The location of the transient(s) in each panel is indicated by the red circle. The orientation and scale is the same in each panel as indicated in the bottom rightmost panel.

magnitude in the image is $U \gtrsim 25.5$ mag (Vega), which we adopt as a limit on the progenitor flux, corresponding to a limit on the absolute magnitude of the progenitor star of $M_U \gtrsim -5.4$ mag (Galactic extinction correction only).

SPIRITS 15ud is located near the nucleus of M101 and was covered in several bands at several epochs with *HST*/WFPC2 and WFC3. We selected the WFC3/UVIS F775W image from 2001 Nov. 12.1 (PID GO-11646; PI A. Crots) for registration with the *Spitzer*/IRAC [4.5] discovery image, for which we obtained an rms uncertainty on the position of the transient of 0.84 WFC3 pixels ($0''.034$). The transient is located in a prominent, nearly opaque dust lane (see Figure 6), and we detect no source consistent with the transient position to a limiting depth of $I \gtrsim 24.5$ mag ($M_I \gtrsim -6.3$ mag; Galactic extinction only). We also examined this position in the ACS/HRC F814W frame from 2005 May 31.0 (PID GO-9776; PI D. Richstone), deriving a limit on the flux from the progenitor of $I \gtrsim 24.4$ mag ($M_I \gtrsim -6.4$ mag).

SPIRITS 17lb is located near the edge of the Southern spiral arm of IC 2163, with possible extinction by the foreground spiral arm of the companion galaxy NGC 2207. This location was covered in WFC3/UVIS F625W and F814W images taken on 2012 December 4.5 (PID SNAP-13029; PI A. Filippenko). We selected the F814W image for registration with the *Spitzer*/IRAC [4.5] discovery image, for which we obtained an rms uncertainty of 0.94 WFC3 pixels ($0''.038$). The transient location is coincident with a patch of unresolved, diffuse starlight, characterized by variable extinction in the vicinity. The limits on the progenitor flux from these images are $I \gtrsim 26.2$ and $R \gtrsim 26.8$, corresponding to limits in absolute magnitude of $M_I \gtrsim -8.9$ mag and $M_R \gtrsim -9.4$ mag.

We reported on the analysis of the WFC3/UVIS and IR frames covering the site of SPIRITS 17pc and SPIRITS 17qm in Jencson et al. (2018a) and Jencson et al. (2018b), respectively. The site of SPIRITS 17pc was covered in WFC3/UVIS and IR F336W, F438W, F814W, F110W, and F160W images taken on 2011 June 8 (PID GO-12185; PI J. Greene). We registered the F110W frame with a high-resolution, *J*-band image taken with the Keck II/NIRC2 adaptive optical image of the active transient from 2017 December 8.6, obtaining a registration rms uncertainty of 0.15 WFC3 pixels (0.02 arcsec). There are several blended sources near the location of SPIRITS 17pc in the WFC3 frames. We analyzed the sources near the location using PSF-fitting photometry with DOLPHOT (Dolphin 2000, 2016). We identify a source consistent with the precise transient position and rated as a “good star” by DOLPHOT in the F814W, F110W, F160W images. There is coincident emission in the F336W and F438W frames, but it not point-like and is blended with nearby objects. Our PSF-photometry from DOLPHOT on the candidate progenitor gives

$F336W > 26.06$, $F438W > 26.18$, $F814W = 24.21 \pm 0.05$, $F110W = 21.76 \pm 0.04$, and $F160W = 20.60 \pm 0.02$ mag. At the distance to NGC 4388, the photometry can be well fit by a single blackbody component of $T = 1900 \pm 100$ K and $L = 2.1^{+0.4}_{-0.3} \times 10^5 L_\odot$.

There are two epochs of WFPC2 F606W images taken on 2001 March 8.3 and 2001 June 9.1 (PIDs SNAP-8597; PI M. Regan) covering the site of SPIRITS 17qm. We registered the first WFPC2 image with the *Spitzer*/IRAC [3.6] discovery image and obtained an rms uncertainty of 3.0 WFPC2 pixels (0.3 arcsec). As shown in Figure 6, there is a single, isolated point source consistent with the location of SPIRITS 17qm in both WFPC2 frames. We obtained magnitudes from the Hubble Legacy Archive source catalogs of $V = 22.45$ mag (2001 March 8) and $V = 20.77$ mag (2001 June 9), indicating the source is highly variable and brightened by ≈ 1.7 mag during the 3 months between the two epochs. The absolute magnitudes then are $V \approx -9.3$ and -11.0 mag for each epoch, respectively, indicating the star is highly luminous. While the localization of SPIRITS 17qm in the WFPC2 frames is coarse, the marked variability of the coincident star strongly suggests a physical association.

There is no archival *HST* imaging available for the sites of SPIRITS 15ade in NGC 5921 or SPIRITS 16ix in NGC 4461.

4.2. *Spitzer* light curves

The [4.5] light curves and [3.6]–[4.5] color curves of the IR selected obscured SN candidate sample are shown in Figure 2. In the left panel for each object, we compare to those of the optically discovered control sample. We define zero phase in a uniform way for each object across both samples as the time of peak brightness in the *Spitzer*/IRAC bands. For SN 2017eaw, we adopt 2017 September 13.6 as the observed time of peak brightness, however, the SN was saturated in the images taken on this date and we do not have a reliable flux measurement of the peak.

The [4.5] light curves of the IR selected sample appear broadly similar to those of the control sample, usually showing a luminous initial peak and subsequent fade over a timescale of ≈ 200 –600 days. SPIRITS 17pc and SPIRITS 17qm represent notable exceptions as both sources underwent previous luminous IR outbursts, up to nearly 1500 days before the observed peak in the case of SPIRITS 17qm. While both sources have begun to decline in IR brightness since their discovery, we will continue to monitor their IR with *Spitzer* throughout Cycle 14 (2019).

The [3.6]–[4.5] color curves are also qualitatively similar between the two samples. Most objects are found with red colors between $0 \lesssim [3.6] - [4.5] \lesssim 1$ mag throughout their evolution, with a few events achieving even redder colors of $\gtrsim 1$ –3 mag. The reddest object we observe is SPIRITS 15c with $[3.6] - [4.5] = 3.0 \pm 0.2$ mag at the time of the

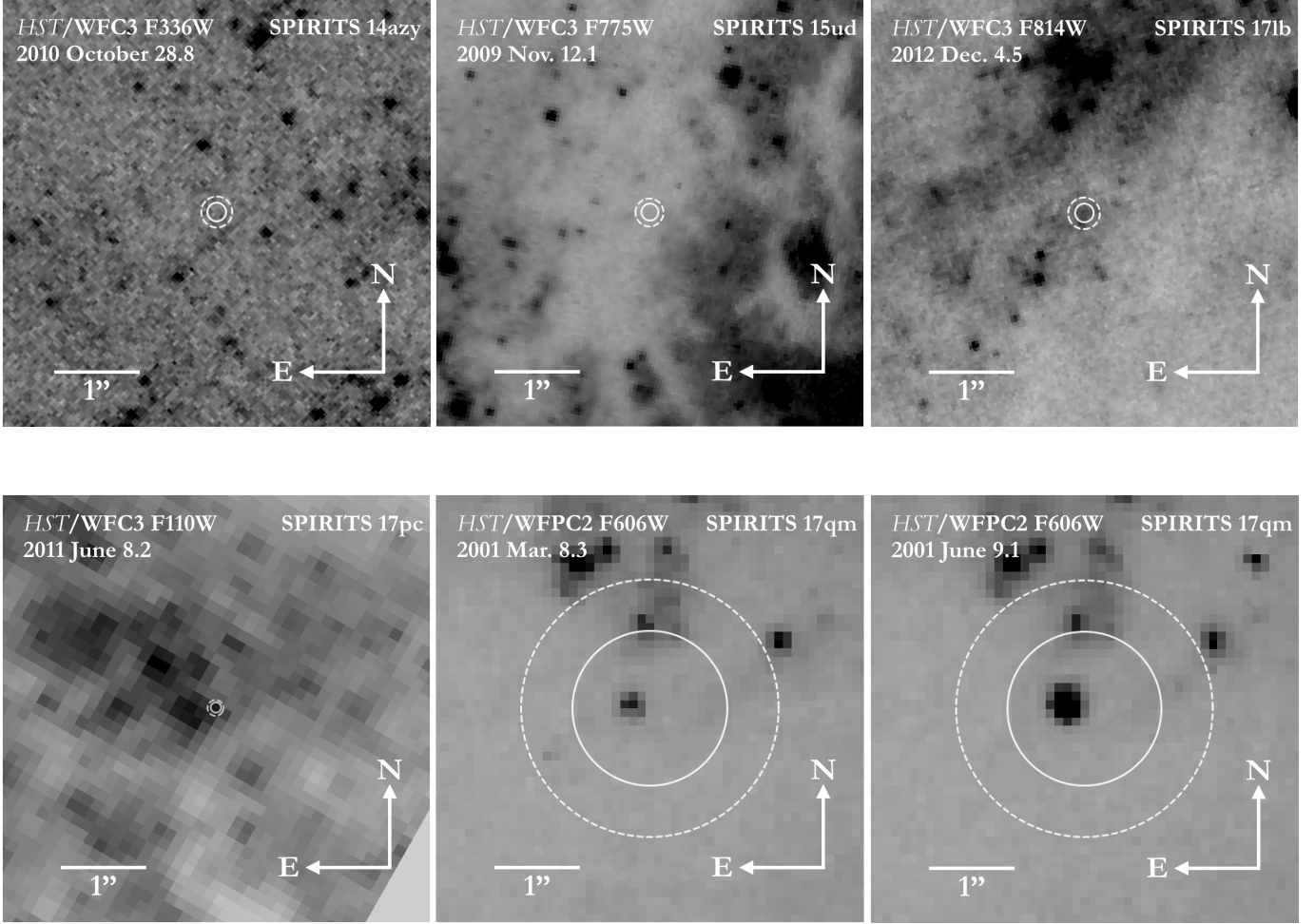


Figure 6. Archival *HST* images of the locations, from left to right, of SPIRITS 14azy, SPIRITS 15ud, and SPIRITS 17lb (top row), and SPIRITS 17pc and the two epochs covering SPIRITS 17qm (bottom row). The portion of each image shown is a $5'' \times 5''$ box, oriented with North up and East to the left. The 3σ (5σ) error circles on the locations of the transients in each image are shown as the solid (dashed), white circles. Each image is labeled with the instrument/filter combination used, and the date of the observation.

observed IR peak, rivaled by SN 2014bi with $[3.6] - [4.5] = 2.9 \pm 0.2$ mag at 225.5 days post peak.

We can make a more quantitative comparison between the IR-selected and optically-selected control samples based on properties derived from the $[3.6]$ and $[4.5]$ light curves. In Figure 7, we show histograms for both samples in their the peak absolute magnitudes at $[4.5]$, $M_{[4.5],\text{peak}}$, their $[3.6] - [4.5]$ colors at peak, and the characteristic fade timescales of their $[4.5]$ light curve, $t_{\text{fade},[4.5]}$, defined as the time in days for the light curve to decline by 1 mag from a linear (in magnitudes) fit to the post-peak light curve.

Both samples span a range in peak $[4.5]$ luminosity, $M_{[4.5],\text{peak}}$, between -14 and -18.5 . The distributions in $M_{[4.5],\text{peak}}$ appear similar, with both peaking between ≈ -16.3 and -17.4 . We note that there is a larger fraction of low-luminosity events in the IR selected sample, i.e., 3 of 9

objects ($\approx 33\%$) have $M_{[4.5],\text{peak}}$ fainter than -16 , while there is only 1 such object of 8 ($\approx 13\%$) in the control sample. In $[3.6] - [4.5]$ color at peak, the two samples again show similar distributions that peak in the range $0.0 \lesssim [3.6] - [4.5] \lesssim 0.9$ with one-sided tails extending to redder colors. Finally, in the distributions of $t_{\text{fade},[4.5]}$, we once again note the broad similarity between the two samples. The distributions extend between ≈ 50 and 500 days, with peaks between ≈ 130 and 250 days. Notably though, the two most rapidly fading events in either sample are SPIRITS 16ix and SPIRITS 16tn, both from the IR discovered sample, with $t_{\text{fade},[4.5]} = 55$ days for both, while the next fastest events are SPIRITS 15c and SN 2016bau (Type Ib) with $t_{\text{fade},[4.5]} \approx 80$ days.

We performed Kolmogorov-Smirnov tests between the two samples in each of the light curve derived parameters discussed above. For the distributions in $M_{[4.5],\text{peak}}$, $[3.6] - [4.5]$

color at peak, and $t_{\text{fade},[4.5]}$, the tests return p-values of 0.31, 0.91, 0.97, respectively. Thus, we are unable to reject the null hypotheses that the IR-selected and optically-discovered samples are drawn from the same parent distribution in all three parameters. The overall similarity of the two samples in their IR properties supports the suggestion that the IR-selected objects presented in this work may represent a population of SNe that were systematically missed by optical transient searches.

4.2.1. Comparison to Spitzer SNe

In the right panel for each object in Figure 2, we compare the SPIRITS transients to the entire sample of SNe yet detected by *Spitzer*/IRAC. A large compilation including every available *Spitzer*/IRAC detection of known SNe through 2014 was recently presented by Szalai et al. (2018), including the previously published compilations of Szalai & Vinkó (2013), Tinyanont et al. (2016), and Johansson et al. (2017), detections of individual SNe originally reported by several authors, and new, previously unpublished detections. To this, we add new detections since 2014 of the optically discovered SNe in our control sample.

We divide this large comparison sample by subtype into hydrogen-rich SNe II (and interacting SNe IIn), stripped-envelope SNe I Ib and SNe Ib/c (and interacting SNe Ibn), and thermonuclear SNe Ia (and interacting SNe Ia-CSM) to demonstrate the diagnostic utility of IR light curves.

In the IR, as found by Johansson et al. (2017), SNe Ia are clearly separated from CCSNe by their rapidly declining [4.5] light curves, and evolution to blue [3.6]–[4.5] colors for the first 200 days. The IR emission of SNe Ia is powered by the tail of the hot thermal component of the SN peaking in the optical, and Johansson et al. (2017) placed stringent limits on the presence of dust within $\lesssim 10^{17}$ cm of $M_{\text{dust}} \lesssim 10^{-5} M_{\odot}$ for the Types Ia SN 2014J, SN 2006X, and SN 2007le. Characterized by strong interaction with a dense circumstellar medium (CSM), SNe Ia-CSM may display redder colors from $0.0 \lesssim [3.6] - [4.5] \lesssim 1.0$ mag, and show a clear IR excess over a normal SN Ia in their [4.5] light curves. Similarly, the unusual, dusty Type Iax SN 2014dt showed redder colors and developed a clear dust excess at [4.5] peaking at ≈ 500 days. With the exception of the ongoing outburst SPIRITS 17pc that shows an initial rise, all of the SPIRITS transients are characterized by declining [4.5] light curves and red IR colors throughout their evolution, inconsistent with the characteristic evolution of SNe Ia and largely dissimilar to the thermonuclear SN subtypes of SNe Ia-CSM and SNe Iax that have been now been characterized by *Spitzer*.

CCSNe, on the other hand, are characterized by more slowly declining IR light curves and redder IR colors with $0 \lesssim [3.6] - [4.5] \lesssim 3$ mag. The IR emission of CCSNe may

be powered by thermal emission from the SN itself, or warm circumstellar dust that may be newly formed in the ejecta or pre-existing dust heated by the light from the explosion. Additionally, if CO has formed in the ejecta as in the case of (Banerjee et al. 2018), the emission at [4.5] may be additionally powered by the fundamental CO vibrational transition in this band, producing a significant [4.5] excess over the other IR bands. This likely contributes to the extreme observed [3.6]–[4.5] colors in several cases. Among the sample of CCSNe, stripped-envelope events (including the interacting subtype Ibn) are relatively more homogeneous in their IR properties, characterized by monotonically declining [4.5] light curves with $M_{[4.5]}$ peaking between -17.5 and -19 , and fading at a typical rate of ≈ 0.01 mag day $^{-1}$. SNe II show a larger spread in both peak luminosity, spanning $M_{[4.5]}$ between -16 and -19 , and decay rates, with some objects having nearly constant [4.5] flux for the first ≈ 500 days. Strongly interacting SNe IIn may exhibit extreme [4.5] luminosities of $M_{[4.5]}$ brighter than -22 , though some SNe IIn have IR light curves similar to more typical SNe II.

SPIRITS 14azy, peaking at only $M_{[4.5]} = -14.4 \pm 0.2$, is fainter than any previously observed CCSN. While consistent with the luminosity of an SN Ia at a phase of ≈ 120 days, the [4.5] fade rate is much slower, and the source is overluminous compared to an SN Ia by 400 days post discovery. Furthermore, its color evolution is inconsistent with an SN Ia. Based only on the IR light curves and considering only SN subtypes, SPIRITS 14azy would be most consistent with a faint SN II, however the as discussed below in Sections 4.4 and 5, optical light curves bear strong similarity to the LRN M101 OT2015-1, arguing against SPIRITS 14azy as a true CCSN.

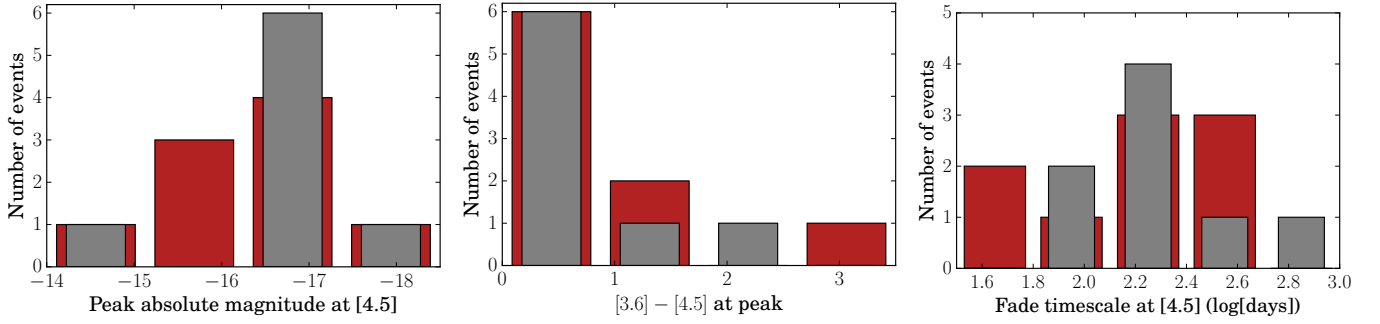
SPIRITS 15c, spectroscopically confirmed as an SN Ib/Ib in Jencson et al. (2017), is fully consistent with the sample of stripped-envelope SNe in its [4.5] light curve. At $[3.6] - [4.5] = 3.0$ at peak light, it is the reddest stripped-envelope SN yet observed by *Spitzer*. The extreme IR color is likely attributable to CO emission at [4.5], corroborated by the detection of emission from the CO $\Delta v = 2$ vibrational overtone transitions in the K band also reported in Jencson et al. (2017).

The [4.5] light curve of SPIRITS 15ud appears most similar to the sample of SNe II. With an observed peak at $M_{[4.5]} = -16.4$, however, it may also be consistent with the class of SN 2008S-like transients (also including the luminous 2008 optical transient in NGC 300, [NGC 300 OT2008-1]; Adams et al. 2016b). Given the large uncertainty in the phase of SPIRITS 15ud of $\gtrsim 400$ days, however, it is likely that the transient was significantly more luminous than SN 2008S, but the IR peak was missed by our observations.

SPIRITS 15ade again appears consistent with either a low-luminosity SN II or an SN 2008S-like event in both its [4.5]

Table 6. Properties derived from light curves and likely classifications

| Name | t_0 | Max age | t_{peak} | $M_{[4.5],peak}$ | $[3.6] - [4.5]$ | $t_{fade,[4.5]}$ | A_V | Classification |
|---------------|---------|---------|------------|------------------|-----------------|------------------|---------------|----------------|
| | (MJD) | days | (MJD) | (mag) | (mag) | (days) | (mag) | |
| SPIRITS 14azy | 56772.0 | 27.9 | 57245.1 | -14.4 | 0.55 | 270 | 3.2 | LRN |
| SPIRITS 15c | 56890.4 | 27.0 | 57057.4 | -17.1 | 3.03 | 85 | 2.2 | SN I/Ib |
| SPIRITS 15ud | 57271.7 | 381.4 | 57271.7 | -16.4 | 0.55 | 170 | $\gtrsim 3.7$ | SN II |
| SPIRITS 15ade | 57276.5 | 34.0 | 57337.9 | -15.7 | 0.67 | 220 | 1.6 | ILRT |
| SPIRITS 16ix | 57477.9 | 195.2 | 57477.9 | -15.8 | 1.61 | 55 | $\gtrsim 5.5$ | SN II |
| SPIRITS 16tn | 57615.0 | 82.0 | 57615.1 | -16.7 | 0.68 | 55 | 7.8 | SN II |
| SPIRITS 17lb | 57901.7 | 149.8 | 57901.7 | -18.2 | 1.09 | 160 | $\gtrsim 2.5$ | SN II |
| SPIRITS 17pc | 57878.8 | 249.9 | 58250.4 | -16.3 | 0.39 | ... | 12.5 | MSE |
| SPIRITS 17qm | 58062.2 | 234.0 | 58062.2 | -15.9 | 0.21 | 480 | 12.1 | MSE/LBV |

**Figure 7.** We show the observed distributions of peak absolute magnitude at [4.5] (left), $[3.6] - [4.5]$ color at time of peak (middle), and fade timescale at [4.5] (right) for the IR-discovered sample (red) and the optically discovered control sample (grey).

light curve and $[3.6] - [4.5]$ color evolution. We examine the classification of this object as an SN 2008S-like event also considering its near-IR spectrum and limits on the presence IR progenitor star in Section 5.

SPIRITS 16ix and SPIRITS 16tn, with largely similar IR properties, are unique among the SPIRITS IR transients presented here, and among all SNe previously observed by *Spitzer*. Their light curves at [4.5] decline more rapidly than any CCSN yet observed, and appear consistent with the decline of an SN Ia. However, their red $[3.6] - [4.5]$ colors at $\gtrsim 0.7$ mag rule out a SN Ia scenario. In Jencson et al. (2018c), we argued that the properties of SPIRITS 16tn were most consistent with a weak SN II, where the early bright IR emission was powered by a luminous dust echo, and the redder $[3.6] - [4.5]$ color at later times was likely attributable a [4.5] excess from CO emission. This interpretation may also apply to SPIRITS 16ix given the similarity of these objects in the *Spitzer* bands.

SPIRITS 17lb is our most luminous transient at $M_{[4.5]} = -18.2 \pm 0.4$, and its light curve and color evolution are consistent with either a luminous SN II, or stripped-envelope SN Iib or Ib/c. While we are unable to distinguish between CCSN subtypes based on the *Spitzer* data alone, we discuss the likely classification of SPIRITS 17lb as an SN II based on the rest of our follow-up data at optical, near-IR and radio wavelengths in Section 5.

SPIRITS 17pc and SPIRITS 17qm are remarkable among the SPIRITS sample due the presence of multiple IR outbursts in the *Spitzer* light curves over the last ≈ 1000 –1500 days. As reported in Jencson et al. (2018a), SPIRITS 17pc shows three distinct IR peaks at [3.6] and [4.5], growing progressively more luminous and longer in duration. During the current, ongoing outburst, SPIRITS 17pc brightened to $M_{[4.5]} = -16.3 \pm 0.4$ mag over a period of at least 400 days, with a fairly constant $[3.6] - [4.5]$ color between 0.2 and 0.4 mag. The increasing IR emission may indicate

ongoing interaction of an SN blastwave with the surrounding CSM, or alternatively, active dust formation during a less extreme, non-explosive outburst.

SPIRITS 17qm, as reported in (Jencson et al. 2018b), underwent a previous IR outburst ≈ 1300 days at $M_{[4.5]} = -15.2 \pm 0.1$ before the discovery by SPIRITS. The observed peak at discovery of $M_{[4.5]} = -15.9 \pm 0.1$, and subsequent slow decline are consistent with an SN II, or even some previously observed interacting SN IIn. Given its eruptive history however, the discovery outburst of SPIRITS 17qm may be due to a more intense non-terminal outburst, rather than a true SN explosion.

4.3. Optical/near-IR spectroscopic properties

Our optical spectroscopy of SPIRITS 16tn (79.5 days), SPIRITS 17pc (192.8 days), and SPIRITS 17qm (9.3 days) are shown in Figure 3. The spectrum of SPIRITS 16tn, previously presented in Jencson et al. (2018c), shows only a featureless red continuum beyond ≈ 8000 Å. The spectrum of SPIRITS 17qm is dominated by strong H α emission with a full width at half maximum (FWHM) velocity of 2400 km s^{-1} (upper-left panel of Figure 8), consistent with ejecta velocities of massive LBV eruptions. We do not detect any broader components that would indicate higher, explosive velocities of an interacting SN IIn. Additionally in SPIRITS 17qm, we detect weaker emission features of O I ($\lambda\lambda 8446, 9266$), but with no clear detection of the 7771 Å O I line, as well as detections of the Ca II IR triplet ($\lambda\lambda 8498, 8542, 8662$). In contrast, for SPIRITS 17pc, we detect narrow, unresolved emission features of the underlying star-forming region (including H α), along with the Ca II triplet in emission, but no significant O I emission or broader components of H α associated with the transient. We confirmed the veracity of the weaker features reported here by close inspection of the reduced 2D spectra.

A zoom-in to the region around O I ($\lambda 8446$) and the Ca II triplet in the spectra of SPIRITS 17pc and SPIRITS 17qm is shown in Figure 9. The Ca II lines in SPIRITS 17pc are each double-peaked, with a blueshifted component at $\approx -240 \text{ km s}^{-1}$, and a redshifted component at $\approx 100 \text{ km s}^{-1}$. For SPIRITS 17qm, the lines show a single component centered at a velocity consistent with the host, and with a FWHM velocity of $\approx 230 \text{ km s}^{-1}$. We also note the O I line at 8446 Å present in SPIRITS 17qm, is absent or much weaker in SPIRITS 17pc.

The full set of our near-IR spectroscopy is shown in Figure 4, including spectra of 6 of the 9 IR-discovered transients. In the near-IR, these objects are spectroscopically diverse, showing a range of properties and features. Our clearest example of a spectroscopically confirmed CCSN is SPIRITS 15c. In Jencson et al. (2017), we compared the near-IR spectra of SPIRITS 15c to those of the well stud-

ied type IIb SN 2011dh. We found strong similarities and identified several features in SPIRITS 15c based on the comparison, including He I (10830 Å), emission features of neutral or singly ionized intermediate mass elements and Fe, and emission from the $\Delta v = 2$ vibrational overtone transitions of CO (see Figure 10 in comparison to SPIRITS 17lb and SPIRITS 17pc). We do not detect any hydrogen in the spectrum, but cannot rule out the presence of hydrogen at earlier times. Thus, we find the spectrum to be consistent with a Type Ib or IIb classification.

Our near-IR spectroscopy of SPIRITS 16tn was first presented in Jencson et al. (2018c), where the spectrum was characterized as a largely featureless red continuum. The spectrum, however, displays broad bumps in each of the *H* and *K* bands that we originally believed may have been due to difficulty in properly flux calibrating low S/N data, especially in the regions of strong telluric H₂O absorption where little to no flux from the transient is received through the atmosphere. Here, in contrast, we suggest a real, astrophysical origin for these broad features as absorption by water vapor at higher temperatures than the narrower atmospheric features. Such features have been observed in the atmospheres of cool giants with spectral types no earlier than M6 (Rayner et al. 2009), where models of pulsating Mira variables show the formation of water in the dense, cool ($< 1000 \text{ K}$) layers formed beyond periodic, outward-propagating shocks in their extended atmospheres (Bessell et al. 1989, 1996). To our knowledge, this would be the first detection of water vapor absorption associated with a luminous transient or SN, and we discuss possible interpretations in Section 5. As we detected no unambiguous SN features, however, we cannot definitively classify SPIRITS 16tn.

For SPIRITS 17lb, we detect a red continuum in the *H* and *K* regions, plausibly attributable to emission from warm dust. We note only possible excess emission beyond 23000 Å from CO in the 123 day spectrum, but which appears to fade by 157 days. As with SPIRITS 16tn, there are no clear, broad features indicative of an SN. We find, however, that a lack of such features does not rule an SN altogether for these objects. As discussed below in Section 4.5, non-thermal synchrotron emission from the interaction of high-velocity ejecta with CSM was detected in SPIRITS 17lb, confirming the core-collapse nature of this event. The strength of the radio emission suggests an SN II classification, possibly indicating that SNe II may be characterized by only weak or absent near-IR features at late phases.

The spectra of SPIRITS 15ade show only the H I recombination lines Br γ in the *K* band and Pa β in the *J* band. As shown in Figure 11, the peak velocities are consistent with the recession velocity of the host, and the velocity profiles can be approximated by simple gaussians with FWHM velocities of ≈ 360 and 390 km s^{-1} , respectively. These are similar

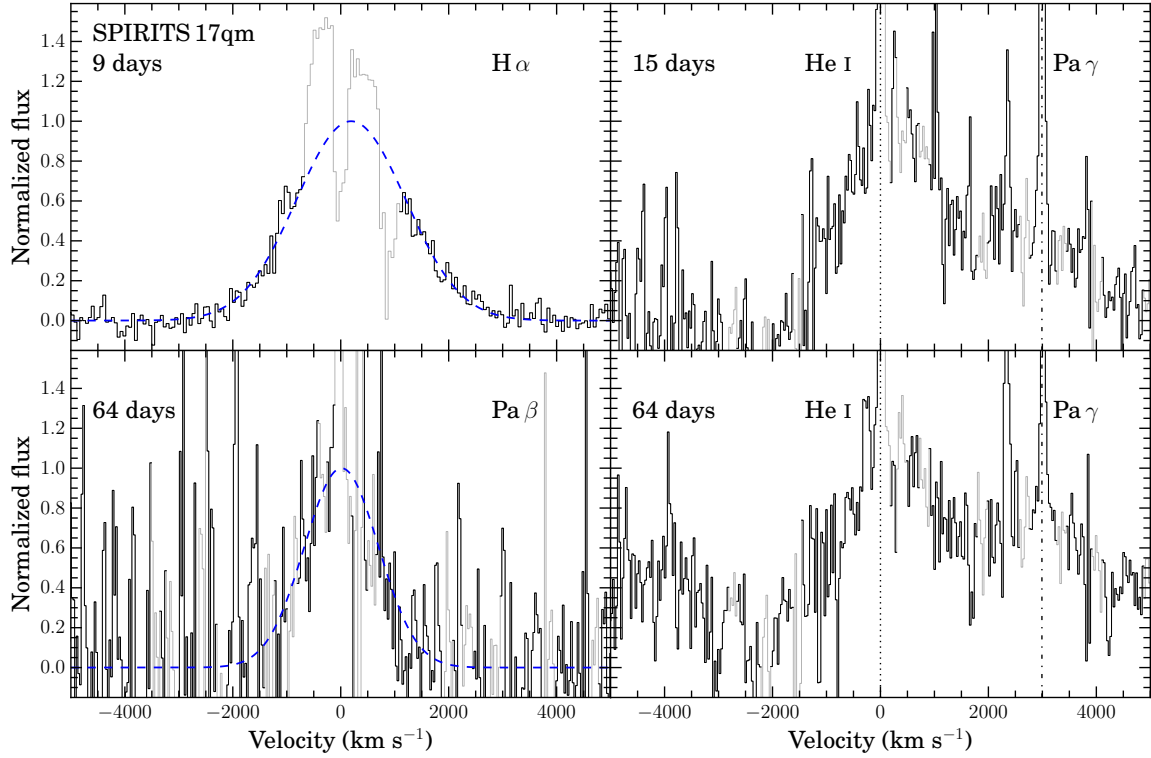


Figure 8. In the left 2 panels we show the $H\alpha$ (top; 9 days) and $Pa\beta$ (bottom; 64 days) velocity profiles of SPIRITS 17qm in black. Gaussian fits to the data with FWHM velocities of 2400 and 1600 km s^{-1} , respectively, are plotted as blue dashed curves, where spectral bins contaminated by emission features of the underlying star-forming region or bright OH airglow emission lines are shown in light gray and excluded from the fits. In the right 2 panels, we show the velocities profiles of He I ($\lambda 10830$; dotted vertical lines) at 15 days (top) and 64 days (bottom), with FWHM velocities of $\approx 2000 \text{ km s}^{-1}$. The red wing of the line is blended with emission from $Pa\gamma$ (dash-dotted vertical lines)

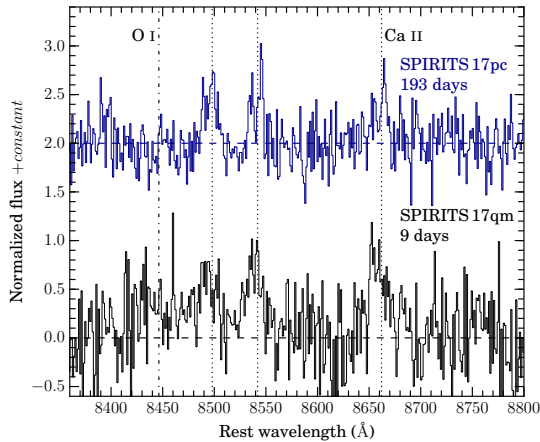


Figure 9. Comparison of the spectral region around O I ($\lambda 8446$; dash-dotted vertical line) and the Ca II IR triplet (dotted vertical lines) in the optical spectra of SPIRITS 17pc (193 days) and SPIRITS 17qm (9 days). A linear approximation to the continuum emission off the spectral features has been subtracted from the spectra. The spectra were then normalized in flux, and the SPIRITS 17pc spectrum has been shifted vertically for clarity. The dashed blue and black horizontal lines show the zero-levels for SPIRITS 17pc and SPIRITS 17qm, respectively.

to the low expansion velocities seen in the H I lines in optical spectra of the prototypical members of the class of ILRTs SN 2008S (e.g., Botticella et al. 2009b) and NGC 300OT-2008 (Bond et al. 2009; Humphreys et al. 2011). The similarity of the [4.5] light curve of SPIRITS 15ade to that of SN 2008S (Section 4.2) strengthens its association with this class. There is also an apparent secondary peak in the $Br\gamma$ and $Pa\beta$ velocity profiles in SPIRITS 15ade at $\approx 300 \text{ km s}^{-1}$, possibly indicative of a bipolar or toroidal outflow geometry. Double-peaked profiles were also seen in the H I and Ca II emission features in NGC 300OT-2008 (Bond et al. 2009), but at lower velocities of $\approx 70\text{--}80 \text{ km s}^{-1}$.

The near-IR spectra of SPIRITS 17pc, taken between 199 and 364 days, show a relatively smooth continuum, with a few notable features. We identify an absorption band of molecular CN at $1.1 \mu\text{m}$ along with the CO $\Delta v = 2$ band heads beyond $2.3 \mu\text{m}$ (shown in more detail in Figure 10). These features are characteristic of mid-G to early-K type stellar spectra, and the spectra bear particular resemblance to G6 Ia–Ib supergiants (c.f., the NASA Infrared Telescope Facility [IRFT] spectral library of cool stars, Rayner et al. 2009). Despite good coverage of several near-IR H I recombination lines, we detect only narrow H lines from the un-

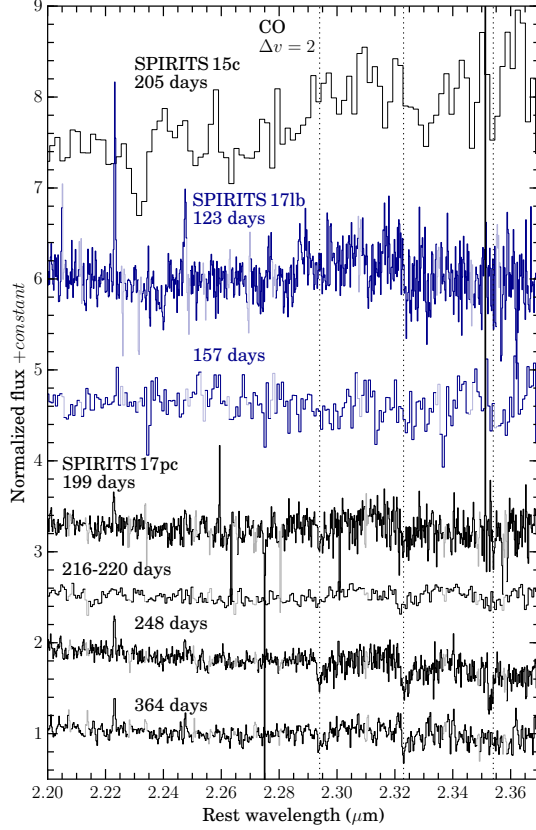


Figure 10. Comparison of the region of the K band between 2.2 and 2.37 μm in the near-IR spectra of SPIRITS 15c, SPIRITS 17lb, and SPIRITS 17pc. The spectra, shown in alternating colors for each object, are labeled on the figure along with their respective phases. Spectral bins of low S/N due to coincidence with bright OH airglow emission lines are plotted in lighter colors. The band heads of the $\Delta v = 2$ vibrational transitions of CO are indicated by the dotted vertical lines.

derlying star-forming region and no broader features associated with the transient (also for He I $\lambda\lambda$ 10830, 20581). As described above, the Ca II IR triplet emission (seen in absorption in mid-G to early K-type stellar spectra) suggests an outflow with velocities of $\approx 100\text{--}240 \text{ km s}^{-1}$. While we do not detect H recombination features from the transient, this is consistent with a temperature of $\approx 5400\text{--}5600$ inferred by the presence of CN/CO absorption and the presence of Ca II in the spectrum, as such temperatures are too low for a significant fraction of the hydrogen to be ionized. The relatively low outflow velocities observed for SPIRITS 17pc and cooler, star spectrum suggest this event is likely associated with non-terminal outbursts or eruptions of its progenitor, rather than a true SN.

In the near-IR, SPIRITS 17qm shows emission features of H I as well as the 10830 \AA line of He I. As shown in Figure 8, these lines are relatively broad. The Pa γ line at 64 days, well approximated by a gaussian with a FWHM velocity of

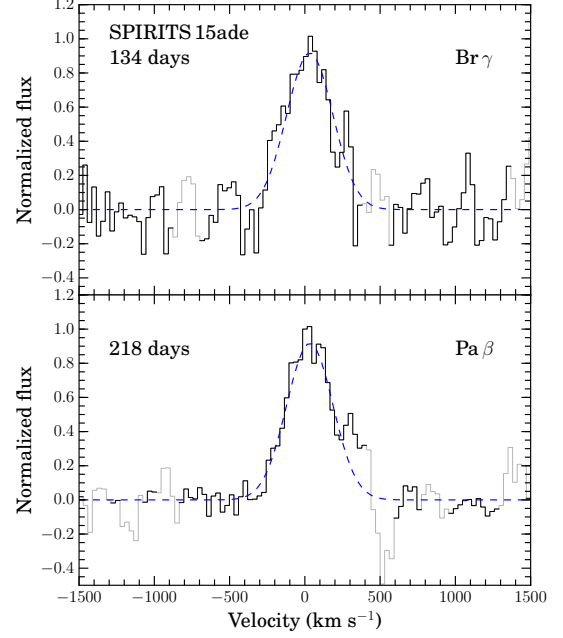


Figure 11. The velocity profiles of Br γ (134 days) and Pa β (218 days) in the spectra of SPIRITS 15ade are shown as the black solid lines in the top and bottom panels, respectively, in the rest frame of the host galaxy, NGC 5921. Gaussian fits to the profiles, excluding velocity bins of low S/N due to coincidence with bright OH airglow emission lines (plotted in light gray), are shown as the blue dashed curves.

1600 km s^{-1} , is somewhat narrower than the H α emission line observed at an earlier phase of 9 days. The spectra are consistent with a massive eruption from an LBV, and while a low-energy SN IIn may also be possible, the lack of higher velocity features argues against the terminal explosion of the progenitor.

4.4. Multi-band light curves and extinction estimates

Using available data, we compiled multi-band light curves from the optical to near-IR for each luminous SPIRITS transient in our sample. These light curves are shown in Figure 12. We then estimate the visible extinction, A_V (after correcting for the Galactic contribution), which may come from the foreground interstellar medium (ISM) of the host galaxy, from the local circumstellar environment of the progenitor, or by dust formed in the event itself. We provide our estimates, based on the analysis below, in Table 4.2. In most cases, we are unable to make strong statements about the origin of the extinction, and throughout this section we assume a standard Milky Way ISM extinction law with $R_V = 3.1$ (Fitzpatrick 1999). To obtain A_V estimates where we have a reasonably secure classification of the transient, we attempt to make a direct comparison with template light curves from a well-studied object. Where the classification of a transient is less secure, or where good template light curves were not

available, we adopt $m_X - m_{[4.5]}$ near the observed peak of the transient as an estimate of A_X , the extinction in broadband filter X (preferably optical), and convert to A_V with our assumed extinction law.

The light curves of SPIRITS 15c were discussed in detail in (Jencson et al. 2017), where we estimated $A_V \approx 2.2$ mag based on comparison the well studied type IIb SN 2011dh. Similarly, for SPIRITS 16tn we estimated $A_V \approx 7.8$ mag based on a comparison to the low-luminosity type IIP SN 2005cs (Jencson et al. 2018c).

The light curves of SPIRITS 14azy are shown in Figure 12 in comparison to the 2015 LRN in M101 (M101 OT2015-1), a well-studied example of a common-envelope ejection in a merging stellar binary system (Blagorodnova et al. 2017, and in preparation). SPIRITS 14azy, shows a short-lived, optical counterpart peaking at $g' = 20.0$ ($M_{g'} = -10.7$), which rises to peak and fades within $\lesssim 60$ days. The optical, broad-band colors near peak are red, with $g' - r' = 0.9$ and $g' - i' = 1.1$. The transient display a longer lived, IR excess detected out to $\gtrsim 300$ days in the near-IR and to $\gtrsim 700$ days in the *Spitzer*/IRAC bands. Shifted in apparent magnitude to the distance of SPIRITS 14azy in NGC 2997, we see that M101 OT2015-1 matches the light curves of SPIRITS 14azy both in the absolute brightness of the transient in g' and the *Spitzer*/IRAC IR bands, as well as in the timescale of the optical transient. While M101 OT2015-1 is characterized by somewhat redder optical colors, and an even longer lived IR excess, the overall similarity of the two events is readily apparent. We characterize the reddening for SPIRITS 14azy as $A_{g'} \approx g'_{\text{peak}} - [4.5]_{\text{peak}} = 3.7$ mag, corresponding to $A_V = 3.2$ mag. We caution that this estimate should not be directly interpreted as a measurement of the extinction from the host galaxy or local environment, and may also be indicative of “intrinsic” reddening of the transient due to dust-formation or the relatively cool effective temperatures associated with LRN-like events.

SPIRITS 15ud was inaccessible for ground-based observing due to its proximity to the sun from Earth at the time of the *Spitzer* discovery, and thus, our constraints on any optical emission associated with the transient are only from phases before/after $\approx \pm 100$ days. As discussed below in Section 5, we find the most likely interpretation of the IR light curves of this event to be an SN II. Our deepest limits on the post-peak optical flux of SPIRITS 15ud are in the r' band, and we compare to the light curve in this band of the Type IIP SN 2004et from to obtain a constraint on the extinction. We shift the light curves in phase to match the time of the observed [4.5] peak of SPIRITS 15ud and in apparent magnitude to match the observed [4.5] brightness, and find that our optical limits then require $A_{r'} \gtrsim 3.1$ mag to be consistent with the declining light curve of SN 2004et. This corresponds $A_V \gtrsim 3.7$ mag,

which we adopt as a lower limit on the extinction to SPIRITS 15ud.

The *Spitzer* light curves of SPIRITS 15ade, as discussed above in Section 4.2, shows distinct similarity those of SN 2008S, a prototype of the class of ILRTs, in both IR luminosity at $M_{[4.5],\text{peak}} \approx -16$ mag and the subsequent IR light curve decline. The first detection of the source was in an unfiltered optical CCD image taken on 2015 September 11.5, where the transient was identified as PSN J15220552+0503160 by M. Aoki (CBAT). A subsequent unfiltered image taken on 2015 September 11.8 by G. Masi detected the transient at 17.5 mag (-14.4 mag absolute, calibrated to R -band magnitudes with UCAC-4 reference stars), 61.0 days before the first detection by SPIRITS. The optical luminosity is similar to the R -band peak of SN 2008S (from Botticella et al. 2009b, assuming $A_V \approx 1$ mag in excess of the Galactic contribution as in Botticella et al. 2009b and Szczygiel et al. 2012), and our late-time optical limits are consistent with the optical fading of SN 2008S within ~ 200 days. We detect an near-IR excess in the J , H , and K_s bands at a phase of ≈ 170 days, again similar to that observed in SN 2008S. We characterize the reddening to SPIRITS 15ade, though it may be intrinsic to the source, as $A_R = R_{\text{peak}} - [4.5]_{\text{peak}} = 1.3$ mag, corresponding to $A_V = 1.6$ mag.

SPIRITS 16ix is a near twin to SPIRITS 16tn in both their observed peak IR luminosities at $M_{[4.5],\text{peak}} \approx -16$ mag, and their rapid IR decline rates (Section 4.2). Furthermore, both objects are remarkably red, as shown for SPIRITS 16ix in Figure 12. Our deepest optical limit during the IR observed peak of SPIRITS 16ix reached $g \gtrsim 22.2$ mag ($\gtrsim 9.3$ mag), indicating $A_g \gtrsim 6.3$ mag. Corresponding to $A_V \gtrsim 5.5$ mag, we adopt this as a lower limit on the extinction to SPIRITS 16ix.

Similar to our analysis for SPIRITS 15ud, we compare our photometric data for SPIRITS 17lb to those of SN 2004et. Shifting SN 2004et in phase to match the time of the observed [4.5] peak and in apparent magnitude to the distance of SPIRITS 17lb, we find that their [4.5] light curves track each other remarkably well, though SPIRITS 17lb is significantly redder than SN 2004et in $[3.6] - [4.5]$ until $\gtrsim 150$ days. Applying reddening with $A_V \gtrsim 2.5$ mag is then required for the SN 2004et light curves to be consistent with our V -band limit at 11.7 days, which we adopt as a lower limit on the extinction to SPIRITS 17lb.

As discussed in Section 4.2, the *Spitzer* light curves of SPIRITS 17pc are characterized by multiple outbursts over the last ≈ 4 years that appear to be progressively increasing in both brightness and duration. Deep optical limits constrain the optical variability of the source between ≈ -1200 and -300 days, and we note the IR outburst peaking at $[4.5] = 15.8$ mag near -400 days was extremely red with $g' - [4.5] > 5.9$ mag. During the brightest, longest-duration IR outburst seen in the *Spitzer*/IRAC bands lasting

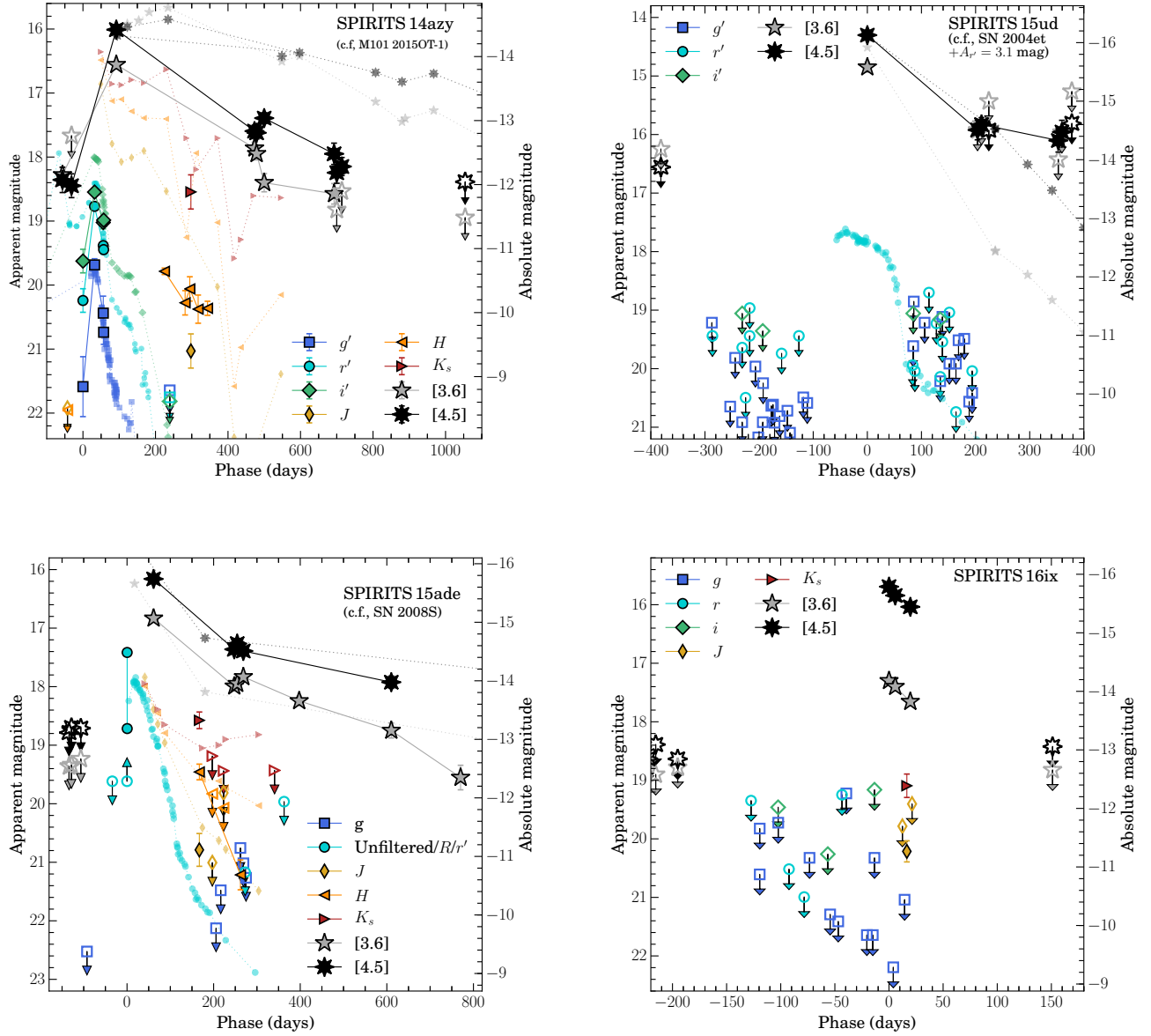


Figure 12. Multi-band light curves of the SPIRITS sample of transients. The large, black-outlined symbols are detections of the SPIRITS transient indicated in the upper-right corner of each panel. Upper limits from non-detections are shown as the large, unfilled symbols with downward arrows. The smaller, faint symbols show corresponding light curves of a well-studied comparison object, also listed in parentheses in the upper-right corner of each panel. All light curves have been corrected for Galactic extinction, and comparison light curves are also corrected for additional host/intrinsic reddening as described in the text. Comparison light curves are then shifted in apparent magnitude to the distance of their corresponding SPIRITS event. The SN 2004et light curves, in comparison to SPIRITS 15ud, have additionally been shifted in apparent magnitude to match in [4.5] peak luminosity, then reddened by $A_V = 3.7$ mag to be consistent with our r' -band limits. Similarly, in comparison to SPIRITS 17lb, the SN 2004et light curves have been reddened by $A_V = 2.5$ mag to be consistent with our V -band limit.

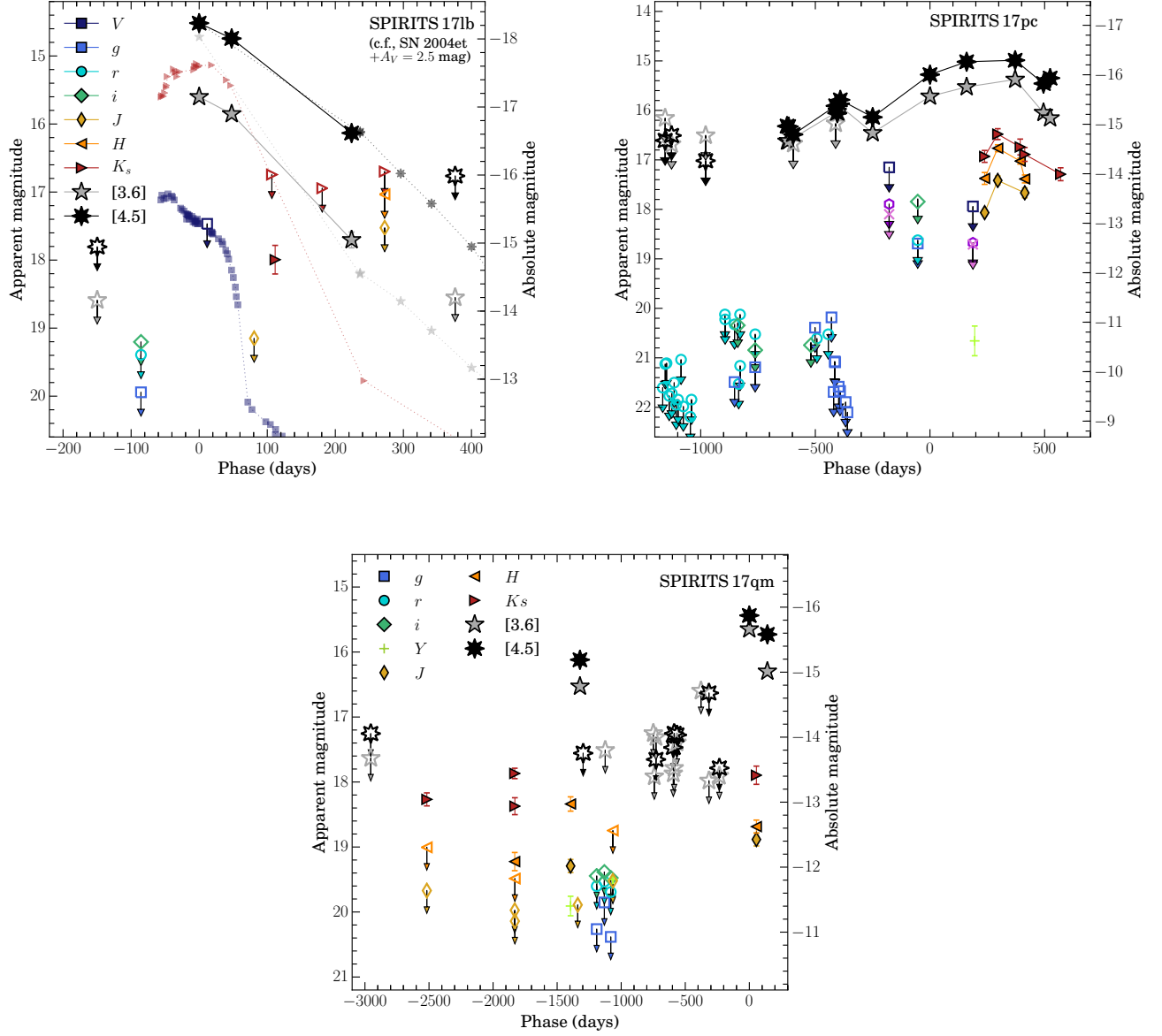


Figure 12, continued.

$\gtrsim 500$ days, we detected underlying near-IR variability peaking at $K_s = 16.5$ mag at 295.6 days with a red near-IR color of $J - K_s = 0.9$ mag with a comparatively shorter duration of $\lesssim 200$ days. We also obtained our only optical detection of SPIRITS 17pc at $Z = 20.7$ mag at 195.1 days, indicating $A_Z = Z - [4.5] = 5.7$ mag. To estimate the extinction in Table 4.2, we convert this to $A_V = 12.5$ mag, but again caution the extreme optical-IR color may be intrinsic to the source and is not necessarily indicative of extinction by the host ISM or local environment of the progenitor.

The light curves of SPIRITS 17qm also indicate multiple epochs of significant variability across the near-IR and *Spitzer*/IRAC bands extending back to at least a phase of -2500 days before the discovery detection and observed IR peak at $[4.5] = 15.4$ mag ($M_{[4.5]} = -15.9$). During the pre-discovery outburst detected by *Spitzer*, our photometry indicates an notably red SED with $Y - [4.5] = 3.8$ mag. Similarly, our near-IR follow-up observations during the post-peak decline at $t = 55.1$ days indicate $A_J = J - [4.5] = 3.3$ mag, corresponding to $A_V = 12.1$ mag. As with SPIRITS 17pc, rather than indicating host or environmental extinction, the extreme colors we observe may be intrinsic to the SED of the source or caused by dust formation.

4.5. Radio constraints

Radio observations of CCSNe probe the non-thermal emission generated when the fastest ejecta interact with the CSM produced by the pre-explosion stellar wind of the progenitor. The spectrum is dominated by synchrotron emission as the blastwave propagates through the CSM, where turbulent instabilities may accelerate electrons to relativistic energies and amplify magnetic fields (Chevalier 1982). At early times, the synchrotron spectrum is self-absorbed at high frequencies, with possible additional contributions from internal free-free absorption, and free-free absorption by the external, pre-shocked, ionized CSM (e.g., Chevalier 1982, 1998). As the shock propagates out into the CSM, the peak in the spectrum, below which the source is opaque, shifts to lower frequencies. As no SN Ia has been detected in the radio to deep limits in radio luminosity of $L_\nu \lesssim 10^{24}$ erg s $^{-1}$ Hz $^{-1}$, detection of this characteristic signature can provide strong confirmation our sources as CCSNe.

In Figure 13, we show the radio light curves of SPIRITS 15c and SPIRITS 17lb. For both sources, we detect a declining radio source consistent with optically thin synchrotron emission. At $t = 546.7$ days for SPIRITS 15c, the transient is detected at both 10 and 6 GHz, with a spectral index $\alpha = 1.32^{+0.05}_{-1.01}$, where the flux density is given by $S_\nu \propto \nu^{-\alpha}$. The source is observed to fade at 6 GHz, with a spectral index of $\alpha = 0.7 \pm 0.1$ between 3 and 6 GHz at $t = 1356.6$ days. We infer from these observations that SPIRITS 15c peaked at a 6 GHz radio luminosity of $L_\nu \gtrsim 3.5 \times 10^{26}$ erg s $^{-1}$ Hz $^{-1}$

a time $t \lesssim 546.7$ days (maximum age $\lesssim 573.7$ days). For SPIRITS 17lb, the source fades at 6 GHz between $t = 222.5$ and 345.3 days, with a spectral index of $\alpha = 0.78 \pm 0.13$ between 3 and 6 GHz at the later epoch. SPIRITS 17lb thus peaked at 6 GHz at $L_\nu \gtrsim 8.8 \times 10^{25}$ erg s $^{-1}$ Hz $^{-1}$ a time $t \lesssim 222.5$ days (maximum age $\lesssim 372.3$ days). The remaining SPIRITS events were undetected in our radio follow-up observations.

In Figure 14, we show the the peak luminosities of radio CCSNe of various subtypes and the time to peak times the frequency of observation compared to our constraints for SPIRITS 15c and SPIRITS 17lb, as well as our limits on the radio luminosity of the rest of the sample. Following our discussion in Section 4.2.1 of Jencson et al. (2018c), we use the self-similar solution for the propagation of the SN blastwave into the CSM described in Chevalier (1998) and Chevalier & Fransson (2006). If synchrotron self-absorption (SSA) is the dominant absorption mechanism, and assuming the emitting electron population is described by a power law with an energy spectral index $p = 3$, then, as calculated by (Chevalier 1998), the size of the radio emitting region is given by

$$R_s = 4.0 \times 10^{14} q^{-1/19} \left(\frac{f}{0.5} \right)^{-1/19} \left(\frac{F_p}{\text{mJy}} \right)^{9/19} \times \left(\frac{D}{\text{Mpc}} \right)^{18/19} \left(\frac{\nu}{5 \text{ GHz}} \right)^{-1} \text{ cm}, \quad (1)$$

where $q \equiv \epsilon_e/\epsilon_B$ is the ratio of the energy density in relativistic electrons to that in the magnetic field, f is the filling factor of the radio emitting region, F_p is the peak flux at frequency ν , and D is the distance to the source. We show the inferred shock velocities assuming energy equipartition ($q = 1$) and $f = 0.5$ (as estimated by Chevalier & Fransson 2006) as the dashed lines in Figure 14.

Assuming the CSM was produced by a steady pre-SN stellar wind, its density profile as a function of radius, r , will be given by $\rho_w = A/r^2 \equiv \dot{M}/(4\pi r^2 v_w)$, where \dot{M} is the mass loss rate and v_w is the wind velocity. We define $A \equiv \dot{M}/(4\pi v_w)$ as the normalization of the CSM density profile and $A_* \equiv A/(5 \times 10^{11} \text{ g cm}^{-1})$ is a dimensionless proxy for A as in (Chevalier 1982). The radio emission at time t since explosion is then sensitive to the density profile of the CSM as

$$A_* \epsilon_{B-1} q^{8/19} = 1.0 \left(\frac{f}{0.5} \right)^{-8/19} \left(\frac{F_p}{\text{mJy}} \right)^{-4/19} \times \left(\frac{D}{\text{Mpc}} \right)^{-8/19} \left(\frac{\nu}{5 \text{ GHz}} \right)^2 \left(\frac{t}{10 \text{ days}} \right)^2, \quad (2)$$

where $\epsilon_{B-1} \equiv \epsilon_B/0.1$ (Chevalier & Fransson 2006). The inferred value of A_* depends very sensitively on t_{peak} , shown in Figure 14 as the nearly vertical dotted lines.

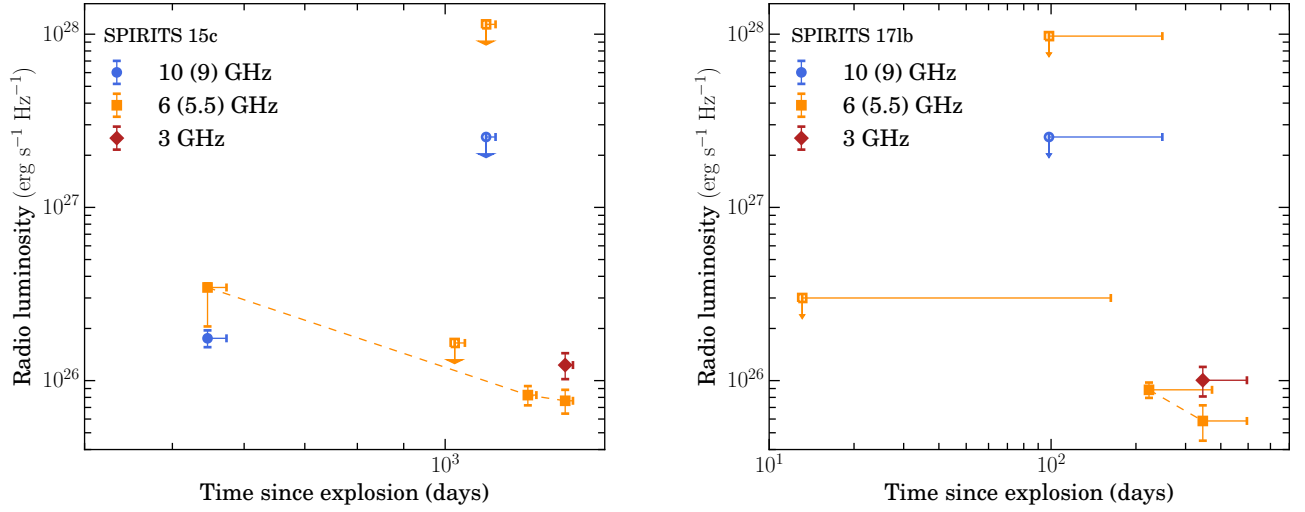


Figure 13. Radio light curves of SPIRITS 15c (left) and SPIRITS 17lb (right) in multiple frequency bands. Detections are indicated by filled symbols, while upper limits from non-detection are indicated by unfilled symbols with downward arrows. Horizontal error bars indicate our uncertainty the absolute phase since explosion for these events.

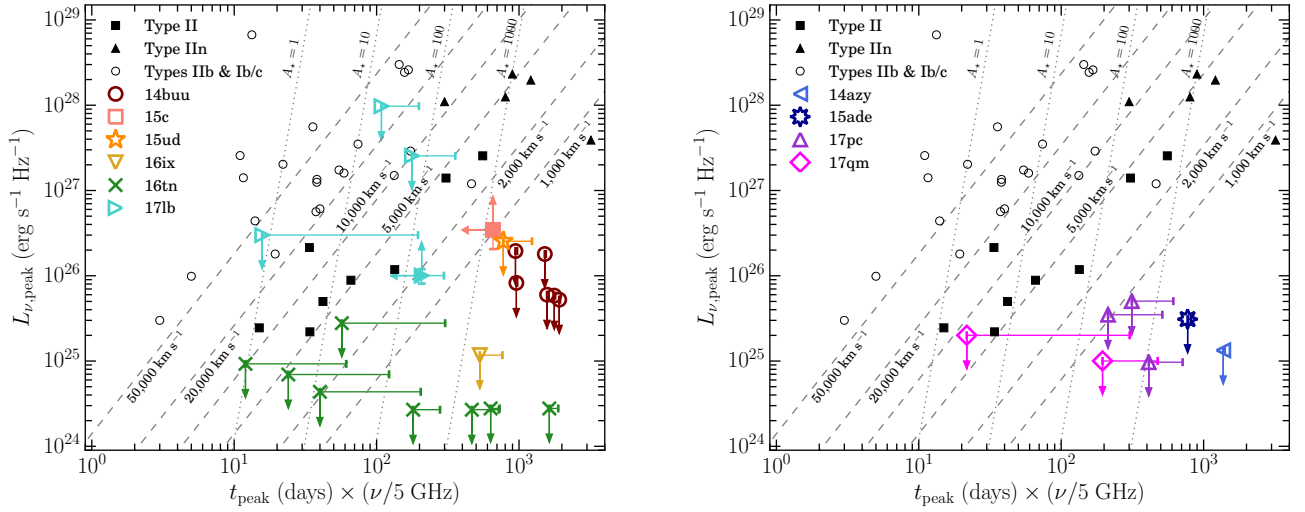


Figure 14. In each panel, we show the peak radio luminosity vs. time of peak times the frequency of observation for radio CCSNe adapted from, e.g., [Chevalier et al. \(2006\)](#) and [Romero-Cañizales et al. \(2014\)](#). This is an updated version of Figure 10 from [Jencson et al. \(2018c\)](#). SNe II are shown as black squares, and strongly interacting SNe II are shown as black triangles. Open circles represent stripped-envelope SNe IIb and Ib/c. Upper limits on the radio luminosity of SPIRITS transients at a given phase are shown as multi-color, open symbols with downward-pointing arrows, where the horizontal error bars represent our uncertainty in the absolute phase since explosion. The likely CCSNe are shown in the left panel, while the non-SN events are shown in the right panel. Filled symbols for SPIRITS 15c and SPIRITS 17lb represent constraints on t_{peak} and $L_{\nu, \text{peak}}$ from detections of the transients. Symbols corresponding to each object are labeled in the legend on the left side of the Figure. Assuming an SSA model with an electron distribution with $p = 3$ for the shock wave propagating through the CSM, one can infer the shock velocity (dashed lines) and CSM density parameter (A_* ; dotted lines) from the position on this diagram.

Our constraint on the peak radio luminosity for SPIRITS 15c is consistent with its spectroscopic classification as an SN I Ib or Ib, which tend to be more luminous radio sources ($10^{26} \lesssim L_{\nu, \text{peak}} \lesssim 10^{28} \text{ erg s}^{-1} \text{ Hz}^{-1}$) peaking on timescales between 10–100 days. Our observations require $v_s \gtrsim 1000 \text{ km s}^{-1}$ and $A_* \lesssim 1400$. This translates to a limit on the pre-SN mass loss rate of $\dot{M} \lesssim 1.4 \times 10^{-3} \left(\frac{\epsilon_B}{0.1}\right) \left(\frac{v_w}{100 \text{ km s}^{-1}}\right) M_{\odot} \text{ yr}^{-1}$, consistent with a yellow supergiant (YSG) or He star progenitor of a Type I Ib or Ib SN, respectively.

SPIRITS 17lb, despite its younger phase at the time of first observation with the VLA, is notably less luminous, more consistent with the population of radio SNe II. We find $v_s \gtrsim 800 \text{ km s}^{-1}$ and $A_* \lesssim 800$, corresponding to a limit on the pre-SN mass loss rate of $\dot{M} \lesssim 8.0 \times 10^{-5} \left(\frac{\epsilon_B}{0.1}\right) \left(\frac{v_w}{10 \text{ km s}^{-1}}\right) M_{\odot} \text{ yr}^{-1}$. This is consistent with a RSG progenitor of an SN IIP.

As discussed in Jencson et al. (2018c), our deep radio non-detections for SPIRITS 16tn rule out a stripped-envelope classification, except possibly the most rapidly evolving, high velocity events that may have fast-peaking radio light curves. The new late-time limits beyond $t \gtrsim 500$ days presented here also rule out a strongly interacting SN IIn. A weak SN II is the most consistent with our observations for SPIRITS 16tn, and specifically, our inferred constraint on the pre-SN mass loss rate of $\dot{M} \lesssim 2.4 \times 10^{-6} \left(\frac{\epsilon_B}{0.1}\right) \left(\frac{v_w}{10 \text{ km s}^{-1}}\right) M_{\odot} \text{ yr}^{-1}$ may suggest a RSG progenitor of lower initial mass (10–15 M_{\odot}). Similarly, the late time limit for SPIRITS 16ix is again sufficiently deep to rule out a strongly interacting SN IIn or luminous stripped-envelope SN, and is most consistent with an SN II. Our weaker constraint for SPIRITS 15ud may be consistent with either an SN II or stripped-envelope classification.

As discussed below in Section 5, based on the sum of all available observational data, we do not believe SPIRITS 14azy, SPIRITS 15ade, SPIRITS 17pc or SPIRITS 17qm were terminal CCSN explosions. Thus, we do not expect strong radio counterparts for these events, but show our radio limits in the right panel of Figure 14 for completeness. Specifically though for SPIRITS 17qm, while the most likely interpretation is a massive LBV eruption, an SN IIn is consistent with the optical/IR data, but is strongly disfavored by the radio non-detections.

5. PUTTING IT ALL TOGETHER: TRANSIENT CLASSIFICATIONS

Here, we discuss the most likely classification for each SPIRITS event in our sample based on the combined observational constraints across radio, IR, and optical wavelengths. We find that 5 of our 9 IR events are confirmed or likely to be CCSNe, while the remaining 4 are non-SN massive star outbursts of various origins. The preferred classification for each event is given in Table 4.2.

5.1. The confirmed and likely CCSNe

As discussed in detail in Jencson et al. (2017), SPIRITS 15c is a clear example of a confirmed, moderately obscured, CCSN. Our assessment is based primarily on near-IR spectroscopy showing distinct similarity to the Type I Ib SN 2011dh, and in particular the presence of a broad ($\approx 8400 \text{ km s}^{-1}$) double-peaked emission line of He I at $1.0830 \mu\text{m}$. The optical/near-IR light curves were well matched to those of SN 2011dh assuming $A_V = 2.2 \text{ mag}$ and a standard Milky Way ISM extinction law with $R_V = 3.1$. In this work we present new radio observations of SPIRITS 15c, which are characterized by the detection of a declining, optically-thin synchrotron source consistent with the radio counterparts of other, previously observed stripped-envelope CCSNe. Furthermore, we derived a limit on the pre-SN mass loss rate consistent with a YSG or He star progenitor of an SN I Ib or Ib, respectively.

SPIRITS 17lb, our most luminous IR transient at $M_{[4.5]} = -18.2 \text{ mag}$, clearly falls in the IR luminosity range of CCSNe (see Figure 2), and is more luminous than any other class of known IR transient. The IR light curves and color evolution are consistent with either a hydrogen-rich Type II or stripped-envelope Type Ib/c or I Ib. The near-IR spectra, taken at phases of 123 and 157 days, show no strong features indicative of a CCSN or specific SN sub-type. There is a possible weak detection of the CO $\Delta v = 2$ features in the 123 day K -band spectrum, which is not present at 157 days. We note that some SNe II, including the recent SN 2017eaw, have shown strong CO K -band features may fade on timescales of months (e.g., S. Tanyanont et al., in preparation), but this does not provide a definitive classification for SPIRITS 17lb. As discussed in Section 4.5, we detected a declining, optically thin synchrotron source at the location of SPIRITS 17lb, confirming this source as a CCSN. Our constraints on the peak radio luminosity and time of the synchrotron peak are most consistent with previously observed radio SNe of Type IIP, rule out a strongly interacting SN IIn, and disfavor typically more luminous stripped-envelope events. Assuming a steady pre-SN wind, we derive constraints on the mass loss rate of $\dot{M} \lesssim 8.0 \times 10^{-5} \left(\frac{\epsilon_B}{0.1}\right) \left(\frac{v_w}{10 \text{ km s}^{-1}}\right) M_{\odot} \text{ yr}^{-1}$, consistent with a RSG progenitor. We infer a lower limit on the extinction to SPIRITS 17lb of $A_V \gtrsim 2.5 \text{ mag}$ in Section 12 comparing to the Type IIP SN 2004et.

The evidence for SPIRITS 15ud, SPIRITS 16ix, and SPIRITS 16tn is more circumstantial, but we find a reddened CCSN to be the most likely interpretation for each of these events. For SPIRITS 15ud, at $M_{[4.5], \text{peak}} = -16.4 \text{ mag}$ the IR light curves are broadly consistent with an SN II, stripped-envelope Type Ib/c or I Ib, or alternatively, an SN 2008S-like ILRT. Given the large uncertainty in the age of SPIRITS 15ud at discovery ($< 381.4 \text{ days}$), it is highly likely that our *Spitzer* observations missed the peak of the this event, and that its

true peak luminosity was substantially higher. This would place SPIRITS 15ud firmly in the IR luminosity range characteristic of CCSNe and disfavors the ILRT interpretation. Despite the large uncertainty in its age in Section 12 and under the assumption that SPIRITS 15ud was an SN II, we placed a lower limit on the extinction of $A_V \gtrsim 3.7$ mag. This interpretation is further supported by the location of SPIRITS 15ud in a prominent, nearly opaque dust lane in archival *HST* imaging.

We examined the observational constraints for SPIRITS 16tn in Jencson et al. (2018c) and again found an SN II, possibly a low-luminosity event similar to SN 2005cs, heavily obscured by $A_V = 7-9$ to be the most likely interpretation of this event. A new piece of the puzzle is the possible identification of water vapor absorption in the near-IR spectrum of SPIRITS 16tn (Section 4.3). In the CCSN scenario, a possibility is that the progenitor was encased in a dense molecular cloud, and water in the vicinity was heated by the explosion to produce the observed, broad absorption. The high extinction for SPIRITS 16tn is consistent with this interpretation. This would constitute the first direct identification of a CCSN associated with a molecular cloud, though Galactic candidates for SN remnants interacting with molecular gas have been previously noted (e.g., W44 & IC 443, Chevalier 1999). Interestingly, Chevalier (1999) argued the progenitors of such events must be relatively low mass, i.e., early B-type stars on the main sequence ($8-12 M_\odot$), as the ionizing flux from a more massive O-type progenitor will clear a region ≈ 15 pc in radius of molecular material. Our inferred limit on the pre-SN mass loss rate from radio observations of SPIRITS 16tn, were also consistent with a lower-mass RSG progenitor, which may further support to this hypothesis.

Alternatively, given the apparent similarity of the water absorption features to those of late-type Mira variables, SPIRITS 16tn, may represent a previously unknown class of transient associated with such stars. It is unclear, however, that water in the atmosphere would survive a luminous outburst or mass loss event. Finally, an additional possibility is chance positional coincidence between SPIRITS 16tn and an unrelated Mira variable. Continued monitoring for ongoing Mira-like variability in the near-IR is required to confirm or rule out this possibility.

SPIRITS 16ix is a near twin of SPIRITS 16tn in their IR properties, and thus we also consider a CCSN, possibly another weak or low-luminosity SN II, as the most likely interpretation. SPIRITS 16tn was clearly associated with active star-formation, indicating a likely massive-star origin further suggestive of a CCSN. We note that for SPIRITS 16ix, however, there is not clear evidence of star-formation at the site, and given the classification of the host as a lenticular S0 galaxy, the association is more ambiguous. We noted in Jencson et al. (2018c), that given the low explosion en-

ergy inferred for SPIRITS 16tn and lack of spectroscopic features distinctive of a CCSN, a non-terminal “impostor” explosion or eruption remains a viable scenario. Neither SPIRITS 16ix nor SPIRITS 16tn have shown any evidence of prior or subsequent IR variability other than the singular events described in this work. This further supports our interpretation they were isolated, and possibly terminal, events in the lives of their progenitors. It is particularly notable that SPIRITS 16ix and SPIRITS 16tn, while distinctly similar to each other in their IR light curves, are also unique compared to the rest of the IR- and optically-discovered transients. Furthermore, they are the two most severely reddened likely CCSNe ($A_V \gtrsim 5.5$ mag) presented in this work. We thus speculate that may represent a new class of IR-dominated transients, possibly associated with low-energy CCSNe arising preferentially in particularly extinguished environments and/or from progenitors that are directly associated with or encased in dense molecular clouds.

5.2. ILRT: SPIRITS 15ade

As a distinct class of IR-dominated events, the nature of ILRTs remains unclear. The prototypical objects are the “imposter” SN 2008S and the 2008 transient in NGC 300 (NGC 300 2008OT-1; Bond et al. 2009). ILRTs are observed to have dust-obscured, IR-luminous ($M_{[4.5]} < -10$ mag) pre-explosion counterparts, suggested to be extreme asymptotic giant branch (AGB) stars of intermediate mass ($\approx 10-15 M_\odot$) self-obscured by a dusty wind (Prieto et al. 2008; Bond et al. 2009; Thompson et al. 2009). Less luminous than typical CCSNe at peak, emission lines in their spectra (including H recombination and strong [Ca II] and Ca II features) also indicate lower velocities up to $\text{few} \times 100 \text{ km s}^{-1}$ (e.g., Botticella et al. 2009b; Bond et al. 2009; Humphreys et al. 2011). A suggested physical scenario involves weak explosion, possibly an electron-capture SN, or massive stellar eruption that initially destroys the obscuring, circumstellar dust and produces a short-lived optical transient. In the aftermath, the development of a significant IR excess indicates the recondensation of dust and consequent re-obscuration of the transient (Thompson et al. 2009; Kochanek 2011; Szczygieł et al. 2012). There is currently no evidence that the progenitor stars survive such events, as both prototypes have now faded below their pre-explosion luminosities in the IR (Adams et al. 2016b).

SPIRITS 15ade shares many properties with this class. While we do not directly detect a progenitor star, our limit from archival *Spitzer*/IRAC imaging at $M_{[4.5]}$ fainter than -12.8 is consistent with the IR progenitors of SN 2008S and NGC 300 OT2008-1. As we found in Section 12, the IR light curves (peaking at $M_{[4.5]} = -15.7$) and the observed peak and duration of the associated optical transient are also very similar to known ILRTs. Finally, we detect H recombination

emission in our near-IR spectra, suggestive of an outflow at 300–400 km s⁻¹, similar to the low expansion velocities of known ILRTs (e.g., Botticella et al. 2009b; Bond et al. 2009; Humphreys et al. 2011).

5.3. LRN: SPIRITS 14azy

The class of extragalactic transients referred to as luminous red novae (LRNe) are believed to be more massive analogs of the population of stellar mergers observed in the Galaxy, including the striking example of the $\approx 1\text{--}3 M_{\odot}$ contact binary merger V1309 Sco (Tylenda et al. 2011) and the B-type stellar merger V838 Mon (Bond et al. 2003; Sparks et al. 2008). While sharing several properties with ILRTs, LRNe are distinctly characterized by multi-peaked, irregular light curves. At early times, their spectra show H emission features, but they develop red optical colors, atomic and molecular absorption features, and significant IR excesses as they evolve. Recent examples include the 2011 transient in NGC 4490 (NGC 4490 OT2011-1; Smith et al. 2016), and the 2015 event in M101 (M101 OT2015-1; Blagorodnova et al. 2017). Specifically in the case of NGC 4490 OT2011-1, the late-time IR excess was too luminous to be explained as an IR echo, indicating the presence of a surviving, merged remnant. With unobscured, directly detected progenitor systems in archival imaging estimated at 20–30 M_{\odot} and $\approx 18 M_{\odot}$, respectively, these events extend a correlation noted by Kochanek et al. (2014) for LRNe between progenitor masses and the transient peak luminosity. Specifically, the progenitor of M101 OT2015-1 was identified in archival imaging as having properties of an F-type supergiant with $L \approx 8.7 \times 10^4 L_{\odot}$ and $T_{\text{eff}} \approx 7000$ K, likely having recently evolved off the main sequence and crossing the Hertzsprung gap as it expands.

Based primarily on our analysis of its multi-band light curves, we find SPIRITS 14azy is most consistent with the LRN class of IR transients, and in particular bears strong similarity to M101 OT2015-1 in its peak luminosity both at $[4.5]$ and g' . Thus, we suggest it may have a similar mass progenitor system. In Section 4.1, we placed a limit on the flux of the progenitor in the HST/WFC3 UVIS F336W filter corresponding to M_U fainter than -5.4 . As the transient is located in a prominent dust lane of the host, the foreground extinction in U band may be significant. Even in the absence of host extinction, and assuming bolometric corrections from (Flower 1996), with corrections by Torres (2010) using a consistent choice of $M_{\text{bol},\odot} = 4.73$ and Crowther (1997) filter transformations, this limit is approximately consistent with a zero-age main sequence O9 star ($T_{\text{eff}} \approx 30,000$ K, $L \approx 40,000 L_{\odot}$) of similar mass to the progenitor of M101 OT2015-1.

5.4. MSEs: SPIRITS 17pc and SPIRITS 17qm

SPIRITS 17pc has undergone multiple, IR-dominated outbursts over a time period spanning at least 1100 days. These

outbursts are extremely red (we infer $A_V \approx 12.5$), possibly indicative of copious dust formation. Near-IR spectra taken during the most recent, longest duration, and most luminous outburst show features similar to a mid to late G-type supergiant spectrum, including CN and CO absorption. An optical spectrum shows double-peaked Ca II emission, but no H or He features, indicative of a cool, few $\times 100$ km s⁻¹ outflow. We identified a luminous ($L \approx 2 \times 10^5 L_{\odot}$) star detected in 2011 archival, multi-band *HST* imaging at the precise location of SPIRITS 17qm as a likely progenitor. The luminosity is lower than that of a classical LBV, but still likely indicates a very massive progenitor. The progenitor photometry is consistent with a blackbody temperature of $T = 1900 \pm 100$ K, likely indicating active dust formation was occurring around the underlying star. Given the previous history of strong IR variability, cool spectral features, low outflow velocities, and lack of strong radio emission, we argue that the most recent outburst of SPIRITS 17pc represents a more intense mass loss event or eruption, rather than a terminal SN explosion.

Similar to SPIRITS 17pc, SPIRITS 17qm has also undergone multiple IR outbursts in SPIRITS, and furthermore was also extremely red (estimated $A_V = 12.1$ mag). However, we highlight several notable differences. The spectra of SPIRITS 17qm were dominated by broader ($v \approx 1500\text{--}2000$ km s⁻¹) features of H and He, and also showed prominent Ca II emission, consistent with a massive LBV eruption. Again, the lack of strong radio emission argues against the interpretation of SPIRITS 17qm as a terminal, Type IIn CCSN explosion. The presumed progenitor of SPIRITS 17qm detected in multi-epoch *HST* imaging was highly luminous and variable ($L \approx 2 \times 10^6 L_{\odot}$, $\Delta V = 1.7$ mag), also consistent with the properties of an LBV. Assuming the progenitor was undergoing S Doradus-like variability, the foreground extinction (host or circumstellar) was likely no larger than $A_V \approx 0.5$ mag at the time of the *HST* observations in 2001. Thus, the extreme optical/IR color observed for SPIRITS 17qm must be due to the formation of copious dust in the intervening years and/or during the observed massive eruption. Incorporating ongoing monitoring, the physical details SPIRITS 17qm and SPIRITS 17pc as self-obscuring, MSEs will be explored more fully in a future publication.

6. THE “REDNESS” DISTRIBUTION OF LUMINOUS IR TRANSIENTS

In Figure 15, we show the distribution of A_V (including lower limits) inferred for our sample of luminous SPIRITS transients. This includes confirmed and likely CCSNe as the filled portions of the histograms, as well the Type Iax SN 2014dt from the optical control sample and the non-SN IR transients as the unfilled portions. For the non-SN transients, we emphasize that our A_V estimates are only a proxy for the observed optical–IR color, and may be indicative of

internal reddening (due to dust formation) or the intrinsically cool SEDs, rather than external extinction. We note that our IR discovered events are overall much redder, with 8 of the 9 objects having $A_V \gtrsim 2$ mag, compared to the optical control sample with 7 of 9 objects having $A_V \lesssim 2$ mag. In particular, the MSEs SPIRITS 17pc and SPIRITS 17qm stand out as the reddest events in our sample with $A_V > 12$ mag. For the 5 IR-discovered events interpreted as likely CCSNe, the estimates range from $2.2 \lesssim A_V \lesssim 7.8$ mag. The optically discovered CCSNe in our control sample are again notably less reddened, ranging from $A_V \sim 0$ up to 4.3 mag, with 6 of the 8 events having $A_V \lesssim 2$ mag. This strongly suggests that the IR-selected sample of luminous SPIRITS transients represent populations of much redder events than the optically selected objects, namely heavily obscured CCSNe, and a population of exceptionally red transients associated with massive star outbursts of various origins.

The sample of all known CCSNe discovered between 2000 and the end of 2011 hosted by galaxies within 12 Mpc along with literature estimates of their host extinction compiled by Mattila et al. (2012, hereafter M12) provides another useful comparison for the SPIRITS sample. In Figure 16, we directly compare the distribution of host A_V for the SPIRITS sample of confirmed and likely CCSNe (both optically and IR-selected events) to the M12 sample. In the SPIRITS sample, 7 of the 13 likely CCSNe (58.3%) have $A_V \gtrsim 2$ mag, and the median value is 2.2 mag. For M12, only 6 of 18 events (33.3%) have $A_V \gtrsim 2$ mag, and the median is significantly lower at 0.25 mag. Shown as cumulative distributions in the right panel of Figure 16, we find the M12 sample is bracketed between the optically known CCSNe in SPIRITS and the full SPIRITS sample including the IR discovered events, where again, a larger fraction of events were found with large host extinction. Here, it is particularly important to re-emphasize that for 3 of the 5 IR discovered CCSNe in the SPIRITS sample, our A_V estimates are only lower limits, meaning that the true distribution is likely even more skewed to large host extinctions.

7. THE OPTICALLY MISSED FRACTION OF NEARBY CCSNE

We now consider constraints from our sample on the fraction of optically missed CCSNe in nearby galaxies, an important consideration for measurements of the local CCSN rate. $N_{\text{CCSNe}} = 13$ confirmed/likely CCSNe were recovered by SPIRITS and pass our selection criteria, with $N_{\text{mCCSNe}} = 5$ events unreported by any optical search. If we assume the completeness of our IR survey to optically discovered and optically missed SNe is the same (we examine this assump-

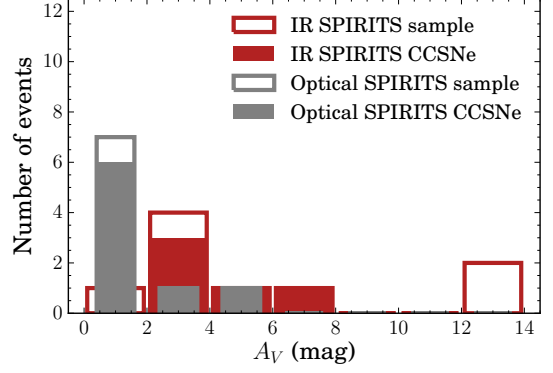


Figure 15. Distribution of A_V inferred for the IR selected sample of luminous SPIRITS transients (red), and the optically selected control sample (gray). The solid-filled regions of the histograms represent confirmed or likely CCSNe. The unfilled regions include the Type Ia SN 2014dt from the control sample, and the non-SN stellar outbursts from the IR sample.

tion in more detail below), then the fraction of missing SNe, f , is given by the binomial distribution

$$P(f) \propto (1-f)^{N_{\text{CCSNe}}} f^{N_{\text{mCCSNe}}} \quad (3)$$

and the requirement that $\int_0^1 P(f) df = 1$ sets the normalization. The nominal, observed missed fraction is 0.385 with a 90% confidence interval of $0.166 < f < 0.645$.

Since 2 of 10 optically discovered and classified CCSNe, SN 2014bc and SN 2016adj, were not recovered in SPIRITS and selected as part of our sample with the criteria outlined in Sections 2.3 and 2.4, our selection efficiency for optically known CCSNe is 0.8. SN 2016adj in Cen A was itself flagged as a saturated source in our transient identification pipeline. An optically obscured CCSN in a galaxy as near as Cen A at a similar IR brightness would have been similarly flagged, and it is natural to assume our survey incompleteness to optically bright and optically obscured CCSNe in the nearest galaxies ($D \lesssim 5$ Mpc) is the same. SN 2014bc was located in the saturated core of NGC 4285. We expect the optical extinction to be higher for events located near the core of the hosts, and thus our survey completeness to optically missed events is likely lower than that to optically known events. Still, we may obtain a more conservative estimate of f if we assume our sample was complete in optically missed events. With $N_{\text{CCSNe}} = 15$ total CCSNe in SPIRITS galaxies, and again with $N_{\text{mCCSNe}} = 5$, we obtain a missed fraction of 0.333 with a 90% confidence interval of $0.142 < f < 0.577$.

Next, we consider the effects of selection biases in our galaxy sample. For the first 3 years (2014–2016), the full sample of 190 SPIRITS galaxies was more representative across galaxy types, though primarily composed of luminous and massive galaxies beyond 5 Mpc. IC 2163, producing both SPIRITS 15c and SPIRITS 17lb, also stands out

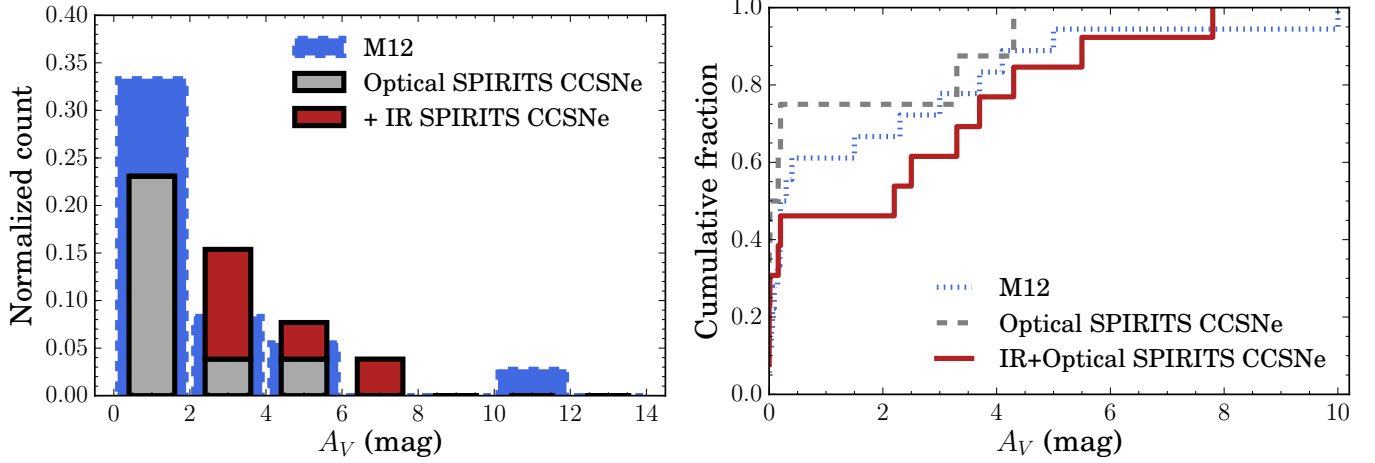


Figure 16. Left: Normalized distribution of A_V for CCSNe from M12 sample, and the sample of confirmed/likely CCSNe in SPIRITS (solid-filled histogram), including events from the optically discovered control sample (gray) and IR discovered events (red). **Right:** Cumulative distribution functions in host A_V estimates for M12 (blue, short-dashed curve), optically known SPIRITS CCSNe from the control sample (gray, dashed curve), and the full sample of likely SPIRITS CCSNe including both optically known and IR-discovered events (red, solid curve).

from the sample in that with recent distance estimates, it lies much farther than the rest of the sample at 35.5 Mpc, and is currently undergoing strong tidal interactions with its companion galaxy, NGC 2207. Including only events discovered during the original 3 year survey, and further excluding SPIRITS 15c in IC 2163, we have $N_{\text{CCSNe}} = 8$, and $N_{\text{mCCSNe}} = 3$, giving $f = 0.375$ with a 90% confidence interval of $0.111 < f < 0.711$. This is notably similar to our nominal estimate from the full sample, but with a larger 90% confidence interval due to the smaller number of events.

Finally, we consider the possibility that some events interpreted here as likely CCSNe have been misclassified. SPIRITS 16tn and SPIRITS 16ix have uniquely fast-fading IR light curves compared to the full sample of CCSNe observed by *Spitzer*, and while SPIRITS 16tn is clearly associated with a region of active star formation, there is not such a clear association for SPIRITS 16ix. Excluding these 2 events, we have $N_{\text{CCSNe}} = 11$, and $N_{\text{mCCSNe}} = 3$, giving $f = 0.273$ with a 90% confidence interval of $0.079 < f < 0.564$.

M12 estimated that locally $18.9^{+19.2}_{-9.5}\%$ of CCSNe are missed by optical surveys, substantially higher than previous estimates by Mannucci et al. (2007) at 5%–10%. Our nominal estimate of $38.5^{+26.0}_{-21.9}\%$ of CCSNe missed in nearby galaxies is even higher, falling at the upper end of the allowed range by M12, but with substantial overlap with our 90% confidence interval. The estimates of Mannucci et al. (2007) and M12 rise steeply to $> 30\%$ and $\sim 40\%$ by $z = 1$, respectively, and substantial work has also been dedicated to uncovering missing supernovae at higher redshift, particularly in the densely obscured and highly star-forming nuclear regions of starburst galaxies and (U)LIRGs. With

seeing-limited imaging (e.g. Mannucci et al. 2003; Miluzio et al. 2013) and high-resolution space- or ground-based adaptive optics imaging (Cresci et al. 2007; Mattila et al. 2007; Kankare et al. 2008, 2012; Kool et al. 2018), a total of 16 individual CCSNe have been uncovered in the IR in these galaxies. Radio very long baseline interferometry (VLBI) imaging of multiple (U)LIRGs (e.g., Lonsdale et al. 2006; Pérez-Torres et al. 2009; Romero-Cañizales et al. 2011, 2014; Bondi et al. 2012; Varenus et al. 2017, and references therein) have also revealed scores of radio sources interpreted as SN and SN remnants. Even with resolution of the upcoming *James Webb Space Telescope* (JWST), probing the innermost nuclear regions of such systems will remain challenging, and recently, Yan et al. (2018) undertook a successful pilot study examining the spatially integrated IR light curves of high redshift (U)LIRGs for variability suggestive of ongoing SN explosions. In this context, we emphasize that our work represents the first attempt to uncover the obscured population and directly constrain the missing fraction of CCSNe in nearby galaxies in the IR.

Our nominal estimate is consistent with an optically missed fraction of CCSNe in nearby galaxies as high as 64.5%, and indicates that accounting for obscured CCSNe may be sufficient to explain the claimed factor of 2 discrepancy by Horiuchi et al. (2011) between the measured rate of CCSNe and rate of cosmic star formation at $z = 0$. Some local studies even have suggested that CCSNe may be overproduced compared to H α - and ultraviolet- (UV-) inferred star formation rates (Botticella et al. 2012; Horiuchi et al. 2013; Xiao & Eldridge 2015), and interestingly, accounting for the population heavily obscured nearby events may

actually increase this tension in the other direction. More recent volumetric CCSN rate estimates from the Supernova Diversity and Rate Evolution (SUDARE; Botticella et al. 2013) also now suggest better agreement between CCSN and star-formation rates at medium redshift ($0.2 < z < 0.8$; Cappellaro et al. 2015).

8. SUMMARY AND CONCLUSIONS

We have presented a sample of 9 luminous IR transients discovered in nearby ($D \lesssim 35$ Mpc) galaxies by the SPIRITS survey between 2014–2018. These events were selected as having M_{IR} brighter than -14 in either the [3.6] or [4.5] channels of *Spitzer*/IRAC, and we required at least two SPIRITS detections and that these events were not present in the first epoch of SPIRITS imaging. Combining archival imaging constraints from *Spitzer* and *HST*, concomitant monitoring of SPIRITS galaxies with several ground-based telescopes, coverage in the iPTF survey from Palomar Observatory, and a dedicated ground- and space-based follow-up effort for our transients at optical, near-IR and radio wavelengths, we construct detailed observational characterizations and attempt to determine their nature. Here, we summarize our analysis of the sample and primary conclusions:

- The IR-discovered sample of transients were predominantly found in the spiral arms of star-forming hosts, except for one event, SPIRITS 16ix, in a lenticular S0 galaxy. This strongly suggests an association with young stellar populations and massive stars. They span IR luminosities with $M_{[4.5],\text{peak}}$ between -14 and -18.2 , show IR colors between $0.2 < [3.6] - [4.5] < 3.0$, and fade on timescales between $55 < t_{\text{fade}} < 480$ days.
- We define a control sample of optically discovered and classified transients recovered in SPIRITS using the same selection criteria (as outlined in Section 2.3). The control sample also consists of 9 events, including known 8 CCSNe and 1 SN Iax. Overall, the control sample and IR-selected sample are similar in their IR properties, with similar distributions in $M_{[4.5],\text{peak}}$, their $[3.6] - [4.5]$ colors at peak, and t_{fade} .
- Of the 9 IR-discovered events, we believe 5 are likely to be significantly dust-obscured CCSNe. SPIRITS 15c was confirmed via a near-IR spectrum similar to the Type IIb SN 2011dh and detection of a radio counterpart consistent with an SN I/IIb (Jencson et al. 2017). SPIRITS 17lb, as the most luminous IR transient in our sample and despite a lack of unambiguous SN features in its near-IR spectrum, was confirmed via its radio counterpart most consistent with an SN II. Our radio data constrain the pre-SN mass loss rates of the progenitors of SPIRITS 15c and SPIRITS 17lb

to $\dot{M} \lesssim 1.4 \times 10^{-3} \left(\frac{\epsilon_B}{0.1}\right) \left(\frac{v_w}{100 \text{ km s}^{-1}}\right)$, consistent with a yellow supergiant (YSG) or He star progenitor, and $\dot{M} \lesssim 8.0 \times 10^{-5} \left(\frac{\epsilon_B}{0.1}\right) \left(\frac{v_w}{10 \text{ km s}^{-1}}\right) M_{\odot} \text{ yr}^{-1}$, consistent with a RSG progenitor, respectively. The IR light curve of SPIRITS 15ud is also most consistent with a CCSN classification. SPIRITS 16ix and SPIRITS 16tn may constitute a previously, unknown class of rapidly fading, luminous IR transients occurring in the most densely obscured environments. We believe these two events are also CCSNe, possibly directly associated with or occurring within dense molecular clouds.

- The 4 remaining luminous IR SPIRITS transients represent a diverse array of IR-dominated transients arising from massive star progenitor systems. The multi-band optical and IR light curves of SPIRITS 14azy and SPIRITS 15ade are most similar to a LRN (possible massive stellar merger similar to M101 OT2015-1) and ILRT (possible weak or electron-capture SN similar to SN 2008S), respectively. SPIRITS 17pc underwent multiple, extremely red outbursts over several years, now showing G-type spectral features in the near-IR, and double-peaked Ca II emission indicative of a few $\times 100 \text{ km s}^{-1}$ outflow. We identified a luminous ($L \approx 2 \times 10^5 L_{\odot}$) star detected in multi-band archival *HST* as a likely progenitor. SPIRITS 17qm, also undergoing multiple-IR dominated outbursts, showed high velocity ($\sim 1500\text{--}2000 \text{ km s}^{-1}$) H and He features consistent with a massive LBV eruption. We identified a visually luminous ($L \approx 10^6 L_{\odot}$), highly variable progenitor in archival *HST* imaging. Future observations and continued monitoring of SPIRITS 17pc and SPIRITS 17qm may determine the physical origin of their IR outbursts and constrain the ultimate fate of their progenitors.
- We estimated the visible extinction, A_V —either as a direct estimate of the host extinction (in the case of a CCSN), or as a proxy for the optical–IR color for non-SN transients that may be self-obscured or intrinsically red—for each event in our sample based on their multi-band optical and IR light curves. 8 of the 9 IR-discovered events, including all 5 likely CCSNe, have $A_V \gtrsim 2$ mag, while only 2 of the 9 objects in the optically discovered control have extinction estimates so high. This strongly indicates that the IR-discovered events represent a separate population of remarkably red events that are systematically missed by optical searches. Compared to a volume- and time-limited sample of CCSNe within 12 Mpc compiled by Mattila et al. (2012), we find that the SPIRITS sample of optically known and newly IR discovered CCSNe contains a larger fraction of significantly obscured events

($A_V \gtrsim 2$ mag). Furthermore, as 7 of 13 of the likely CCSNe in SPIRITS were significantly obscured, it is likely that optical searches for SNe to larger distances are vastly incomplete to obscured events.

- 13 likely CCSNe recovered in SPIRITS passed our selection criteria, including 8 optically discovered events in control sample, and 5 IR-discovered events presented here. For our galaxy sample, this implies a large fraction, nominally $38.5^{+26.0}_{-21.9}\%$ (90% confidence), of CCSNe are being missed by optical surveys in nearby galaxies.

We thank C. Contreras and the staff of Las Campanas Observatory for help with conducting observations and data reduction. We also thank K. Mooley, D. Dong, M. Anderson, M. Eastwood, and A. Horesh for valuable discussions and help with VLA data reduction.

This material is based upon work supported by the National Science Foundation Graduate Research Fellowship under Grant No. DGE-1144469. HEB acknowledges that support for *HST* Program numbers GO-13935, GO-14258, and AR-15005 was provided by NASA through grants from the Space Telescope Science Institute, which is operated by the Association of Universities for Research in Astronomy, Incorporated, under NASA contract NAS5-26555. RDG was supported by NASA and the United States Air Force. This work is part of the research programme VENI, with project number 016.192.277, which is (partly) financed by the Netherlands Organisation for Scientific Research (NWO).

This work is based in part on observations made with the Spitzer Space Telescope, which is operated by the Jet Propulsion Laboratory, California Institute of Technology under a contract with NASA. This work is based in part on observations with the NASA/ESA *Hubble Space Telescope* obtained at the Space Telescope Science Institute, and from the Mikulski Archive for Space Telescopes at STScI, which are operated by the Association of Universities for Research in Astronomy, Inc., under NASA contract NAS5-26555. Some of the data presented herein were obtained at the W. M. Keck Observatory, which is operated as a scientific partnership among the California Institute of Technology, the

University of California and the National Aeronautics and Space Administration. The Observatory was made possible by the generous financial support of the W. M. Keck Foundation. The authors wish to recognize and acknowledge the very significant cultural role and reverence that the summit of Maunakea has always had within the indigenous Hawaiian community. We are most fortunate to have the opportunity to conduct observations from this mountain. Based on observations obtained at the Gemini Observatory (acquired through the Gemini Observatory Archive* and processed using the Gemini IRAF package, which is operated by the Association of Universities for Research in Astronomy, Inc., under a cooperative agreement with the NSF on behalf of the Gemini partnership: the National Science Foundation (United States), National Research Council (Canada), CONICYT (Chile), Ministerio de Ciencia, Tecnología e Innovación Productiva (Argentina), Ministério da Ciência, Tecnologia e Inovação (Brazil), and Korea Astronomy and Space Science Institute (Republic of Korea). UKIRT is owned by the University of Hawaii (UH) and operated by the UH Institute for Astronomy; operations are enabled through the cooperation of the East Asian Observatory. When the data reported here were acquired, UKIRT was supported by NASA and operated under an agreement among the University of Hawaii, the University of Arizona, and Lockheed Martin Advanced Technology Center; operations were enabled through the cooperation of the East Asian Observatory. Based on observations obtained at the Gemini Observatory acquired through the Gemini Observatory Archive and processed using the Gemini IRAF package, which is operated by the Association of Universities for Research in Astronomy, Inc., under a cooperative agreement with the NSF on behalf of the Gemini partnership: the National Science Foundation (United States), the National Research Council (Canada), CONICYT (Chile), Ministerio de Ciencia, Tecnología e Innovación Productiva (Argentina), and Ministério da Ciência, Tecnologia e Inovação (Brazil). The National Radio Astronomy Observatory is a facility of the National Science Foundation operated under cooperative agreement by Associated Universities, Inc.

Facilities: Spitzer (IRAC), HST (WFPC2, WFC3), Swift (UVOT), Hale (WIRC), PO:1.5m (SEDM), Keck:I (LRIS, MOSFIRE), Keck:II (NIREs), OANSPM:HJT (RATIR), UKIRT (WFCAM), Gemini:Gillett (GNIRS), Gemini:South (FLAMINGOS-2), EVLA, ATCA, AMI

REFERENCES

- Adams, S. M., Jencson, J. E., & Kasliwal, M. M. 2016a, *The Astronomer’s Telegram*, 9441
- Adams, S. M., Kochanek, C. S., Prieto, J. L., et al. 2016b, *MNRAS*, **460**, 1645
- Amanullah, R., Goobar, A., Johansson, J., et al. 2014, *ApJL*, **788**, L21
- Aoki, M. 2016, *Transient Name Server Discovery Report*, 4
- Arbour, R. 2016, *Transient Name Server Discovery Report*, 215

- Arcavi, I., Valenti, S., Hosseinzadeh, G., et al. 2014, *The Astronomer's Telegram*, 6466
- Banerjee, D. P. K., Joshi, V., Evans, A., et al. 2018, ArXiv e-prints, [arXiv:1808.04766 \[astro-ph.SR\]](https://arxiv.org/abs/1808.04766)
- Bessell, M. S., Brett, J. M., Scholz, M., & Wood, P. R. 1989, *A&A*, 213, 209
- Bessell, M. S., Scholz, M., & Wood, P. R. 1996, *A&A*, 307, 481
- Blagorodnova, N., Kotak, R., Polshaw, J., et al. 2017, *ApJ*, 834, 107
- Bock, G., Dong, S., Kochanek, C. S., et al. 2016, *The Astronomer's Telegram*, 9091
- Bond, H. E., Bedin, L. R., Bonanos, A. Z., et al. 2009, *ApJL*, 695, L154
- Bond, H. E., Henden, A., Levay, Z. G., et al. 2003, *Nature*, 422, 405
- Bondi, M., Pérez-Torres, M. A., Herrero-Illana, R., & Alberdi, A. 2012, *A&A*, 539, A134
- Botticella, M. T., Smartt, S. J., Kennicutt, R. C., et al. 2012, *A&A*, 537, A132
- Botticella, M. T., Pastorello, A., Smartt, S. J., et al. 2009a, *MNRAS*, 398, 1041
- . 2009b, *MNRAS*, 398, 1041
- Botticella, M. T., Cappellaro, E., Pignata, G., et al. 2013, *The Messenger*, 151, 29
- Butler, N., Klein, C., Fox, O., et al. 2012, in *Proc. SPIE, Vol. 8446, Ground-based and Airborne Instrumentation for Astronomy IV*, 844610
- Cao, Y., Kasliwal, M. M., McKay, A., & Bradley, A. 2014, *The Astronomer's Telegram*, 5786
- Cao, Y., Nugent, P. E., & Kasliwal, M. M. 2016, *PASP*, 128, 114502
- Cappellaro, E., Botticella, M. T., Pignata, G., et al. 2015, *A&A*, 584, A62
- Casali, M., Adamson, A., Alves de Oliveira, C., et al. 2007, *A&A*, 467, 777
- Cenko, S. B., Fox, D. B., Moon, D.-S., et al. 2006, *PASP*, 118, 1396
- Cheng, Y.-C., Chen, T.-W., & Prentice, S. 2017, *The Astronomer's Telegram*, 10374
- Chevalier, R. A. 1982, *ApJ*, 259, 302
- . 1998, *ApJ*, 499, 810
- . 1999, *ApJ*, 511, 798
- Chevalier, R. A., & Fransson, C. 2006, *ApJ*, 651, 381
- Chevalier, R. A., Fransson, C., & Nymark, T. K. 2006, *ApJ*, 641, 1029
- Cortini, G., Masi, G., Nocentini, F., et al. 2014, *Central Bureau Electronic Telegrams*, 3876
- Cresci, G., Mannucci, F., Della Valle, M., & Maiolino, R. 2007, *A&A*, 462, 927
- Crowther, P. A. 1997, in *IAU Symposium, Vol. 189, IAU Symposium*, ed. T. R. Bedding, A. J. Booth, & J. Davis, 137
- Dolphin, A. 2016, *DOLPHOT: Stellar photometry*, *Astrophysics Source Code Library*, [ascl:1608.013](https://www.ascl.net/asn/ascl:1608.013)
- Dolphin, A. E. 2000, *PASP*, 112, 1383
- Eikenberry, S., Elston, R., Raines, S. N., et al. 2006, in *Proc. SPIE, Vol. 6269, Society of Photo-Optical Instrumentation Engineers (SPIE) Conference Series*, 626917
- Elias, J. H., Joyce, R. R., Liang, M., et al. 2006, in *Proc. SPIE, Vol. 6269, Society of Photo-Optical Instrumentation Engineers (SPIE) Conference Series*, 62694C
- Fazio, G. G., Hora, J. L., Allen, L. E., et al. 2004, *ApJS*, 154, 10
- Ferrarese, L., Mould, J. R., Kennicutt, Jr., R. C., et al. 2000, *ApJ*, 529, 745
- Fitzpatrick, E. L. 1999, *PASP*, 111, 63
- Flower, P. J. 1996, *ApJ*, 469, 355
- Foley, R. J., Van Dyk, S. D., Jha, S. W., et al. 2015, *ApJL*, 798, L37
- Fossey, S. J., Cooke, B., Pollack, G., Wilde, M., & Wright, T. 2014, *Central Bureau Electronic Telegrams*, 3792
- Gehrels, N., Chincarini, G., Giommi, P., et al. 2004, *ApJ*, 611, 1005
- Gehrz, R. D., Roellig, T. L., Werner, M. W., et al. 2007, *Review of Scientific Instruments*, 78, 011302
- Goodrich, R., & Cohen, M. 2003, in *Proc. SPIE, Vol. 4843, Polarimetry in Astronomy*, ed. S. Fineschi, 146
- Granata, V., Benetti, S., Cappellaro, E., et al. 2016, *The Astronomer's Telegram*, 8818
- Grossan, B., Spillar, E., Tripp, R., et al. 1999, *AJ*, 118, 705
- Hess, K. M., Pisano, D. J., Wilcots, E. M., & Chengalur, J. N. 2009, *ApJ*, 699, 76
- Horiuchi, S., Beacom, J. F., Bothwell, M. S., & Thompson, T. A. 2013, *ApJ*, 769, 113
- Horiuchi, S., Beacom, J. F., Kochanek, C. S., et al. 2011, *ApJ*, 738, 154
- Hosseinzadeh, G., Howell, D. A., Arcavi, I., McCully, C., & Valenti, S. 2016, *The Astronomer's Telegram*, 8859
- Hosseinzadeh, G., Valenti, S., McCully, C., et al. 2018, *ApJ*, 861, 63
- Humphreys, R. M., Bond, H. E., Bedin, L. R., et al. 2011, *ApJ*, 743, 118
- Itagaki, K. 2016, *Transient Name Server Discovery Report*, 234
- Jencson, J. E., Bond, H. E., Adams, S. M., & Kasliwal, M. M. 2018a, *The Astronomer's Telegram*, 11577
- . 2018b, *The Astronomer's Telegram*, 11579
- Jencson, J. E., Kasliwal, M. M., Johansson, J., et al. 2017, *ApJ*, 837, 167
- Jencson, J. E., Kasliwal, M. M., Adams, S. M., et al. 2018c, ArXiv e-prints, [arXiv:1803.00574 \[astro-ph.HE\]](https://arxiv.org/abs/1803.00574)
- Johansson, J., Goobar, A., Kasliwal, M. M., et al. 2017, *MNRAS*, 466, 3442
- Kankare, E., Mattila, S., Ryder, S., et al. 2008, *ApJL*, 689, L97

- . 2012, *ApJL*, **744**, L19
- Kasliwal, M. M., Bally, J., Masci, F., et al. 2017, *ApJ*, **839**, 88
- Khan, R. 2017, *ApJS*, **228**, 5
- Kilpatrick, C. D., & Foley, R. J. 2018, ArXiv e-prints, [arXiv:1806.00348](https://arxiv.org/abs/1806.00348) [astro-ph.SR]
- Kim, M., Zheng, W., Li, W., et al. 2014, Central Bureau Electronic Telegrams, 3777
- Kiyota, S., Holoien, T. W.-S., Stanek, K. Z., et al. 2014, The Astronomer’s Telegram, 6460
- Kochanek, C. S. 2011, *ApJ*, **741**, 37
- Kochanek, C. S., Adams, S. M., & Belczynski, K. 2014, *MNRAS*, **443**, 1319
- Kochanek, C. S., Fraser, M., Adams, S. M., et al. 2017, *MNRAS*, **467**, 3347
- Kool, E. C., Ryder, S., Kankare, E., et al. 2018, *MNRAS*, **473**, 5641
- Kumar, S., Zheng, W., Filippenko, A. V., et al. 2014, Central Bureau Electronic Telegrams, 3892
- Li, W., Mo, J., Wang, X., et al. 2014, Central Bureau Electronic Telegrams, 3788
- Lonsdale, C. J., Diamond, P. J., Thrall, H., Smith, H. E., & Lonsdale, C. J. 2006, *ApJ*, **647**, 185
- Maiolino, R., Vanzì, L., Mannucci, F., et al. 2002, *A&A*, **389**, 84
- Mannucci, F., Della Valle, M., & Panagia, N. 2007, *MNRAS*, **377**, 1229
- Mannucci, F., Maiolino, R., Cresci, G., et al. 2003, *A&A*, **401**, 519
- Marples, P., Bock, G., & Parker, S. 2016, The Astronomer’s Telegram, 8651
- Masci, F. J., Laher, R. R., Rebbapragada, U. D., et al. 2017, *PASP*, **129**, 014002
- Mattila, S., Väisänen, P., Farrah, D., et al. 2007, *ApJL*, **659**, L9
- Mattila, S., Dahlen, T., Efstathiou, A., et al. 2012, *ApJ*, **756**, 111
- McLean, I. S., Steidel, C. C., Epps, H., et al. 2010, in *Proc. SPIE*, Vol. 7735, *Ground-based and Airborne Instrumentation for Astronomy III*, 77351E
- McLean, I. S., Steidel, C. C., Epps, H. W., et al. 2012, in *Proc. SPIE*, Vol. 8446, *Ground-based and Airborne Instrumentation for Astronomy IV*, 84460J
- Milisavljevic, D., Margutti, R., Kamble, A., et al. 2015, *ApJ*, **815**, 120
- Miluzio, M., Cappellaro, E., Botticella, M. T., et al. 2013, *A&A*, **554**, A127
- Monard, L. A. G., Kneip, R., Brimacombe, J., et al. 2014, Central Bureau Electronic Telegrams, 3977
- Morgan, C. W., Byard, P. L., DePoy, D. L., et al. 2005, *AJ*, **129**, 2504
- Muñoz-Mateos, J. C., Sheth, K., Gil de Paz, A., et al. 2013, *ApJ*, **771**, 59
- Nakano, S., Itagaki, K., Guido, E., et al. 2014, Central Bureau Electronic Telegrams, 4011
- Nasonova, O. G., de Freitas Pacheco, J. A., & Karachentsev, I. D. 2011, *A&A*, **532**, A104
- Nousek, J. A. 2004, in *Proc. SPIE*, Vol. 5165, *X-Ray and Gamma-Ray Instrumentation for Astronomy XIII*, ed. K. A. Flanagan & O. H. W. Siegmund, 169
- Ochner, P., Tomasella, L., Benetti, S., et al. 2014, The Astronomer’s Telegram, 6648
- Pérez-Torres, M. A., Romero-Cañizales, C., Alberdi, A., & Polatidis, A. 2009, *A&A*, **507**, L17
- Persson, S. E., Murphy, D. C., Smee, S., et al. 2013, *PASP*, **125**, 654
- Prieto, J. L., Kistler, M. D., Thompson, T. A., et al. 2008, *ApJL*, **681**, L9
- Querejeta, M., Meidt, S. E., Schinnerer, E., et al. 2015, *ApJS*, **219**, 5
- Rayner, J. T., Cushing, M. C., & Vacca, W. D. 2009, *ApJS*, **185**, 289
- Riess, A. G., Macri, L. M., Hoffmann, S. L., et al. 2016, *ApJ*, **826**, 56
- Rodríguez, Ó., Clocchiatti, A., & Hamuy, M. 2014, *AJ*, **148**, 107
- Romero-Cañizales, C., Mattila, S., Alberdi, A., et al. 2011, *MNRAS*, **415**, 2688
- Romero-Cañizales, C., Herrero-Illana, R., Pérez-Torres, M. A., et al. 2014, *MNRAS*, **440**, 1067
- Roming, P. W. A., Kennedy, T. E., Mason, K. O., et al. 2005, *SSRv*, **120**, 95
- Sahu, D. K., Anupama, G. C., Srivastav, S., & Chakradhari, N. K. 2016, The Astronomer’s Telegram, 8514
- Schlafly, E. F., & Finkbeiner, D. P. 2011, *ApJ*, **737**, 103
- Schlegel, D. J., Finkbeiner, D. P., & Davis, M. 1998, *ApJ*, **500**, 525
- Sheth, K., Regan, M., Hinz, J. L., et al. 2010, *PASP*, **122**, 1397
- Simcoe, R. A., Burgasser, A. J., Bernstein, R. A., et al. 2008, in *Proc. SPIE*, Vol. 7014, *Ground-based and Airborne Instrumentation for Astronomy II*, 70140U
- Simcoe, R. A., Burgasser, A. J., Schechter, P. L., et al. 2013, *PASP*, **125**, 270
- Smartt, S. J., Smith, K. W., Wright, D., et al. 2014, Central Bureau Electronic Telegrams, 3877
- Smith, N., Miller, A., Li, W., et al. 2010, *AJ*, **139**, 1451
- Smith, N., Andrews, J. E., Van Dyk, S. D., et al. 2016, *MNRAS*, **458**, 950
- Sorce, J. G., Tully, R. B., Courtois, H. M., et al. 2014, *MNRAS*, **444**, 527
- Sparks, W. B., Bond, H. E., Cracraft, M., et al. 2008, *AJ*, **135**, 605
- Stetson, P. B. 1987, *PASP*, **99**, 191
- Stritzinger, M., Hsiao, E. Y., Morrell, N., et al. 2016, The Astronomer’s Telegram, 8657
- Szalai, T., & Vinkó, J. 2013, *A&A*, **549**, A79
- Szalai, T., Zsifros, S., Fox, O. D., Pejcha, O., & Müller, T. 2018, ArXiv e-prints, [arXiv:1803.02571](https://arxiv.org/abs/1803.02571) [astro-ph.HE]

- Szczygieł, D. M., Prieto, J. L., Kochanek, C. S., et al. 2012, [ApJ](#), **750**, 77
- Theureau, G., Hanski, M. O., Coudreau, N., Hallet, N., & Martin, J.-M. 2007, [A&A](#), **465**, 71
- Thompson, T. A., Prieto, J. L., Stanek, K. Z., et al. 2009, [ApJ](#), **705**, 1364
- Tinyanont, S., Kasliwal, M. M., Fox, O. D., et al. 2016, [ApJ](#), **833**, 231
- Torres, G. 2010, [AJ](#), **140**, 1158
- Tully, R. B. 1988, Nearby galaxies catalog
- Tully, R. B., Courtois, H. M., Dolphin, A. E., et al. 2013, [AJ](#), **146**, 86
- Tylenda, R., Hajduk, M., Kamiński, T., et al. 2011, [A&A](#), **528**, A114
- Vacca, W. D., Cushing, M. C., & Rayner, J. T. 2003, [PASP](#), **115**, 389
- Varenus, E., Conway, J. E., Batejat, F., et al. 2017, arXiv e-prints, [arXiv:1702.04772](#)
- Watson, A. M., Richer, M. G., Bloom, J. S., et al. 2012, in [Proc. SPIE](#), Vol. 8444, Ground-based and Airborne Telescopes IV, 84445L
- Werner, M. W., Roellig, T. L., Low, F. J., et al. 2004, [ApJS](#), **154**, 1
- Wiggins, P. 2017, Central Bureau Electronic Telegrams, 4390
- Wilson, J. C., Eikenberry, S. S., Henderson, C. P., et al. 2003, in [Proc. SPIE](#), Vol. 4841, Instrument Design and Performance for Optical/Infrared Ground-based Telescopes, ed. M. Iye & A. F. M. Moorwood, 451
- Xiao, L., & Eldridge, J. J. 2015, [MNRAS](#), **452**, 2597
- Yan, H., Ma, Z., Beacom, J. F., & Runge, J. 2018, [ApJ](#), **867**, 21
- Zhang, J., Zheng, X., Wang, X., & Rui, L. 2016, The Astronomer's Telegram, 9093
- Zhang, T., Wang, X., Mo, J., & Chen, J. 2014, Central Bureau Electronic Telegrams, 3795